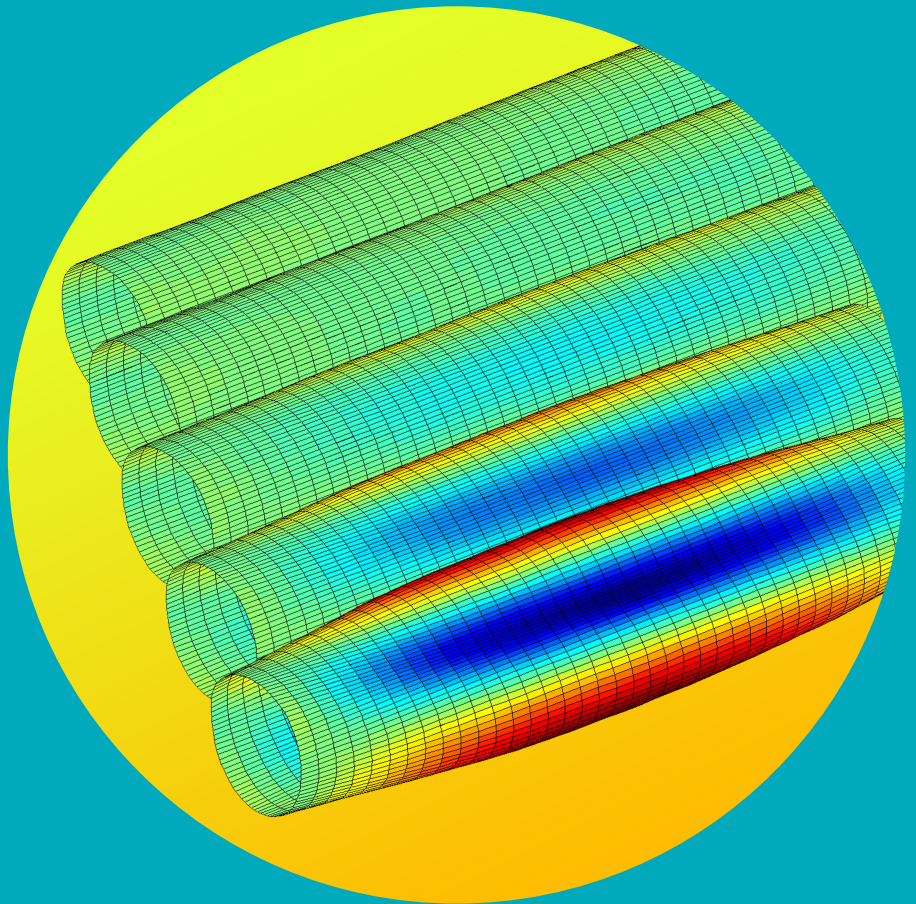


Department of Engineering Design and Production

Dynamic geometry of a rotating paper machine roll

Jari Juhanko



Dynamic geometry of a rotating paper machine roll

Jari Juhanko

Doctoral dissertation for the degree of Doctor of Science in Technology to be presented with due permission of the School of Engineering for public examination and debate in Auditorium K216 at the Aalto University School of Engineering (Espoo, Finland) on the 18th of November 2011 at 12 o'clock noon.

Aalto University
School of Engineering
Department of Engineering Design and Production

Supervisor

Prof. Petri Kuosmanen

Instructor

Prof. Petri Kuosmanen

Preliminary examiners

Prof. Jouko Karhunen, Oulu University, Finland

Prof. Dr.-Ing. René Theska, Technical University Ilmenau, Germany

Opponents

Prof. Juhani Niskanen, Oulu University, Finland

Prof. Dr.-Ing. René Theska, Technical University Ilmenau, Germany

Aalto University publication series

DOCTORAL DISSERTATIONS 117/2011

© Jari Juhanko

ISBN 978-952-60-4363-0 (printed)

ISBN 978-952-60-4364-7 (pdf)

ISSN-L 1799-4934

ISSN 1799-4934 (printed)

ISSN 1799-4942 (pdf)

Unigrafia Oy

Helsinki 2011

Finland

The dissertation can be read at <http://lib.tkk.fi/Diss/>



Author

Jari Juhanko

Name of the doctoral dissertation

Dynamic geometry of a rotating paper machine roll

Publisher School of Engineering

Unit Department of Engineering Design and Production

Series Aalto University publication series DOCTORAL DISSERTATIONS 117/2011

Field of research Machine technology

Manuscript submitted 13 June 2011

Manuscript revised 31 August 2011

Date of the defence 18 November 2011

Language English

Monograph

Article dissertation (summary + original articles)

Abstract

The research is initiated by the findings that the coating variation of light weight coated LWC paper is in synchronization with a backing roll of a coating station. The frequency of the largest peak in the quality variation spectrum corresponds to the oval geometry of a backing roll, but no such a phenomenon has been measured in a roll shop. It was realized that the cause of the research problem could be the change in the geometry as a function of running speed.

First, a theoretical study is carried out by building a single cross-section FE model of a backing roll using measured wall thickness data with systematic thickness variation. Only the main variation component is used. The analysis shows the wall thickness variation is a possible cause for a dynamic geometry change.

For a more detailed study, a cylindrical FE model is created, and the measured wall thickness matrix is used to define the inner surface nodes. The analysis shows dynamic geometry change although the geometry is more complex due to fixed end plates.

A device is developed to measure the dynamic geometry change. The device is calibrated using a multi-lobe disc as a reference standard. Using the principles of GUM (Guide to the expression of uncertainty in measurements) it is shown that the expanded uncertainty U of the device is less than two micrometers in a typical measuring case.

A full scale backing roll is used as a test roll in laboratory experiments. The measurements of the roll show similar behavior that was observed in the FE analyses. The magnitude of the change in simulation was about 20 % lower than in the measurements. It is concluded that enhancements in the FE model and the processing of the measuring data would lead to more consistent results.

The significance of the phenomenon is studied using a quite large sample of backing rolls at paper mills in Finland and abroad. The measured rolls are classified according to different generations of manufacturing processes and materials used. The study showed that dynamic geometry change is a common phenomenon in industry.

A correlation analysis between machine direction quality variations of LWC paper and the dynamic behavior of a backing roll shows a very strong correlation. In many cases, the dynamic geometry change is the most significant single component causing run-out, and thus the main single cause for the harmonic paper quality variation.

During the research, some methods were used for maintenance purposes to improve the dynamic behavior of backing rolls. According to the measurements, the used maintenance methods proved to be useful.

Keywords rotor dynamics, dynamic geometry, geometry change, paper machine, backing roll

ISBN (printed) 978-952-60-4363-0

ISBN (pdf) 978-952-60-4364-7

ISSN-L 1799-4934

ISSN (printed) 1799-4934

ISSN (pdf) 1799-4942

Location of publisher Espoo

Location of printing Helsinki

Year 2011

Pages 172

The dissertation can be read at <http://lib.tkk.fi/Diss/>

Tekijä

Jari Juhanko

Väitöskirjan nimi

Paperikoneen telan dynaaminen geometria

Julkaisija Insinööritieteiden korkeakoulu**Yksikkö** Koneenrakennustekniikan laitos**Sarja** Aalto University publication series DOCTORAL DISSERTATIONS 117/2011**Tutkimusala** Konetekniikka**Käsikirjoituksen pvm** 13.06.2011**Korjatun käsikirjoituksen pvm** 31.08.2011**Väitöspäivä** 18.11.2011**Kieli** Englanti **Monografia** **Yhdistelmäväitöskirja (yhteenvedo-osa + erillisartikkelit)****Tiivistelmä**

Paperiteollisuudessa on havaittu, että kevyesti päällystetyn LWC-paperin koneensuuntainen laatu vaihtelu on synkronissa paperikoneen päällystysaseman vastatelaan. Suurin yksittäinen vaihtelukomponentti tahdistuu vastatelan toiseen harmoniseen eli soikeutta vastaavaan virheeseen. Tutkimuksen hypoteesina on, että ilmiö johtuu telan geometrian muuttumisesta ajonopeuden funktiona.

Telasta luotiin ensin yksinkertainen poikkileikkausmalli, jonka muodostamiseen käytettiin seinämänpaksuusmittauksessa havaittua suurinta vaihtelukomponenttia. Laskenta osoitti, että todellista suuruusluokkaa oleva seinämänpaksuusvaihtelu aiheuttaa dynaamista geometriamuutosta. Koko telan mallia varten mitattua seinämänpaksuusvaihtelumatriisia hyödynnettiin asettamalla elementtimallin sisäpinnan määrittämät solmupisteet mittaustuloksen mukaan. Analyysin tuloksena saatiin dynaaminen geometriamuutos, jossa telan päätyjen jäykistävä vaikutus on havaittavissa. Havaittu muodonmuutos on mahdollinen selitys tutkittavalle ilmiölle.

Dynaamisen geometrian tutkimiseksi kehitettiin mittalaite. Laite kalibroitiin kehitetyllä kalibrointiekolla, jonka geometria koostui useasta aaltomuodosta. Laajennetuksi mittaasepävarmuudeksi saatiin GUM-periaatteita noudattaen alle kaksi mikrometriä.

Teollisessa tuotannossa olleen päällystysaseman vastatelan laboratoriomittauksissa mitattiin vastaava dynaaminen käyttäytyminen kuin FE-analyysissä oli havaittu. Mallinnuksessa saadut tulokset geometriamuutoksen osalta olivat noin 20 % pienemmät kuin mitatut. Tulosten analysoinnissa havaittiin, että kehittämällä mallin reunaehdoja ja mittaustiedon käsittelyä tulosten yhteneväisyys olisi parempi.

Ilmiön merkittävyyttä tutkittiin paperiteollisuudessa käytössä olevien telojen mittaussarjalla. Mitatut telat luokiteltiin ikäkausittain telan rakenteen ja käytettyjen materiaalien perusteella. Mittaukset osoittivat, että dynaaminen geometriamuutos on yleistä kaikilla vastatelatyypeillä.

LWC-paperin ja telan dynaamisen käyttäytymisen välinen korrelaatio osoittautui analyysissä erittäin vahvaksi. Useissa tapauksissa dynaaminen geometriamuutos on suurin yksittäinen telan heittoa aiheuttava komponentti ja siten suurin yksittäinen harmonisen päällystemäärävaihtelun aiheuttaja. Tutkimuksen aikana vastatelan dynaamisen käyttäytymisen parantamiseksi käytettiin erilaisia kunnostusmenetelmiä. Mittausten perusteella menetelmät osoittautuivat toimiviksi.

Avainsanat roottoridynamiikka, dynaaminen geometria, geometriamuutos, paperikone, vastatela

ISBN (painettu) 978-952-60-4363-0**ISBN (pdf)** 978-952-60-4364-7**ISSN-L** 1799-4934**ISSN (painettu)** 1799-4934**ISSN (pdf)** 1799-4942**Julkaisupaikka** Espoo**Painopaikka** Helsinki**Vuosi** 2011**Sivumäärä** 172**Luettavissa verkossa osoitteessa** <http://lib.tkk.fi/Diss/>

Preface

The research work related to this thesis is carried out in the Department of Engineering Design and Production at Aalto University School of Engineering during 1995-2011. The projects are funded by the National Technology Agency (Tekes), Finnish paper and paper machine industry which are greatly acknowledged.

Professor Petri Kuosmanen deserves my warmest gratitude as a supervisor and as a research colleague for his support and encouragement during the years. Professor Matti Kleimola has inspired my work during the first years as a researcher.

I am grateful to all the colleagues from the industry who have motivated the work during this long journey: Jari Aho, Pekka Bolström, Klaus Enwald, Jani Hakola, Timo Häkkinen, Klaus Jernström, Hannu Junes, Ari Koskinen, Antti Kuusinen, Kristiina Lammila, Tapio Makkonen, Jukka Nikula, Markku Oikarainen, Tero Olander, Antti Ollikainen, Jan Paasonen, Martti Pakkanen, Ilpo Palomäki, Risto Rämänen, Markku Saarela, Kyösti Saastamoinen, Kalervo Salomäki, Pekka Simola, Sakari Toivonen, Arto Turunen, Rami Vanninen, Antti Veistinen and Pertti Weissenfelt. Without you the research would have never started and continued through all these years.

A great number of current and former researchers have been involved in the research. Special thanks are due to Pekka Väänänen for the development of the geometry measuring method, and Jukka Pullinen for co-developing the device and writing the latest measuring software. It has been very fruitful working with you. The work of Esa Porkka, Kimi Forsberg and Aki Koskinen has been very valuable in performing and analyzing the finite element models. The development of the ultrasonic measurement system by Tommi Uski plays an important role in this study. Without Thomas Widmaier's support on practically every issue concerning data acquisition, signal processing, software and the use the laboratory instruments and devices the research would still go on. Discussions with Panu Kiviluoma on the measuring technology, as well as with Jukka Pirttiniemi, Jari Toiva and Raimo von Hertzen on rotor dynamics and balancing made me understand and refine some of the key issues. No experimental work would have been possible without the help of laboratory personnel Jouni Pekkarinen, Santtu Teerihalme, Olli Ylöstalo and Olavi

Turunen who are greatly acknowledged for their support. In the first years of the projects ex-researchers Janne Haikio and Ilkka Väänänen have given lots of support in their special fields of expertise - thank you.

Humble thanks to all the others that have contributed to the nice and supportive working environment. Sometimes this lab does not feel as a workplace at all.

Finally, I would like to thank my wife Ulla and our children Anni, Kaisa and Saara for their patience and support during the most intensive research periods. Now the job is done.

Helsinki, October 2011

Jari Juhanko

Nomenclature

Abbreviations

amp	amplitude
c-s	cross-section
DS	drive side, the end of a roll where a drive unit is connected
FE	finite element
FFT	fast Fourier transform
GUM	Guide to the expression of uncertainty in measurements
LSC	least squares circle
LWC	light weight coated paper grade
M	middle cross-section of a roll or the centerline of a paper web
MCC	minimum circumscribed circle
MIC	maximum inscribed circle
MPEe	maximum permissible error for length measurement
MZS	minimum zones circle
NDT	non-destructive testing
RND	roundness
TOF	time of flight
TS	tending side, the side opposite to the drive side (DS)
TSA	time synchronous averaging
upr	undulations per revolution

Symbols

$2^{\text{nd}} H$	the second harmonic component of a signal
$3^{\text{rd}} H$	the third harmonic component of a signal
$4^{\text{th}} H$	the fourth harmonic component of a signal
a_0, a_n, b_n	Fourier terms from Euler equations
A, B, \bar{A}, \bar{B}	outputs of an incremental rotary encoder and their inverse functions
A_{2H}	amplitude of the 2^{nd} harmonic component
A_{3H}	amplitude of the 3^{rd} harmonic component
A_{4H}	amplitude of the 4^{th} harmonic component
\bar{A}_{ref}	mean harmonic component of the reference instrument
\bar{A}_{DG}	mean harmonic component of the geometry measuring device
ΔA	uncorrected value of the geometry measuring device

ΔA_C	corrected value of the geometry measuring device
$A(\theta)$	geometry profile
A_n, B_n	Fourier series terms
$B(\theta)$	geometry profile
c_i	sensitivity coefficient
c_n	Fourier coefficients in complex plane
C	Fourier amplitude term of a coherent component of a signal
$C(\theta)$	geometry profile
D_b	diameter of a rolling element of a bearing
D_m	average diameter of inner and outer rings of a bearing
EI	flexural stiffness
e_{per}	permissible specific unbalance
f	rotating frequency
f_{co}	filtering cut-off frequency
f_{cr}	critical frequency
f_r	rotating frequency of a roll
f_c	frequency of a cage of a bearing
f_i	frequency of an inner ring of a bearing
f_o	frequency of an outer ring of a bearing
f_b	frequency of the rolling element of a bearing
$f(x)$	periodic function
F	force
g	gravitational force
G	balance quality grade
h	diameter of a roll
I_x, I_y	principal moments of inertia around an axis while rotating around the same axis, also I_{xx}, I_{yy}
k	coverage factor
k_{co}	filtering cut-off frequency factor
L	length
L_{OC}	offset corrected wall thickness
L_{OGC}	offset and gain corrected wall thickness
\bar{L}_{ref}	mean average of a measurement with a precision micrometer
\bar{L}_{US}	mean average of a measurement with the ultrasonic device
ΔL	difference between the reference measurement and the analyzed measurement
ΔL_{OC}	offset corrected value of a wall thickness measurement
ΔL_{OGC}	offset and gain corrected value of a wall thickness measurement
m	mass of a rotor
M	mass required to balance an eigenmode

M_T	moment caused by linear graded thermal distribution
n_i	order of a harmonic
$n(t)$	noise of a signal
$N(t)$	non-synchronous coherent term of a signal
N	number of eigenmodes to be balanced
N	number of averagings
OA	vibration vector without a trial unbalance M_{tr}
OB	vibration vector with a trial unbalance M_{trial}
R	correlation coefficient
$r(\theta)$	radius at a angle θ of a roll
s	thickness of a material
$s_i, s_i(\theta)$	run-out from an observation angle ϕ_i as a function of rotational angle θ
$S_1, s_1(\theta)$	sensor 1 signal at selected an angle $\gamma_1 = 0^\circ$
$S_2, s_2(\theta)$	sensor 2 signal at selected an angle γ_2
$S_3, s_3(\theta)$	sensor 3 signal at selected an angle γ_3
$S_4, s_4(\theta)$	sensor 4 signal at selected an angle 180°
$S(t)$	synchronous coherent term of a signal
\bar{S}_{LSR}	mean of a displacement measurement signal
\bar{S}_{LSRC}	mean of a corrected displacement measurement signal
ΔS	uncorrected displacement measurement signal
ΔS_C	corrected displacement measurement signal
t, t_i	time
$T(t)$	non-synchronous and non-coherent term of a signal
ΔT	temperature difference
u	standard uncertainty of measurement
$u(y)$	standard deviation of the output estimate
U	expanded uncertainty of a measurement
U_{ADG}	expanded uncertainty of a dynamic geometry measurement
U_{Aref}	expanded uncertainty of a reference instrument
U_{even}	expanded uncertainty of harmonic components with even number of undulation components
U_{Lref}	expanded uncertainty of a calibration block measurement with the precision micrometer
U_{LUS}	expanded uncertainty of a calibration block measurement with a ultrasonic measuring device
U_{per}	permissible residual unbalance
U_{SLSR}	experimental expanded uncertainty of a laser displacement measurement
U_Δ	combined uncertainty of a measurement

$x(t)$	a signal consisting periodic signal $f(t)$ and additive noise $n(t)$
X_i	input quantity (in general, case study: speed)
X_j	input quantity (case study: frame eccentricity)
X_k	input quantity (case study: axial position)
x_i	input estimate
\bar{x}	arithmetic mean of an input estimate
Y	output quantity
y	output estimate
α	thermal expansion coefficient
α	attenuation
γ_1	angular position of a sensor S_1
γ_2	angular position of a sensor S_2
γ_3	angular position of a sensor S_3
δ	definition of roundness apart
θ	angular position of a roll
v	deflection of a roll
v	velocity of sound waves
ϕ_i	observation angle
w_2, w_3	weighting factors in roundness algorithm
ω	balancing speed
ω_i	rotating speed of a shaft

Unit conversions

rpm	rounds per minute, 1 rpm = 1/60 Hz
m/min	meters per minute, 1 m/min = 1/60 m/s with the test roll, 1000 m/min corresponds 3.7 Hz

Contents

Preface	7
Nomenclature	9
Contents	13
1 Introduction	17
1.1 Background	17
1.2 Research problem	19
1.3 Aim of the research	21
1.4 Research methods	22
1.5 Scope of the research	23
1.6 Author's contribution	25
2 State of the art review	27
2.1 Pigment coating of paper	27
2.1.1 Light weight coated magazine paper	28
2.1.2 Blade coating	29
2.2 Rotor dynamics	31
2.2.1 Static and dynamic run-out	32
2.2.2 Natural frequency and critical speed	32
2.2.3 Balancing	34
2.2.4 Bearing excitations	41
2.2.5 Asymmetric axis of inertia	42
2.2.6 Initial bending	44
2.2.7 Misalignment	45
2.2.8 Rotating shells	45
2.2.9 Dynamics of paper machine rolls	46
2.2.10 Other phenomena	46
2.3 Roll geometry	48
2.3.1 Geometry definitions	48
2.3.2 Workpiece geometry in machining	50
2.3.3 Roll geometry measurement methods and devices	55
2.3.4 Thermal effects on roll geometry	57
3 Research methods and equipment	60
3.1 Measurement and analysis methods	60
3.1.1 Fourier analysis	60
3.1.2 Synchronous averaging	61
3.1.3 Roundness	64

3.2	Measurement data acquisition	66
3.2.1	Rotary pulse encoder	66
3.2.2	Displacement sensor	66
3.2.3	Low pass filtering board	67
3.2.4	Data acquisition board.....	68
3.2.5	Measurement signal processing	68
3.3	Experimental uncertainty of measurement	69
3.3.1	Expanded uncertainty of measurement	71
3.3.2	Uncertainty interval	71
3.3.3	Error separation	72
3.3.4	Roundness measurement uncertainty	73
3.4	Test roll	76
3.5	Ultrasonic measurement of wall thickness	77
3.5.1	Measurement device and setup	80
3.5.2	Measurement uncertainty	82
3.6	Dynamic behavior measurement of large rotating cylinders	87
3.6.1	Dynamic geometry measurement principle	88
3.6.2	Measurement setup	88
3.6.3	Displacement sensors	89
3.6.4	Speckle pattern effect.....	93
3.7	Calibration procedure and measurement uncertainty	95
3.7.1	Measurement uncertainty of laser displacement sensors	95
3.8	Finite element models	97
3.8.1	Cross-section model.....	97
3.8.2	Cylindrical finite element model	98
3.9	Measurement of coating quality variations	99
3.9.1	Analysis in machine direction	101
3.10	Survey of backing rolls in industrial use	103
3.11	Roll maintenance	103
4	Results	104
4.1	Finite element analysis of cross-section model	104
4.2	Wall thickness of cylinder.....	106
4.3	Finite element analysis using measured wall thickness	107
4.4	Roll measurement device	109
4.4.1	Calibration disc	109
4.4.2	Measuring device calibration measurements	113
4.4.3	Effect of synchronous averaging	116
4.4.4	Effect of cut-off frequency	117
4.4.5	Effect of measuring axial position	118
4.4.6	Measuring frame eccentricity	119
4.4.7	Rotating speed range test	121

4.5	Laboratory measurements of test roll	122
4.5.1	Roundness at measured cross-sections.....	122
4.5.2	Dynamic bending	128
4.5.3	Run-out	130
4.6	Survey of backing rolls in industrial use	133
4.7	Coating quality variation	134
4.8	Roll maintenance and renewal process.....	135
4.8.1	Roll stiffening	136
4.8.2	Internal machining	136
4.8.3	Addition of counterweights	136
4.8.4	3D grinding	136
5	Discussion	138
5.1	Wall thickness	138
5.2	Finite element modeling.....	139
5.3	Measurement accuracy of the device	140
5.3.1	Signal processing system	140
5.3.2	Running speed.....	141
5.3.3	Axial measuring position	144
5.3.4	Frame eccentricity.....	145
5.3.5	Combined measurement uncertainty.....	145
5.3.6	Measurement result versus certified value	147
5.4	Backing roll behavior	150
5.5	Simulation model vs. measured behavior.....	156
5.6	Roll behavior differences by roll structure.....	157
5.7	Roll maintenance	158
5.8	Coating quality variations.....	159
6	Summary	161
	References	164

1 Introduction

1.1 Background

The research group at Aalto University (formerly Helsinki University of Technology) has carried out research on paper machine roll geometry measurements and machine control systems from the beginning of the 1990's. The first research devices were developed to measure the true roundness profile of a roll at a roll grinding machine or at a lathe of a paper mill work shop. The main findings were that machined rolls are typically out of round. Typical ground supercalender soft rolls were oval in shape and turned rolls tend to have more variation in geometry, such as three, four or five lobed geometries, typically. Machine control systems (Väänänen 1993, Haikio 1997, Widmaier et al. 2004) for both lathes and grinding machines were also developed to compensate these geometry errors.

Often, the balancing state of a rotor is a synonym for the dynamic behavior of rolls. When vibration problems exist the rolls are balanced to meet the quality requirements and tolerances. The balancing is carried out with common hard bearing balancing machines, and usually a two plane balancing method (ISO 1940) is applied. Some new methods and devices to balance flexible rotors (ISO 11342) are introduced to reduce the dynamic bending at the operating speed of a paper machine. It is known that the state of balance has a significant effect on the runnability of a paper machine, and even in some cases might have an effect on the paper quality variation.

Asymmetry of paper machine rolls has been studied, because it is known that the asymmetry of the principal inertia moments I_x and I_y (Snellman 1983) causes a bending stiffness variation of a roll. The bending stiffness variation was found to be one cause for the half-critical vibrations which occur at a quite narrow rotating frequency range. In most cases, this vibration problem has been tackled with improved manufacturing technology. A later analysis for the better control of the geometry errors in manufacturing has been presented for example by Sällinen (1998).

Increasing the running speed the way over the design speed of a particular paper machine has brought up some major challenges if the machine is operated with the original rolls. Typically, one or both of the following design criteria for the paper machine rolls has to be met: to limit the

maximum dynamic bending of the roll, and to design the operating speed to be either under the critical speed or under the half-critical speed of the roll.

Both of these qualification criteria cause excessive vibration or run-out of rolls, and in some older paper machines in which the operating speed has been increased during the years, some of the rolls have hit this unwanted frequency range. To reduce the increased vibration either balancing or new rolls are required.

In the middle of the 90's the author visited some paper mills and had discussions with the operation and maintenance personnel about the current and future challenges of a paper making process concerning the roll behavior and the maintenance. It turned out that the analysis of light weight coated (LWC) paper showed significant quality variations in machine direction especially in some of the latest paper machine builds in Finland. Analyses made by a Tapio PMA™ paper machine analyzer showed that the basic wavelength of the variation in thickness, basis weight and ash content matched the perimeter of the backing roll and its harmonics such as twice and three times per perimeter or revolution.

Since the beginning of this study the Finnish pulp and paper industry has undergone some major strategic changes. The profitability of the paper making has been marginal for years. Paper consumption has not been increasing in the traditional markets for Finnish paper products. The increasing manufacturing costs and the decreasing price trend of the paper products require efficient means to improve the productivity and to reduce the cost of paper making. The pulp and paper industry has shut down some paper mills during the past few years.

One of the goals set by the paper industry is to improve the cost efficiency in the paper production and in the asset management (Hagberg et al. 1998). The cost efficiency for every investment on a paper machine or its maintenance has to be analyzed carefully.

In the recent years most of the greenfield investments have been realized in Asia where the consumption of paper is increasing. These paper machines have the latest technology and the competitive edge that the Finnish industry used to have at the 1980's. Increasing the production efficiency without investment on new paper machines is needed.

The maintenance of the paper machine is changing towards proactive maintenance. Depending on a company the maintenance is either the core business or it is outsourced to some specialized maintenance service providers. In both cases, the winner is who takes the most out of the machine with less money.

1.2 Research problem

The research problem has been derived from a quality issue of light weight coated magazine paper (LWC). In the machine direction of the paper web the harmonic coating grammage variation, shown in Figure 1, exceeds the predetermined tolerance values. The wavelength of the variation is the same as the half of the perimeter of the backing roll in a blade coating station.

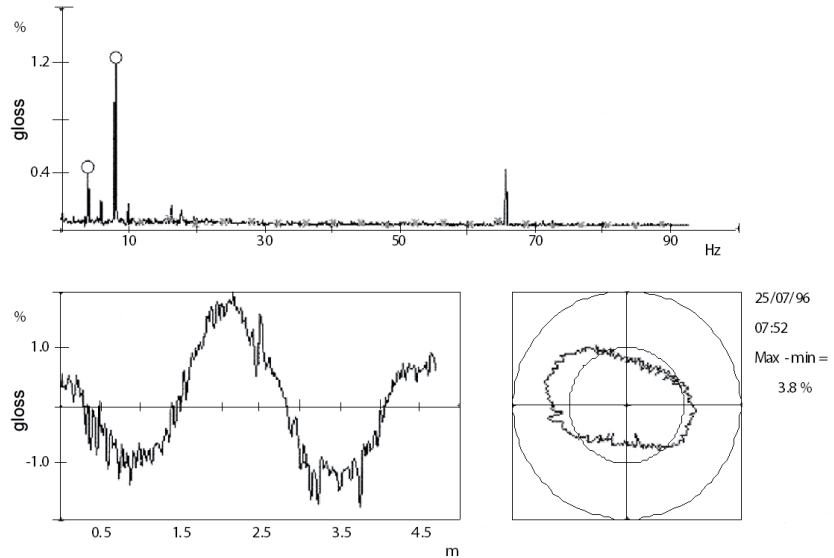


Figure 1 Tapio PMA-analyzer is used to find the source for a single quality variation component of a machine direction paper sample. In the gloss spectrum (top) two major components caused by a backing roll of a coating station are marked (°) at 4 and 8 Hz. The profile (bottom) generated from the harmonic components of one backing roll shows the effect of that very roll on paper quality. (Juhanko 1999)

This measured variation occurs at a wide speed range covering the whole running speed range of the paper machine and the variation seemed to increase as a function of running speed. Resonance vibration occurs in typical cases on a relatively narrow frequency band; therefore this resonance vibration phenomenon does not explain the observed behavior.

At half critical speed i.e. the rotating frequency which is only 0.5 times the natural frequency the harmonic excitations twice per rotation cause excitation at the resonance frequency. This frequency corresponds to the wavelength of the discovered grammage variation.

The first measurements of a backing roll that indicate dynamic geometry change were carried out in 1995 as a run-out measurement with a

triangular laser beam displacement sensor. The maximum running speed of the grinding machine was limited to 3 Hz (180 rpm), which corresponds a web speed of 850 m/min. Radial run-out measurements were carried out in the speed range of 10 to 180 rpm with 1024 samples per revolution for ten revolutions. A data acquisition card (Data Translation DT3831) and a programmable analog low-pass filtering card (Alligator AAF-3) were installed in a PC.

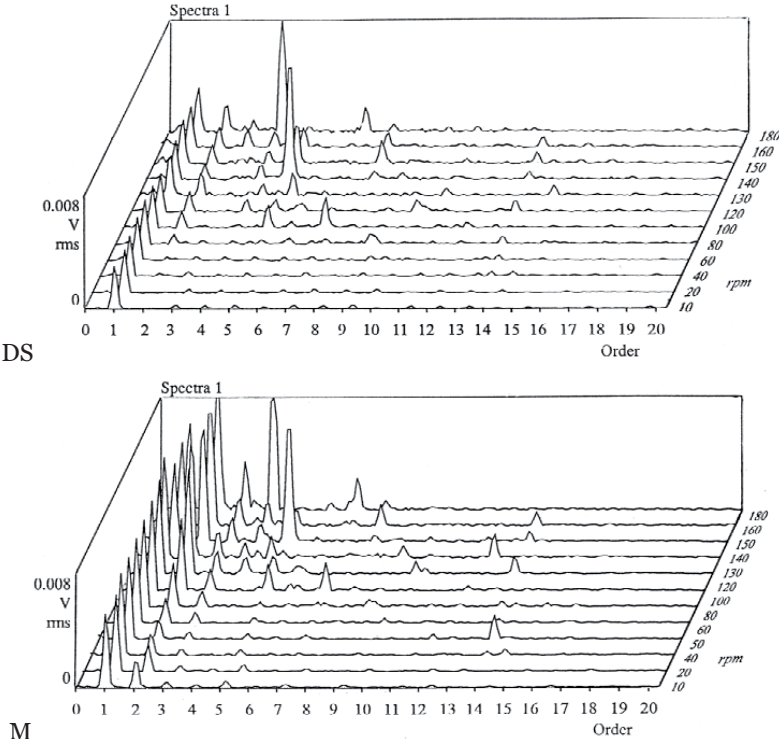


Figure 2 Backing roll run-out spectra measured close to the drive side end plate (DS) and from the middle cross-section (M) of the roll as a function of rotating speed. Tending side (TS) behavior was similar to DS measurement.

Measurement results are shown in Figure 2 as waterfall spectra. Three cross-sections of the roll shell were measured; near the ends (DS, drive side and TS, tending side) of the roll and the middle cross-section (M). The x-axis indicates the order of each component relative to rotating frequency. The frequency of each order component can be calculated from $n_i \cdot f$ where n_i indicates the order and f is the rotating frequency. The amplitude of the first order component remains constant in the measuring range. This indicates that dynamic bending of the roll is not a major issue and the constant static error indicates that there is some eccentricity in the roll. The

second order component shows increasing values especially in the middle cross-section.

The observed peaks at the 4th order measurement at 180 rpm and the 5th order peak at 140 rpm were caused by vibrations of the laser sensor supports.

Run-out measurements carried out by one displacement sensor show an increase in the 2nd harmonic component of run-out as a function of running speed to the power of two. The measured behavior is somewhat similar to the deflection of a flexible roll as a function of running speed caused by unbalance; only the frequency is different.

The cause for the run-out behavior cannot be analyzed with a run-out measurement systems of a typical balancing machine. Run-out consists of the geometry error and the rotational error motion of the rotor axis. These basic components cannot be distinguished from each other with a simple measurement setup. Earlier studies have shown that the geometry of a roll is not perfect after grinding, but there is a varying amount of irregularities in the roundness profile. The hypothesis is that the geometry of a rotating cylinder is not constant, but changes as a function of running speed, mechanical loading and thermal effects. In this study, the focus is on the effect of running speed though the measuring technology may as well be adapted to studying the effects of mechanical and thermal loads.

The challenge is to measure the geometry profile of a rotating cylinder within the accuracy of a few micrometers. The run-out tolerance of a modern high quality process roll is 50 μm typically, and it is set by the operators and manufacturers based on a long-term experience. The set value includes all error components, so the measurement accuracy of a few micrometers is initially justified.

Research is focused on the dynamic behavior of a tube roll and especially on a backing roll of a blade coating station. The increasing quality requirements of paper and the aim for a higher running speed of a machine set tightening requirements also for the dynamic behavior of the rolls (Karlsson 1997). This trend in setting new tolerances applies to all rolls of a paper machine and not just to the backing rolls of a coating station.

1.3 Aim of the research

The aim of the research is to study the dynamic geometry of a paper machine roll. First step is to develop a verified and validated method and device to measure the dynamic behavior of a paper machine roll rotating at normal operating speed of a paper machine. The measurement system must be capable of analyzing the dynamic geometry of a chosen cross-section

from separate and simultaneous run-out measurements. The accuracy of the device is verified and results are validated in co-operation with the Center of Metrology and Accreditation of Finland (Mikes). The results must be independent of rotating speed in the desired speed range. The device is developed for both laboratory experiments and for routine measurements in paper industry as a standard quality assurance procedure.

The aim can be classified as:

- to develop a new measurement device in order to analyze the dynamic behavior of paper machine rolls within an uncertainty of $\pm 2 \mu\text{m}$. For some special cases uncertainty of less than $\pm 1 \mu\text{m}$ would be preferred,
- to understand the relation between roll structure and the dynamic behavior, including the dynamic roundness of the rolls,
- to understand the relation between the dynamic behavior of the backing roll and quality variation of a coated magazine paper,
- to study the effect of operation condition on the dynamic behavior of a backing roll,
- to set demands and tolerances for roll manufacturing, and
- to introduce maintenance procedures to improve the dynamic behavior of backing rolls and to decrease the quality variations of coated magazine paper.

The initial requirement specifications include:

- a non-contacting measurement of a wide variety of surface finishes and materials,
- the measured geometry must be independent of rotating speed, and
- the measurements are carried out at the maximum surface velocity of approximately 33 m/s (2000 m/min).

1.4 Research methods

Literature and patents were studied for the State-of-the-Art section. Known phenomena related to the research problem in wider scope were studied and results are presented and classified. The blade coating is presented briefly to show the importance of the roll run-out to coating weight variation in the machine direction of the paper. The second part presents the phenomena typically introduced in general rotor dynamic analysis. The third part presents geometry error issues in a machining process including material and dimensional errors. The fourth chapter is

focusing on the dynamic behavior of paper machine tube rolls and the common phenomena with relatively thin shells.

The device was designed using systematic design methodology and the experience gained from earlier projects at the Department of Engineering Design and Production of Aalto University, formerly known as the Laboratory of Machine design at the Helsinki University of Technology (TKK). The roundness profile measuring algorithm and a device are developed by Väänänen (1993) to measure the roundness of a slowly rotating cylinder using contacting sensors. The selection of the non-contacting sensors was carried out by a literature study and experimental tests of some chosen commercially available sensor models. Hardware and signal processing algorithms were chosen to fulfill the requirements for the device.

The experimental verification and validation of the measurement device were carried out by reference measurements using a calibration standard disc designed and manufactured for calibration purposes with a known multi-lobe geometry profile. The experimental measurement uncertainty was determined according to GUM (Guide to the expression of uncertainty in measurement). The correlation between manufacturing accuracy and the dynamic geometry error is analyzed using wall thickness measurements as an input data for finite element calculation.

The research problem is also studied by analyzing the roll itself. Manufacturing accuracy of a roll tube is studied using finite element analysis and experimental measurement data retrieved from the rolls used in industry.

Roll measurements were carried out in the laboratory and in several companies, which were participating in the research projects.

1.5 Scope of the research

The developed device uses a formerly introduced algorithm and the further development of the mathematical algorithm is excluded. The front end of the signal conditioning and data acquisition parameters have been redesigned, because of the nature of sensors, the dynamic behavior of the rotor and vibrating surroundings. The uncertainty of measurement analysis is carried out by experimental means, and thorough analysis of the measuring system using error budgeting or sensitivity analysis is excluded. These analyses are vital in the further development of the measurement system, and therefore these methods may be used in the development of the next generation measuring device.

The research is focused on the experimental research of a backing roll of a blade coating machine. A single test roll is used in the laboratory study and therefore some results may not be applicable to the other types of rolls or the other backing rolls which structure or material differs from the one used in the laboratory experiments. The research presents the dynamic behavior measurements of several backing rolls with different structures, but only one roll structure is used in the analysis.

The analysis concentrates on the dynamic behavior at normal operating speeds of a paper machine. Backing rolls are designed to operate below half-critical speed. However, the operating speed window for different paper grades might be quite large, and in some cases, the operation at 1/3-critical speed can be evident. Yet, when the production volume and hence the running speed of older machines have been increased over the original design speed, backing rolls might be running close to or at half-critical speed, which often causes vibrations. The vibration analysis is excluded from the study.

Deep analysis and development of balancing methods are excluded from this study, because the driving force for this study is the second harmonic run-out component of the backing roll running frequency. This restriction derives from the analysis of paper quality variations in the machine direction that shows the main variation component which exists twice per backing roll perimeter.

Perimeter expansion is excluded from the study although it is known that there are some roll structures with inner stiffening rings that might cause error in cylindricity i.e. a diameter profile error. The stiffening ring would affect the perimeter expansion caused by centrifugal force.

Measurements and analyses of dynamic behavior in this study are restricted to the analysis of the geometry change as a function of rotating frequency. Another special program has been developed at the Helsinki University of Technology for analyzing the effects on general imperfections e.g. an asymmetric rotor is included in the model but roundness profile analysis is not. (Hertzen 1994, Paloheimo 2000, Toiva 2002)

The engineering tools i.e. FE analysis and ultrasonic measurements are used as engineering tools to verify and validate the results. Available technologies and programs were used and no emphasis was put on utilizing the latest scientific findings in these areas.

Active and semi-active vibration methods are excluded from the experimental study, because the nature of the studied phenomena is quasi static in a rotating coordinate system at a certain running speed. The goal of this research is to study methods in order to measure and understand the

cause for the dynamic geometry change, and to find means to minimize the error.

The dynamic behavior of the blade supporting beam is excluded from this study although it has a great importance in some cases in which resonance vibration is the cause for the coating grammage variation. This vibration exists on a narrow frequency band and therefore the cause for grammage variation can easily be analyzed by measurements as a function of running speed.

Paper is also coated by some other methods than a blade coating technique. Rolls used in surface sizing or in film coating are excluded from this study although there are some similarities in these rolls. The coating principle is different and the effect of run-out on coating thickness variation is not studied.

1.6 Author's contribution

In the middle of 1990's the author came up with a new phenomenon in run-out measurements of a paper machine roll that could not be explained by commonly known rotor dynamic theory. The first measurements were carried out by the author on a grinding machine of a paper mill. The rotating speed was relatively slow in comparison with the operating speed of a paper machine, but significantly faster than the rotating speed in a normal grinding process. The running speed was limited to 3 Hz (180 rpm) by the grinding machine, which corresponds to the web speed of 850 m/min. This was still significantly less than the normal production speed of the paper machine.

The measurement showed greater run-out that could be explained by the conventional roundness error and rotational error motion of the roll. Further experiments showed that the discovered behavior increased as a function of running speed from the initial value measured at a very low rotating speed. Soon the author realized that the measured result might be caused by an increasing geometry error of the roll shell.

After discovering the nature of the problem the author has carried out the prototype development of the measurement device and software to distinguish the rotational error motion of the roll axis and the geometry of rotors at typical running speed range of a paper machine. In later stages of research other researchers have been working in the development of the measuring device and utilizing the device in both laboratory and industrial experiments. The author has carried out most of the measurements together with the research team, especially M.Sc. Jukka Pullinen, who has

created the latest version of the measurement software and its user interface.

The author is responsible for carrying out the ultrasonic measurements including the calibration and validation of these measurements. The ultrasonic measurement system is developed by Uski (1999) for quality inspections of soft roll covers. The author used the same measurement setup for wall thickness measurements.

FE models are generated and studied comprehensively by Porkka and Forsberg (2006) and the author has only a minor role in developing these models and their respective analyses.

A part of the literature study has been carried out in Väre-project by Pucket and von Herten (1999) as well as by Kärkkäinen and von Herten (1999). The section for general rotor dynamics is based on this work and is extended by the author.

The author has also been working for commercializing the measurement device. Some devices are in operation at roll shops in Finland.

This thesis is based on several projects, the first of which started in 1995. The measurements were carried out in the laboratory and in paper mills and roll workshops, mostly in Finland. Quite many researchers have participated and contributed to this thesis. The research problem was set in early 1996 when the coating quality variations were analyzed to be in synchronization with rotating speed and its multiples of a backing roll.

2 State of the art review

The aim of the literature study has three approaches. First, the aim is to describe the properties of light weight coated paper, present the coating process and how the dynamic behavior of a backing roll relates to paper quality variations therefore showing the significance of the research problem.

Secondly, the research subject is approached from the basics of rotor dynamics to set a theoretical background on the characteristics and dynamic behavior of a paper machine roll. The review is limited to the most important issues related to the theme of this study, and the most recent scientific advances e.g. in balancing are excluded.

The third part presents geometry measurement methods and signal processing technologies. This knowledge is required in designing the new measurement system. The error estimation, calibration and validation methods are briefly described.

2.1 Pigment coating of paper

The aim of coating paper is to obtain a better surface for printing and publishing. There are many paper grades, which can be classified as coated paper. Light weight coated paper is commonly used for example in magazines with color photos. Variation in quality properties such as glossiness or smoothness has an effect on print quality.

An on-line coating process has set new demands for the efficiency of coating machines. Blade coating, which is sensitive on the run-out of the backing roll, can be used also in the future for coating paper and therefore the dynamic behavior of backing rolls will have even greater importance.

In this chapter, the coating process is explained in order to understand the relation between quality variations of light weight coated (LWC) magazine paper and the dynamic behavior of the backing roll in a blade coating station. First, LWC paper, its quality requirements and production are described. Although results can be applied to the other paper grades this study concentrates strictly on LWC.

2.1.1 Light weight coated magazine paper

A typical classification of mechanical printing and writing papers can be done by paper grades of different characteristics (Knowpap 2009) as shown in Figure 3. Only one of the grades is relevant to this thesis and described in more detail.

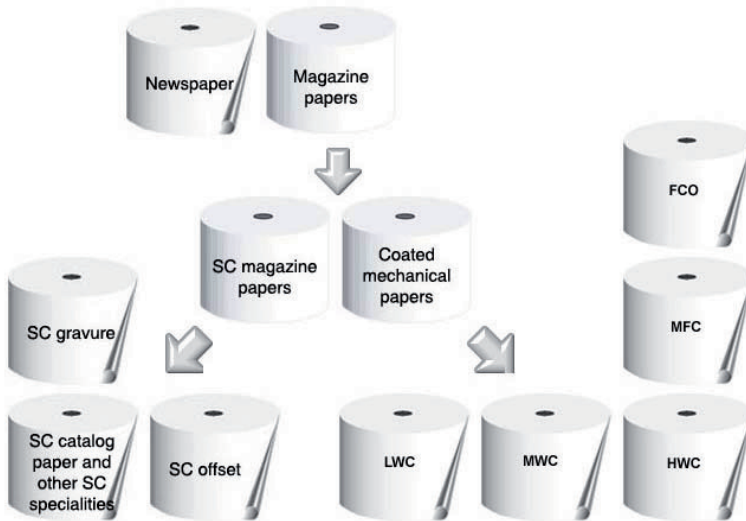


Figure 3 Mechanical printing and writing papers. (Knowpap 2009)

Lightly coated (5...12 g/m² double-side coated paper) LWC grades are manufactured for printing that requires relatively high quality (Haarla 2000). Base paper is made from mechanical and chemical pulp. The strength of the LWC-paper is quite good due to the demands of the coating process on the base paper. The brightness levels of the paper are adjusted to its basis weight so that the highest basis weights are the brightest.

LWC paper has good gloss and brightness and it is used in magazines and catalogues where the proportion of advertisement is large. LWC paper has a significant importance for Finnish paper industry.

When analyzing the quality requirements for a specific printing paper, the starting points are the quality requirements for the customer's publisher or printer product. The amount, cost and desired print quality are deciding factors when choosing the paper grade. The dynamic behavior requirements of a paper machine roll should be traced back to these quality requirements. Typical measured paper properties for printability are gloss, smoothness, opacity, brightness, formation, surface strength and permeability.

The coating layer is relatively thin, only 10...20 µm. The challenge is to cover the paper web with this layer and with traditional technology it cannot be done in one step. (Kiviranta 2000, Linnonmaa and Trefz 2000)

2.1.2 Blade coating

The most common coating methods are blade coating, film coating, air brush coating and spray coating. Blade coating in its different forms is still the most common coating method.

The coating smoothens the irregularities filling the voids of the paper and the end product has even caliper i.e. thickness. Film coating is often referred as contour coating, because a coating film with even thickness is applied on the surface of the paper. This research focuses on blade coating.

In pigment coating a smooth layer of coating color is applied to the surface of the paper one side at a time in a blade coating station. The coating is dried before coating the other side. The forming of the coating can be divided into two process stages: application and control of the coating thickness. (Linnonmaa and Trefz 2000)

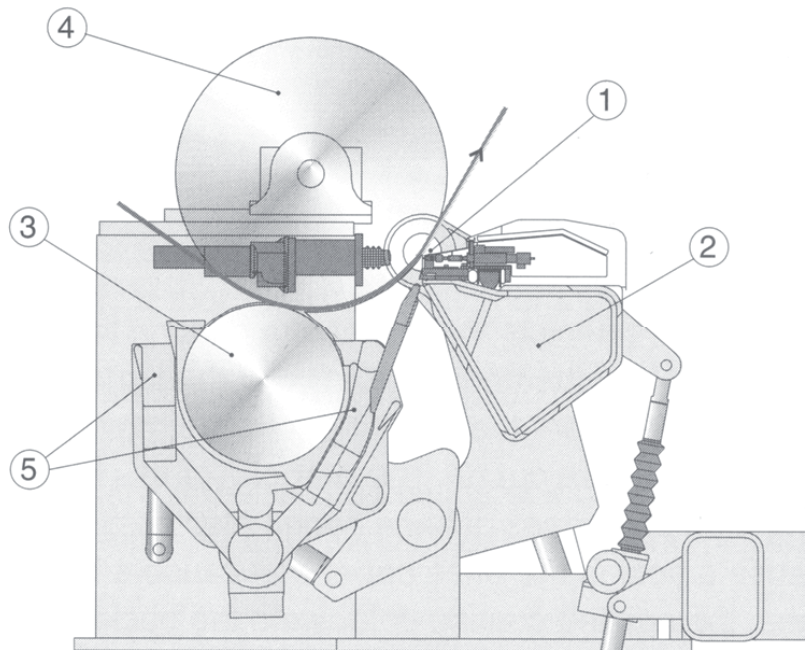


Figure 4 Blade coating station with a backing roll (4) metering blade (1), support beam of the blade (2), applicator (3) and coating color overflow collectors (5). (Lehtinen 2000)

The function of a backing roll is to guide the paper web through the coating station, and to give backup for the coating process, as shown in Figure 4. First, the coating color is applied on the paper web either by a roll application or a nozzle application. Typically, this part of the coating process does not affect the quality variation of the paper.

After application of coating color, the web travels around the backing roll. The dwell time i.e. the time between application and metering of the coating color is controlled by the structure of the coating machine. During that dwell time the paper web picks up moisture from the coating color while dewatering the color itself. Roll applicators are often referred as a long dwell time applicator, because of the relatively long time of 20...50 ms before metering. With nozzle type of applicator the applicator and metering can be arranged closer to each other. Therefore, with these short dwell type applicators lighter paper grades can be coated without excessive moistening of the paper. (Haarla 2000, Linnonmaa and Trefz 2000)

The final coating grammage is controlled by blade metering, rod metering, roll metering or an air knife. In blade metering changing the load of the doctoring blade against the paper web and the backing roll controls the amount of coating color. Typically, the pressure is applied by loading the blade or changing the contact angle between the blade and the paper web. Figure 5 shows a detailed picture of a short dwell coater chamber.

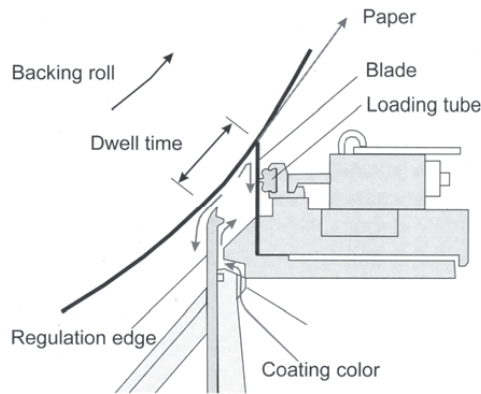


Figure 5 Short dwell coater chamber flows. Run-out of the roll affects the hydrodynamic force balance under the blade. (Linnonmaa and Trefz 2000)

The dynamic behavior of the doctoring blade allows the blade to follow the surface of the paper while small amount of run-out of the backing roll is present. The coating color thickness variation is caused by small changes in the force equilibrium at the coater chamber affecting the contact geometry of the doctoring blade against the web. Two mechanisms are reported: an impulse force towards the blade, and a change in the contact angle that causes a change on hydrodynamic force balance under the doctoring blade thus affecting the gap and therefore coating thickness. (Linnonmaa 1988)

Koskinen (1989) proposes that the characteristics of the backing roll cover material have a big influence on the stability of the coating process. Koskinen lists the quality requirements of rolls as an important issue.

Thus it is crucial to have a steady backup for the coating process. This steady backup is offered by a backing roll which is manufactured with the state of the art technology to fulfill the strict manufacturing tolerances. (Linnonmaa and Trefz 2000)

Backing rolls are typically much larger than any other paper-carrying rolls in a coating machine to provide very straight and stable backing for the paper when coating is being applied and metered. The large diameter is used to increase the natural frequency of the roll.

Reducing and blocking vibrations from the other parts of the coating machine to the backing roll is crucial to prevent the disturbance of the very critical metering process.

The blade coating method will most likely be one of the coating methods in the future. With new techniques even web speeds of 3000 m/min have been reached in pilot scale studies without degrading the coating quality (Lehtinen 2000).

2.2 Rotor dynamics

Basic vibration theory can be read from every book of vibrations; hence the analytical formulae of equations of motions and their solution are not presented. Rotor dynamics has been an important research area for decades, and there are lots of published books and articles starting from the 19th century as a work of Gustav de Laval followed by Henry Jeffcott's research. The development of finite element analysis started during the 1940s and currently there are flexible tools for analyzing non-idealities of rotor systems. The user of these tools should be aware of the software capabilities as not all software can take into account the required phenomena.

In this study some of the phenomena of rotor dynamics are presented by a limited number of papers. A part of the general rotor dynamics section is based on a survey carried out by A. Puckett and R. von Herten (1999) and a report by T. Kärkkäinen and R. von Herten (1999). The study was a part of the Väre-project on rotor dynamics, and parts having influence on the dynamic behavior of paper machine rolls are included.

In industry, the state of balance and dynamic run-out has been synonyms for the dynamic behavior of a paper machine roll. For cylindrical, thin wall rotors, such as paper machine rolls, many analytical and numerical FE models have been developed in which geometry, structure and material properties are included. Models have been used to improve and optimize the design and these models are used in manufacturing and maintenance.

Demand for a better and more comprehensive analysis of roll characteristic requirements has been set by increased running speed.

The following chapters present significant phenomena in paper machine roll dynamics. The term static has been used for a measurement state where the dynamic part of the phenomena can be neglected. Typically, this means a low rotating frequency, such as a grinding speed of only a few rounds per minute, or jogging speed of a paper machine i.e. web speed of 50 m/min. In these cases, the roll behavior does not change as a function of running speed.

A simply supported roll bends due to gravitation. While bending the roundness profile of a hollow cylinder is affected resulting in deformed cross-section geometry. This geometry does not rotate with the roll.

2.2.1 Static and dynamic run-out

Run-out is defined by the standard ISO 1101. Run-out can be expressed in several ways the most common being a peak-to-peak (p-p) value summing up all error components and indicating the difference between the maximum value and the minimum value. Also, total indication read-out TIR has been used. In the geometric tolerancing terms run-out and total run-out are used. Run-out is defined as a radial variation from a true circle.

The run-out can be divided into static and dynamic components. Static run-out is caused by initial bending (not gravitational), roundness error and bearing error motion, for instance. Run-out components that are changing as a function of rotating frequency are called dynamic run-out components and they are caused by bending due to unbalance, the deformation of the roll shell and the bending stiffness variation, for instance. Bearings can act as a vibration excitation. In addition, external excitations might cause dynamic run-out of a roll. These excitations include, but are not limited to excitations from drives, the paper web and other machines and devices in the paper machine.

2.2.2 Natural frequency and critical speed

A roll can be taken as a homogenous beam which has an indefinite number of eigenmodes and corresponding natural frequencies. The lowest natural frequency is typically either a translation mode of a rigid rotor, or the first bending mode (Figure 6). The natural frequency of a roll usually refers to the first bending mode, but other modes may as well be present in operating conditions. The lateral eigenmodes can be differentiated with at least three synchronized run-out or vibration measurement sensors; two at both ends and one in the middle.

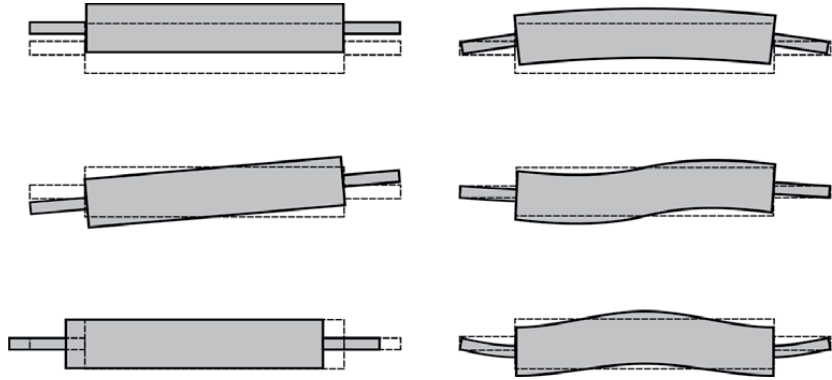


Figure 6 Some eigenmodes of a roll; translational rigid body modes (left) and bending modes of a flexible rotor (right).

Critical speed or critical frequency f_{cr} is defined as a speed when the rotating frequency equals the natural frequency of one particular eigenmode, and the magnification factor is at its maximum causing excessive vibration. Vibration amplitude depends on the excitation force and damping of the structure. Internal damping does not have an effect on the bending due to unbalance, because the bending is a static phenomenon in a rotating coordinate system. At a critical speed even a small excitation force can cause vibration. The vibration amplitude is restricted mostly by external damping from the paper web and felts, for instance.

Below the critical speed there are resonance peaks, typically, where the ratio between the critical speed and the running speed is an integer and the vibration amplitude is increased.

At half-critical speed the roll vibrates at natural frequency although the rotating speed is only half of the critical speed. At the speed $0.5 \cdot \omega_{cr}$, the excitation at natural frequency is caused by some systematic harmonic excitation twice per revolution. Possible causes are bending stiffness variation i.e. $I_x \neq I_y$ (Snellman 1983, Karhunen 1995) and ovality of the rotating bearing surface. In general, these superharmonic vibrations in the sub-critical range are excited by both external and internal sources.

Design criteria for dynamic behavior depend on the type of the roll. Most of the rolls are designed to operate under the critical speed and the dynamic bending is restricted by a dynamic run-out tolerance value. Some rolls are designed to operate under the half-critical speed due to high demands on runnability. The actual operating speed of a paper machine can be significantly lower or even higher than the original design speed. Should the paper machine be run at lower speeds, even one-third critical speed may appear as a problem for a backing roll of a coating station.

The running speed of some older paper machines has been increased during modernization projects; therefore some rolls have had to be changed for ones with a larger diameter to achieve increased stiffness, higher natural frequency and slower rotating speed.

2.2.3 Balancing

Unbalance i.e. imbalance and dynamic bending are the most referred dynamic errors of rotating machinery. Balancing machines are commonly used in industry to minimize either the supporting forces or the dynamic bending. The state of balance and balancing methods are described in standards by International Organization for Standardization ISO. Balancing vocabulary is presented in (ISO1925).

The unbalance can be described as static and dynamic unbalance. Static unbalance is defined as the rotational axis i.e. the shaft axis and the central principal axis are parallel but not coincident. Static unbalance can be observed by deviating the rotor from the state of equilibrium (ISO1925).

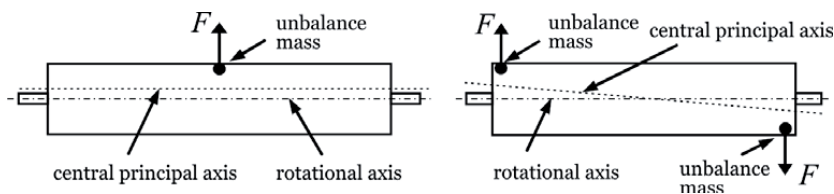


Figure 7 Static unbalance (left) and dynamic unbalance.

Dynamic unbalance is defined as the axis of rotation and the central principal axis are not parallel. Dynamic unbalance can be described as two added masses on the opposite sides of a rotor, as shown in Figure 7. Rotation causes a pair of forces which furthermore may cause bending of the rotor.

In reality, the unbalance is a combination of these ideal unbalance states and eccentric unbalance mass is distributed along the length of the rotor. The unbalance causes centric forces as a function of the rotating frequency to the power of two. Centric forces and the change in eccentricity cause a varying bending moment; thus the rotor deflects due to unbalance. Bending is quasi-static and the stresses are static at a constant rotating frequency.

A rotor is defined as flexible when the state of balance changes as a function of running speed. Otherwise a rotor is rigid (ISO 1925).

In a paper machine unbalance causes vibration and rotating force on bearing supports. Dynamic bending can be observed as run-out. These effects are minimized with a balancing procedure. In balancing, the mass

distribution is fixed that the residual unbalance and dynamic deflection are within a given tolerance.

2.2.3.1 Balancing of rigid rotors

Standard ISO 1940/1 presents the balancing of rigid rotors in one and two planes. According to the standard, one plane balancing can be used for disc-shaped rotors i.e. Jeffcott's type rotors with a point mass (disc) and a long bearing span. Otherwise the rotor has to be balanced in two planes.

The permissible residual unbalance is defined as

$$U_{\text{per}} = e_{\text{per}} \cdot m \quad (1)$$

where

U_{per} permissible residual unbalance (g·mm),
 e_{per} permissible specific unbalance (g·mm/kg) and
 m mass of the rotor (kg).

The greater the mass of the rotor, more permissible residual unbalance is allowed. The balance quality grade of a paper machine roll is defined as

$$G = e_{\text{per}} \cdot \omega, \quad (2)$$

where

G balance quality grade (mm/s),
 e_{per} specific unbalance (g·mm/kg) and
 ω balancing speed (rad/s).

In a certain balancing quality grade class the function $e_{\text{per}} \cdot \omega$ is constant i.e. allowed specific unbalance increases when the rotating frequency decreases. The standard classifies rotors according to the purpose of use. Paper machine rolls are currently placed in a more demanding class. In general, a roll fulfills the requirements if measured unbalance does not exceed permissible residual unbalance U_{per} in balancing planes.

In two plane balancing of paper machine rolls the end plates are chosen as correction planes, because of a natural position for added or removed mass. This method does not have a significant effect on the dynamic bending hence the design speed is chosen for balancing speed. Because in general the rolls are flexible rotors, the residual unbalance of a rotor is changing as a function of rotating speed. Therefore, when balancing is carried out at the actual operating speed, the unbalance reaches its minimum at that operating speed.

In many cases, the balancing speed has been chosen according to the manufacturer's documents. In practice, the balancing speed should be

chosen close to the actual operating speed of a paper machine. This is especially true with the machine that is running far from its original design speed – either lower or higher speed.

Instead of end plates, the balancing planes can be chosen with other criteria such as using Bessel points the maximum internal bending moment is minimized (Savolainen 1996).

2.2.3.2 Balancing of flexible rotors

To balance a flexible rotor $N+2$ balancing planes are required. The N is a number of eigenmodes to be balanced. Flexible rotors are prone to the proper distribution of unbalance mass, because the unbalance mass has an effect on the eigenmodes. When the speed is close to an eigenfrequency, the respective eigenmode is dominating.

A standard ISO 11342 is applied in the balancing of flexible rotors. Rotors are categorized according to balancing requirements. In general, a standardization of balancing procedures for flexible rotors is challenging, because the operating speed as well as characteristics of the supports have a strong influence on the dynamic behavior and the state of balance.

Standard ISO 11342 gives guidance for the experimental balancing of flexible rotors. The quality of balancing can be measured and evaluated as vibration, bending or bearing support forces. The balancing is carried out by one eigenmode at a time starting from the mode that appears at the lowest frequency.

The standard presents an experimental trial mass balancing method where the vector OA represents vibration without a trial unbalance M_{tr} and vector OB depicts vibration with a trial unbalance M_{trial} added on a rotor. The mass M that is required to balance that eigenmode is calculated using equation

$$M = M_{trial} \cdot \frac{OA}{OB} \quad (3)$$

The method presented in the standard is not very practical to balance paper machine rolls, because trial masses need to be used. More practical method is to measure the unbalance forces and using a model of the roll the required correction is calculated. Although the principle and general workflow are presented in the standard. (ISO 11342)

In three plane balancing of flexible rolls the balancing planes are typically the end plates and the mid-point of the roll. The mass added to the middle is sometimes distributed along the length of the roll tube for easier realization and to minimize the internal stresses caused by centrifugal forces due to that added mass.

2.2.3.3 Balancing by roll centring

The first and second mode of rigid body transverse vibrations can be balanced by centring the roll in turning (Figure 8). By moving the shaft axis linearly, the same amount extra mass is removed from the roll equally along the length of the roll, thus providing means to balance the first bending mode. By tilting the roll tube, material is removed symmetrically from opposite sides which has an effect on the second mode. Tilting is also used to optimize the residual unbalance at each bearing support thus minimizing the required added mass.

This centring can be carried out using a simultaneous ultrasonic wall thickness measurement and displacement measurement with eddy-current sensors to find the real mass distribution of the preformed roll tube (Savolainen 1996). The optimum rotational axis can be calculated from the measurement. Using either traditional centring devices or sophisticated machine control systems (Haikio 1997) the outer surface of the roll is manufactured to minimize the need for any further center balancing.

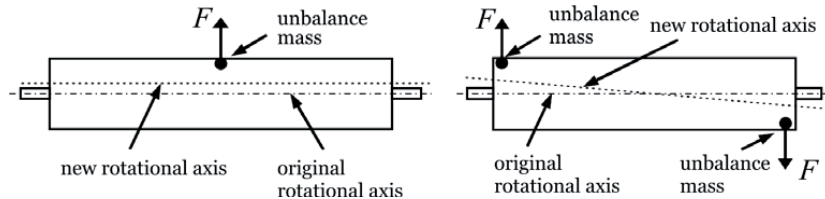


Figure 8 Centering method in balancing consist of parallel transition of the rotating axis and inclination of the rotating axis.

The centring requirement can be retrieved from the actual dynamic behavior measurement of the roll tube, and using a FE model of the roll the required centring values can be calculated. The advantage of these centring methods is that no internal devices or masses are required for center balancing. One disadvantage is that if balancing of the residual unbalance is needed, some other methods than centring needs to be applied.

Unbalance is widely studied research area. Lees and Friswell (1997) present a method characterizing the unbalance of a beam utilizing bearing vibration measurements. A comprehensive model of the rotor is required, but only the stiffness of the bearings is needed. Bearing supports are characterized as stiffness and mass matrices, the factors of which are determined from the measurements. The model is verified in several situations with 15 cases. Several parameters affecting the results are tested to find out the usable parameter range for reliable analysis and the sensitivity to errors in initial parameters.

Plaut and Wauer (1995) have studied coupling of bending and torsional vibrations in an unbalanced and damped rotating beam under gravitational

forces. The damping of the beam is assumed to be viscoelastic and a viscous damping model is used for external damping. Euler-Bernoulli beam model has been used for the equations of motion including time dependent rotating speed. In the analysis the rotating speed is constant. In the paper four resonance cases are studied: rotating frequency is about twice the frequency of the torsional vibrations, rotating frequency is close to the frequency of the torsional vibrations, or rotating speed is close to the sum or subtraction of torsional and bending vibration frequencies.

Wauer and Suherman (1998) are discussing the possibility to pass the resonance frequencies by changing the stiffness of the beam between two values using memory shape metals. In their model asymmetry and limited power of the motor are considered. Both the stationary and the transitional behavior of the beam and the motor are studied. First, they present a state-of-the-art study of rotating systems including non-ideal power sources, changing the system stiffness, or both. In the equations of motion, the beam is assumed to be viscoelastic and external damping as a function of rotating frequency. Wauer and Suherman solve two simplified steady state cases, and they continue of presenting the transient response, as well as minimizing the response by changing the stiffness of the beam when passing the resonance frequency.

Shaw and Shaw (1991) study qualitatively the dynamic response and the stability of an unbalanced beam with internal damping. Gravitational force, shear force and axial and bending inertia are neglected. First, they present periodic steady state responses and related stability issues. Next they present the response after losing the stability with small unbalance masses and speeds close to the first critical speed. In the end, they conclude the results and show e.g. bifurcation graphs as well as some limitations of the model.

2.2.3.4 Balancing of paper machine rolls

A conventional balancing machine supports and rotates a workpiece and indicates the amounts and angular locations of unbalance corrections required. The measurement plane is typically not the same as the correction plane. When the unbalance at the measuring plane has been measured, the correction mass can be calculated respectively using required information of the balancing machine and the rotor.

There are several balancing principles and types of balancing machines. For paper machine rolls majority of balancing machines use a hard bearing principle. The rotor runs on the machine at a speed that is less than critical speed, typically $0.3 \cdot \omega_{cr}$, hence the eigenmode vibration is not dominating.

With these specifications a permanent calibration of the machine can be carried out for all rotors that fulfill the machine specific requirements.

Balancing flexible rotors, such as paper machine rolls, measurement information of the dynamic behavior at central part of the roll is required. Typically, a run-out measurement using a capacitive, an eddy-current or an optical sensor is used. In balancing all other frequencies except the rotating frequency are filtered out from the measurement signal. Dynamic bending is calculated from the bending vectors measured at a low speed (static measurement) and at operating speed by vector subtraction. Only the change in the 1st harmonic should be used for balancing, especially if there is initial eccentricity on the rotor. An analytical or a finite element model can be used to evaluate the required correction mass (or any other corrective means).

A conventional balancing machine cannot measure the other dynamic effects such as the asymmetric principal moments of inertia i.e. bending stiffness variation, geometry changes and rotational error motion of the bearings, mainly because it is not designed to do so.

The dynamic deflection of a roll in operating conditions is mainly caused by unbalance, thermal bending and tension of the paper web or felt. Only unbalance is a phenomenon that is speed dependent. Thermal bending is caused by either inhomogeneous material structure at elevated temperature or an uneven thermal distribution.

By definition a rotor is deflected by unbalance forces only if the rotor is classified as a flexible rotor. In case of long paper machine rolls this is typically the case, therefore the balancing procedure should be carried out using balancing methods for flexible rotors. Many methods have been introduced for this requirement of *N*-plane balancing.

The most common method is center balancing which requires an addition of balancing mass in to the axial midpoint of the roll. The most common method is to apply the mass with some fixing mechanism. Many patented innovations have been introduced by all major paper machine manufacturers (U.S.Pat. 6,370,953 B1, U.S.Pat. 5,331,737, U.S.Pat. 5,397,291, EP 1 722 126 A2, U.S.Pat 5,096,734, U.S.Pat 5,170,547, DE 43 11 936 A1). Although these methods are invented to ensure the fixation of the balancing material, they provide some strength against dynamic shell deformations. The challenge in applying the mass straight on the inner surface of the roll shell is to avoid a point mass that cause central point force on to the roll shell. As found out in some unpublished measurements this point force may have an effect on the geometry of the cylinder and the result is more or less ovoid geometry ("egg-shaped" geometry).

Methods for balancing of flexible paper machine rolls have been developed. One of the first studies is carried out by Julkunen (1974, 1983). Järvelä (1989) has presented a method and procedure for three plane balancing to minimize the dynamic run-out in the middle of the roll shell. Järvelä reports a decrease in the measured value from 1.30 mm to 0.19 mm. Järvelä has also studied the half-critical vibration and the external dampening effect of felts on half-critical vibration. Keskiniva et al. (1995) and Keskiniva (1997) present a balancing method which is based on the measurement of the external radius of the roll i.e. a run-out profile. The whirling response is described by a N number of semidefinite eigenmodes in a body-fixed reference frame. In the optimization process n number of masses is determined. The n and N ($n < N$) are chosen based on the required balancing class. According to Keskiniva, the elimination of the dynamic bearing forces due to constraint equations is the most important criterion when compared with the mode-by-mode methods. Typical modal balancing methods lack that feature. Pirttiniemi (2004) studied the influence of the support stiffness on the balancing process and he proposes a new method to reduce the time to achieve the required state of balance.

More advanced methods include the centring of the roll tube in a manufacturing stage to minimize the dynamic bending of the roll as presented in Chapter 2.2.3.3.

Paper machine rolls are balanced with or without assembled bearings. During manufacturing and maintenance it might be convenient to carry out the balancing process with the roll supported by open rollers, shown in Figure 9. The diameter of the rollers is chosen so that the possible run-out of the rollers does not affect the measurements. On the other hand the manufacturing tolerances of the bearings are in the same scale as the requirements for an accurate process roll, therefore possible eccentricity and other errors would be revealed in the measurement with the original bearing assembly.

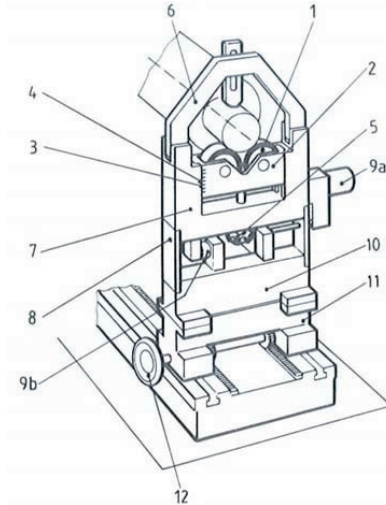


Figure 9 In typical balancing machine the rotor is supported by open rollers (1). The diameter ratio of the shaft and the rollers should be selected to avoid the influence of possible corrugation of rollers in the measurements (ISO 1925).

2.2.4 Bearing excitations

There are both sliding bearings and rolling element bearings used in a paper machine, the majority of being rolling bearings. Also, studied backing rolls are typically equipped with spherical rolling bearings, therefore the focus in this study is on rolling element bearings and their effect on the vibration excitation.

Bearings excite vibrations and transmit the vibrations from the paper machine and supports into the roll. Excitations from outside the roll system can be transmitted into the vibration of the roll, if the excitation hits the resonance frequency of the roll or the roll system. Naturally, these vibrations can't be reduced by improving the manufacturing accuracy of the roll.

The excitations from bearings can be divided as follows: the form errors of the elements of the bearings are typically wall thickness variations of the inner and the outer rings or roundness errors and diameter variations of the balls or rollers. There are always geometry errors to some extent. The excitation frequencies of bearing elements can be calculated as a function of rotating speed. The formulas to calculate the excitation frequencies for the most common case, where the outer ring is fixed and the inner ring is rotating, are presented for the inner ring, the outer ring, the ball and the cage. Because the inner ring never has an absolutely round profile, the rotating frequency f_i of the shaft is multiplied by the undulation component

z of the ring. According to Slocum (1992), when the rotating speed of the shaft is ω_i (*rpm*), the excitation frequency can be expressed

$$f_i = \frac{z \cdot \omega_i}{60}. \quad (4)$$

The frequency of the cage f_c can be calculated

$$f_c = \frac{\omega_c}{60} = \frac{1}{2} \cdot \frac{\omega_i}{60} \cdot \left(1 - \frac{D_b}{D_m} \cdot \cos \beta \right) \quad (5)$$

where β is the contact angle between the race and the rolling element, D_m is the average of the diameter of the inner and the outer rings and D_b is the diameter of the rolling element. The frequency f_b of the rolling element can be calculated

$$f_b = \frac{\omega_b}{60} = \frac{1}{2} \cdot \frac{\omega_i}{60} \cdot \left(\frac{D_m}{D_b \cdot \cos \beta} - 1 \right) \quad (6)$$

Also, the excitation frequency f_b of the rolling element can be expressed as (SKF 1994)

$$f_b = 2 \cdot \frac{D_b}{D_m} \cdot \frac{\omega_i}{60} \cdot \left(1 - \frac{D_b}{D_m} \right)^2 \cdot \cos^2 \beta \quad (7)$$

The base frequency of the inner ring f_{ir} and outer ring f_{or} can be expressed as

$$f_{ir} = |f_i - f_c| \quad (8)$$

and

$$f_{or} = f_c \cdot z, \quad (9)$$

when the outer ring is not rotating. These frequencies are often monitored by condition monitoring systems for fault recognition at the early stages of crack propagation.

The damping effect of roller bearings is considerably lower in comparison with typical sliding bearings. In theory, the damping of the rolling bearing can be increased by squeeze film damper although they are not commonly used in paper machine applications. One advantage of rolling element bearing is low friction (Slocum 1992).

2.2.5 Asymmetric axis of inertia

Manufacturing inaccuracies of a roll shell cause asymmetric principal axes of inertia at each cross-section of the roll. This asymmetry, also known as bending stiffness variation, causes the center-point of the roll to whirl at double speed relative to the rotor speed. This is one of the reasons for half-

critical vibrations. Methods for reducing bending stiffness variation have been introduced (Snellman 1983, U.S.Pat. 5,940,969). The typical amount of bending stiffness variation is in the range of 0...2 % depending on the type of the roll and manufacturing accuracy. At normal running speed of a backing roll the bending stiffness is not an issue, because these rolls are designed to operate below the half-critical speed.

In the literature the deviation of the axial symmetry of the rotor is often referred to as asymmetry and the deviation of axial symmetry of the bearing or support is referred to as anisotropy.

Kang *et al.* (1992) have studied a steady-state response of an asymmetric rotor with finite element method and with a Timoshenko beam model. With an element model deviator inertia and asymmetric stiffness can be taken into account. Element models for linear bearing and rigid asymmetric discs are presented. Kang *et al.* study four cases to outline the effects of the angle between the major axis of a shaft and a disc, bearing stiffness and damping and deviatoric inertia of the asymmetric shaft on steady-state bending vibrations.

Lee *et al.* (1992) have studied a rotor-bearing system with geometrical asymmetry in accelerating through critical resonance speeds. The method and the model are similar to models in article by Kang *et al.* (1992). Lee *et al.* illustrate the results with numerical examples for both steady-state and acceleration phase. The effect of acceleration on the response and the stability is analyzed, and the acceleration process is optimized to minimize the vibration amplitude at resonance frequency.

Kang *et al.* have studied (1994) the steady-state response of a rotor-bearing system, but instead of using a Timoshenko beam model, as Lee *et al.* (1993), the study is carried out with a Rayleigh-Euler model. The article describes the effect of asymmetry instead of unbalance. For simplicity, the equations of motion are presented in a rotating coordinate system. Kang *et al.* present a numerical example.

Joh and Lee (1996) have studied asymmetry and anisotropy of a rotor bearing system concentrating on experimental testing. Joh and Lee use the term asymmetry for the rotor deviating from axial symmetry, and the term anisotropy for the bearing deviating from axial symmetry. Joh and Lee present a short review on frequency functions, the analysis process and the measurement setup. Model is validated.

Wettergren and Olsson (1996) concentrate on asymmetry and anisotropy, and the effect of internal damping of the bearing and the rotor on the stability of the rotating beam. Wettergren and Olsson present the common forms of instability. Difference in the bending stiffness of an asymmetric beam results in two separate natural frequencies. Between these

frequencies the rotor is unstable. Due to internal damping the rotor might be unstable above the first critical speed.

Jei and Lee (1992) have studied the vibrations and stability of asymmetric rotor-bearing systems using modal analysis and a Rayleigh beam model. The paper concentrates on beams with constant and asymmetric geometry from which the precession speed and eigenmodes are calculated. In addition, Jei and Lee study the effect of boundary conditions and asymmetry on the stability and eigenmodes of the rotating beam.

Ganesan (1997) has analyzed the effect of asymmetric bearing clearance on nonlinear excitations. He concentrates on nonstationary state passing the resonance frequency, but steady state vibrations and their stability are also studied. The rotor is modeled using a simple Jeffcott model with asymmetric bearing clearance. After the theoretical part one numerical example with varying parameters is presented.

Wettergren (1997) has studied the effect of asymmetry on the eigenfrequencies of a rotating shaft made of composites. Asymmetry, classified as unbalance and different principal axes of inertia at a cross section, is assumed to be caused by the manufacturing process.

Rajalingham et al. (1993) have studied the stabilization effect of external damping on the dynamic behavior of an asymmetric beam under gravitation.

Modal analysis for studying asymmetric and non-isotropic rotor systems has been studied by Suh et al. (2005). Suh presents the analysis procedure for the asymmetric rotor systems with stationary and rotating parts with asymmetric and isotropic properties. Time-invariant linear differential equations are provided. A numerical example with a flexible rotor is given.

Kuosmanen (1992) has presented a method to optimize a contact nip pressure of two non-ideal asymmetric rotors by using an out-of-round geometry on one of the rotors. With non-circular turning the variation of the contact pressure caused by the asymmetry of the rotor is reduced to one third of the original. The method has been further developed in combination with a balancing procedure (U.S.Pat. 5,940,969).

2.2.6 Initial bending

Leinonen (1969, 1971) has studied the effect of initial bending on the stability of rotors. Leinonen compares the experimental test results with theory. Leinonen gives a short review to the theory of initial bending where the bending is represented as a Fourier series. After explaining the experimental setup he compares the measurement results with calculated results with eight different rotors.

Leinonen expands the theory in another article (Leinonen 1994) and introduces a non-linear model for materials in order to prevent infinite displacements at resonances. Leinonen verifies the model with experimental test results of four rotors.

2.2.7 Misalignment

Nikolajsen (1998) has presented the effects of alignment errors of a rotor with three or more bearings. A method to calculate bearing loads and eccentricity is introduced to define the dynamic behavior of the rotor. The model includes terms for a radial misplacement of bearings and flexible housings. In addition to response function, stiffness and damping of the bearings are determined. The method can be used to optimize the stability of the rotor using bearings. Nikolajsen presents one numerical solution.

Sekhar and Prabhu (1995) have studied the effect of misalignment of couplings on vibrations of a rotor-bearing system. They used beam elements in FE modelling with 8 degrees of freedom per node (displacement, inclination, bending moment and shear force in two directions). The authors take into account forces and moments caused by the misalignment of the coupling. They use one numerical example and show that the effect of misalignment of the coupling can be neglected.

2.2.8 Rotating shells

Rotating shells have been studied by Li et al (2005) and they present an extensive review of the subject including chapters in fundamental theory of rotating shells of revolution, free vibration of thin and thick cylindrical shells as well as critical speed and dynamic stability of thin rotating isotropic cylindrical shells. The research approach starts with governing equations of motion, and a generalized eigenvalue problem is summarized. In the following chapters the fundamental theory is reduced to that of thin and thick rotating cylindrical shells using a Galerkin-based method and Mindlin shell theory for free vibration analysis of these rotating shells.

The critical speed of thin rotating cylindrical shells and the dynamic stability of thin rotating cylindrical shells are investigated. Detailed studies for critical speeds and instability regions with respect to the rotating speed and axial loading are carried out.

The research is based on assumptions that are common in rotor dynamic analyses. One significant parameter is excluded, and it has a significant role in this thesis – “the shells possess constant thickness”.

Free vibrations of thin cylindrical shells have been studied widely and the theory is presented by e.g. Wah (1964) and Leinonen (1972). Further presentation of these vibration phenomena is excluded from this study.

2.2.9 Dynamics of paper machine rolls

There are numerous master theses on paper machine rolls that are supervised and initiated by paper machine and roll manufacturers.

A rotor dynamic program has been developed at Helsinki University of Technology and its development is initiated by von Hertzen and Jorkama (1994, 1995). The first model was developed to analyze bending vibrations of a roll with gyroscopic effect, asymmetry of the rotor, initial bending, stiff end plates, flexible supports and a varying rotating speed. Hamilton principle has been used in deriving the equations of motion. Paloheimo (2000) developed the equations further for more general rotor dynamic applications.

Toiva (2002) added some more imperfections to the analytical equations of motion of which the most important were internal and external damping as well as asymmetric journal damping and modal damping. The damping mechanism has to be chosen by the analyst. Toiva coded the rotor dynamics program and studied the effects of various imperfections on rotor vibrations. The structural imperfections accounted in the model are presented. The model accounts for gyroscopic effects, mass unbalance, rotor asymmetry, asymmetric journal stiffness and damping, modal damping, internal and external damping of the rotor. The possibility to reduce the number of degrees of freedom by modal reduction is used for numerical efficiency. The results are verified and validated by analytical and measured results. Toiva found some additional resonances, unstable zones and changes in the whirling behavior due to rotor asymmetry and asymmetric journal stiffness.

2.2.10 Other phenomena

Frame vibrations are often referred to vibrations from other parts of the paper machine, which are transmitted to the vibration of the roll through bearing assembly, driving shaft or other device that is in contact with the roll such as a doctor blade or a coating knife. The excitations caused by the rolls can be reduced by improving the dynamic behavior of the roll. In a paper machine there are also many other sources of vibration excitations, such as felts, wires and pumps. Also, the tension variation of paper web, felts and wires cause excitation to the vibration system and act as a transmission path of roll vibration to the connecting structures.

In paper machine calenders and in a press section a roll is in contact with another roll and pressed together forming a nip. This induces a vibration mechanism referred as barring. Barring has been studied extensively during the years by e.g. Tervonen (1984) and Toiva (2006). Tervonen (1997) has

extended his research on rolling contact of covered viscoelastic rolls acting with deforming i.e. viscoelastic/elastic paper web. These phenomena may not be present in a blade coating station, but a film coating process have some similarities to calendering process.

Jorkama (1998, 2001) has carried out research on a winding process and the rolls related. In winding there is a relatively soft roll of paper in contact with the supporting system.

Wong and Zu (1999) have studied bending and torsional vibration of a simply supported rotating Timoshenko beam analytically. There is mass unbalance on the rotor and a constant moment is applied. Results from the numerical simulations showed that beating phenomena may exist because the natural frequencies of the bending modes and torsional modes are close to each other.

Stephenson and Rouch (1993) have simulated the behavior of a rotor system using a FE model where the beam elements are replaced by axisymmetric solid elements to reduce the effect of expansion of a cross section caused by rotation. Stephenson and Rouch compare the results with other methods using four examples.

Lee, Shih and Kang (1992) have presented a method to analyze the steady-state response of unbalance of a linear rotor-bearing system. In addition to unbalance, axial force and moment together with moments of inertia, gyroscopic force and moment, and shear force are included in the model. The strength of the presented method is a minimal memory requirement and quite accurate results. The method is compared with a finite element model in one case study.

Nataraj (1993) presents results of a case study for coupling of bending and torsional vibrations of a rotating beam with constant speed. Nataraj uses the same method as Wong and Zu (1999). Nataraj shows that the frequency of torsional vibrations is twice the rotating speed frequency. In addition, Nataraj explains qualitatively some experimentally observed frequencies higher than the rotating frequency.

Melanson and Zu (1998) have presented vibration result from an analytical Timoshenko beam model with internal damping. Both viscous and hysteresis damping are considered. All six combinations of free, simply supported and fixed beam boundary conditions are analyzed for the stability with one numerical example.

2.3 Roll geometry

The geometry errors of a roll are usually indicated by run-out, roundness or straightness, which are measured by specific devices. Some quantities that can be measured in a typical roll shop are

- run-out (both static and dynamic run-out),
- roundness profile and roundness,
- axial diameter variation (axial diameter profile),
- cylindricity,
- conicity of the shell,
- straightness,
- error motion of rotational axis,
- thickness of a roll shell,
- unbalance, and
- surface roughness.

Cylindricity and straightness measurements are typically not carried out according to the strict definition. Unbalance and surface roughness are not geometrical quantities by definition. Systematic surface roughness variation, for example, can be interpreted as geometrical error, if a paper machine roll has been worn by e.g. barring vibration to have visible n -lobe geometry where the amplitude is very little; the surface has polished systematically and only little changes in surface roughness can be measured (Wirtz 2002, Toiva 2006).


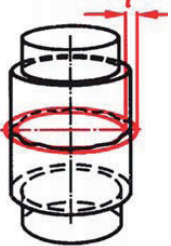

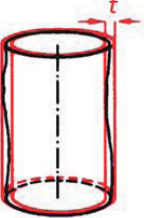
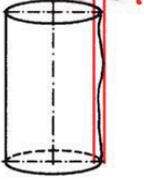
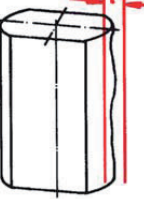
2.3.1 Geometry definitions

The standard ISO 1101 defines the form and location tolerance as well as some measurement methods. The notation in this chapter is based on the standard.

A tolerance zone of a feature is either area or space within or between two lines (circles) or areas (cylinders). For location tolerances, it is necessary to define a datum indicating the exact location of the tolerance zone. A datum is a theoretically exact, geometrical feature (an axis, a plane, a straight line, etc.); datum can be based on one or several datum features. The tolerated feature may be on any form, location or orientation within the tolerance zone, unless a more restrictive indication is given. The tolerance value t is

indicated in the same unit used for linear measurements. If not otherwise specified, the tolerance applies to the whole length or surface of the tolerated feature. The most important geometrical tolerances are presented in Table 1.

Table 1 Geometric tolerance definitions. (ISO 1101)

	<p><i>Roundness</i></p> <p>The tolerance zone in the measuring plane perpendicular to the axis by two concentric circles a distance t apart.</p>		<p><i>Radial run-out</i></p> <p>The tolerance zone is limited in the measuring plane to the axis by two concentric circles a distance t apart, the common center of which lies on the datum axis. The workpiece has to be rotated about the datum axis.</p>
	<p><i>Cylindricity</i></p> <p>The tolerance zone is limited by two coaxial cylinders a distance t apart.</p>		<p><i>Conicity</i></p> <p>The tolerance zone is limited in the measuring plane by two straight lines a distance t apart and parallel to the datum.</p>
	<p><i>Straightness</i></p> <p>The tolerance zone is limited in the measuring plane by two parallel straight lines distance t apart"</p>		<p><i>Parallelism</i></p> <p>The tolerance zone is limited in the measuring plane by two straight lines a distance t apart and parallel to the datum."</p>

For roundness the tolerance zone in a plane perpendicular to the axis of rotation is defined by two concentric circles a distance δ apart. The roundness is defined using concentric circles enclosing the circular profile and having the least radial separation.

$$\delta = \max(r(\theta)) - \min(r(\theta)) \quad (10)$$

The determination of roundness can be carried out with four methods, shown in Table 2 (Whitehouse 1994). The methods produce different values for roundness. For computerized application either regression circle i.e. least squares circle (LSC) or minimum zone circles (MZC) are preferred. These bounding references are studied by formulating their definitions

mathematically as optimization problems (Chetwynd and Phillipson 1980). The algorithms are presented for the determination of these references. The utilization of least squares method in roundness evaluation is studied by Tan et al (1992) and Kim and Kim (1996), for instance. They present a mathematical method for estimating the center point that gives the minimum value for roundness.

Table 2 Definition of the center point of the reference circle to calculate roundness. (ISO 1101)

	<p>Regression circle (Gaussian straight circle)</p> <p>Circle laid into the measured circular profile such that the sum of the squares of all profile deviations is a minimum. The center is that of the least squares circle. (LSC=Least Square Circle)</p>
	<p>Circular zone with minimum radial separation MZC</p> <p>Concentric circles enclosing the circular profile and having the least radial separation. (MZC=Minimum Zone Circles)</p>
	<p>Minimum circumscribed circle MCC</p> <p>Smallest possible circle which can be fitted around the circular profile.</p>
	<p>Maximum inscribed circle MIC</p> <p>Largest possible circle which can be fitted within the circular profile.</p>

2.3.2 Workpiece geometry in machining

The geometry errors that are typical to a ground or a turned workpiece are presented, because some of those may contribute also to the dynamic behavior of the roll.

The geometry of the workpiece is a sum of different characteristics and process disturbances. Some aspects on the geometry of a workpiece in

machining are presented by Väänänen (1993). Many of the factors are human based, therefore the result depends on the professional ability of the employee. The most significant factors are:

- guideway error,
- alignment of the roll,
- rotational error motion of the workpiece during machining,
- center point motion caused by bending stiffness variation and natural bending by gravity,
- vibrations of the machine tool or the workpiece, and
- uneven thermal distribution during machining.

2.3.2.1 Guideway error

Guideway error motion includes three linear and three angular error motion components. Only error motions affecting the straightness of the tool path linear motion are usually observed. Error motion in the direction of the tool path normals, especially towards the workpiece, is copied into the geometry error of the workpiece. (Juhanko and Väänänen 1999)

Straightness of the guideways is often out of the required tolerance for the paper machine rolls. According to the information from roll shops, mechanical accuracy of a lathe or a grinding machine has been around 0.01...0.05 mm.

Modern machine tools for paper industry are equipped with an error compensating system for guideway errors. Typically, these systems are based on axial diameter variation measurements of machined workpiece. The measurement is used in a control system which operates the cutting tool by the either linear or angular motion of the carriage to generate a straight tool path.

The diameter profile is also affected by errors in roundness profile of the roll. If the roundness profile is oval at both ends, and the ovality is in different angle relative to each other, the axial diameter profile is different depending on the rotational angle which the measurement takes place. Therefore, the control system should take the roundness error profile and especially diameter variation components into account when calculating the control curve. This phenomenon can be seen in Figure 10.

2.3.2.2 Roll and machine tool alignment

The alignment of the roll relative to the cutting tool path affects the axial diameter profile of the machined roll. If the rotational axis of the roll is not

aligned with the guideways or motion of the tool path, the roll will have conical geometry after machining.

The alignment of the roll requires either stiff and accurately adjustable supports or a control system by which the tool path is aligned to be parallel with the rotational axis of the roll. (Juhanko and Väänänen 1999)

2.3.2.3 Rotational accuracy in machining

The rotational accuracy of the bearing assembly during the machining process affects the geometry of the roll, because the rotational error motion component in the direction of the cutting tool is copied into the geometry of the roll. When the roll is moving away from the tool, the radius of the workpiece will be larger than the nominal radius and *vice versa*. If there is harmonic systematic motion caused by e.g. bending stiffness variation, the path of rotational error motion is two circles during one revolution of the roll.

The effect of bearing assembly has been tested in a simple experiment by Juhanko and Väänänen (1999). A roll with straight shafts was equipped with spherical roller bearings which were assembled on the shaft by conical adapter sleeves. First, the roll was machined, and the geometry of the roll was measured (Figure 10 a). Geometry of the rolling path of the inner ring of the bearing is influenced by the geometry of the shaft, the thickness variation of the adapter sleeve and the inner ring of the bearing and diameter variation of the rolling elements.

The effect of the adapter sleeve on the geometry of the roll was tested by rotating only the adapter sleeve by close to 90° relative to the shaft and inner ring of the bearing, which were kept in the same angular position relative to each other. The roll was machined after the rotation of the adapter sleeve and the geometry of the roll was measured, as shown in Figure 10 b.

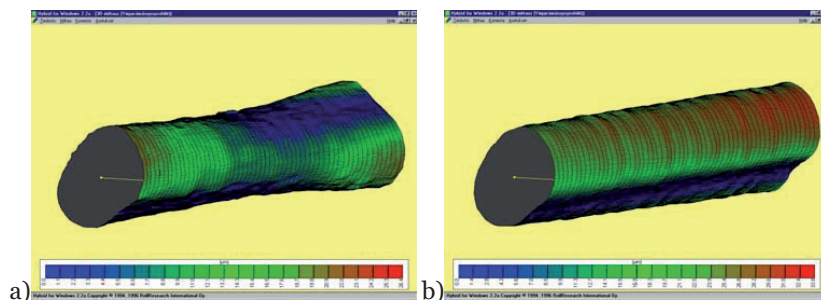


Figure 10 Geometry of a roll before a) and after b) the rotation of the adapter sleeve while the inner ring was kept in the same angular position relative to the shaft. The roll was machined before each measurement. (Juhanko & Väänänen 1999)

Before the test the amount of ovality at the ends of the roll was about the same, but the direction of the main axis had a phase difference close to 90° . After rotating the adapter sleeve, the ovality error was in the same range, but there was no phase difference between the roll ends. In this case, the adapter sleeve was a probable cause for the ovality.

2.3.2.4 Bending stiffness variation and natural bending

Bending stiffness variation is caused by differences between principal moments of inertia I_x and I_y of a cross-section. Although the geometry is intended to be circular, due to manufacturing inaccuracy the cross section has at least some roundness profile errors, which cause the bending stiffness variation. Also, material inhomogeneity and structural discontinuities, such as welding seams, might cause bending stiffness variation.

Bending stiffness variation causes rotational error motion of the rotor. During one full revolution, a point on the center axis draws two full circles and the frequency is two times higher than the rotating speed of the rotor. The sinusoidal error motion towards the cutting tool is copied onto the roll and causes oval geometry to the machined workpiece.

The amount of ovality can be estimated by the amount of natural bending caused by gravity force g and the amount of bending stiffness variation. Typically, a roll with natural bending of 3 mm (supercalender roll) and the difference in the principal moments of inertia of approximately 1 % has ovality of about $30\ \mu\text{m}$ in the center cross-section. In case of backing rolls the bending stiffness variation can usually be neglected, because of the quite high section modulus which derives from the large diameter to length ratio (Kuosmanen 1992).

2.3.2.5 Vibrations of the workpiece and tool

Machining vibrations can be divided into external and internal forced vibration and self-excited or regenerated vibrations. In Table 3 some factors affecting the cutting process are presented (Väänänen 1993). External forced vibrations are not caused by the cutting machine, the workpiece or the machining process, but they still can cause serious vibration between the cutting tool and the workpiece. Internal forced vibrations are caused by the machining process. Self-excited vibrations are more harmful than forced excitations, because the vibration amplitude increases significantly at certain cutting parameter values.

Table 3 Vibrations in machining (Väänänen 1993).

Forced vibrations		Self-excited vibrations
External	Internal	
- transferred vibrations	- intermittent chip breaking	1. Primary phenomena
- imbalance of rotating components	- discontinuous cutting surface	- reduction of cutting forces with higher cutting rate
- gear vibrations	- stick-slip on rake face	- friction of front rake and workpiece
- geometry errors of bearing components, bearing area variation	- material homogeneity e.g. hardness variation	- modal coupling of several degrees of freedom
- bending stiffness variation	- built-up edge	2. Regenerative phenomena
- asymmetric stiffness of supports		- the effect of previously machined surface
		- partial or full loss of contact of the tool from the workpiece (multiregenerative phenomenon)

In general, vibrations deteriorate the surface quality and dimensional accuracy, increase the tool wear and cause damage to the machine.

2.3.2.6 Thermal bending in machining

Thermal expansion of materials causes geometry errors by either uneven thermal distribution or inhomogenous material in the roll. The thermal expansion coefficient of steel is about $10 \mu\text{m}\cdot\text{C}^{-1}\text{m}^{-1}$ thus a gradual one-sided temperature distribution causes bending that quite easily reaches a millimeter scale. If the roll is machined either by turning or grinding in a bent state, roll deflects in a steady thermal state, seen as initial bending.

Linear graded thermal distribution in a cross-section causes a moment M_T (Niskanen 1970)

$$M_T = -\frac{\alpha EI \Delta T}{h} \quad (11)$$

where α is the thermal expansion coefficient, EI is flexural stiffness, ΔT is the temperature difference and h is the diameter. The deflection v is

$$v = \frac{\alpha \cdot \Delta T \cdot L^2}{6h} \cdot \left[\frac{2x}{L} - \frac{3x^2}{L^2} + \frac{x^3}{L^3} + \frac{2(L-x)}{L} - \frac{3(L-x)^2}{L^2} + \frac{(L-x)^3}{L^3} \right] \quad (12)$$

where L is the length of the roll and x is the lengthwise observation point. A steel roll with length of 10 m and diameter of 1 m, deflects 0.12 mm due to gradual one-sided 1°C temperature deviation.

This harmful effect is usually minimized at roll shops by rotating the roll long enough before the machining process starts. One way to generate a gradual one-sided thermal distribution is letting either a cold roll heat up or a hot roll to cool down without constantly rotating. Rotation is required to minimize the effect of surroundings (e.g. thermal reflectors as a floor) and

gradual temperature change of room air as a function of height which is approximately $0.5^{\circ}\text{C}/\text{m}$.

There have been claims that viscoelastic deformation of roll material causes some initial bending of rolls. The rotation of rolls has been carried out for an elastic recovery of the roll. At least with steel rolls this viscoelastic behavior is practically impossible at normal operating temperatures and stress levels.

2.3.3 Roll geometry measurement methods and devices

Diameter measuring devices cannot measure the true roundness profile, yet the measuring method suffers from a harmonic filtration, as shown in Figure 11, where a Relax triangle is illustrated. Using this type of diameter measuring device one cannot measure odd lobe shapes like triangular, 5-lobe, 7-lobe etc. geometries, because the method is unable to separate the geometry error of the cross-section from the error motion of the rotating axis (Whitehouse 1994). If the rotor has no rotational error, the roundness measurement could be carried out with a single run-out measurement sensor.

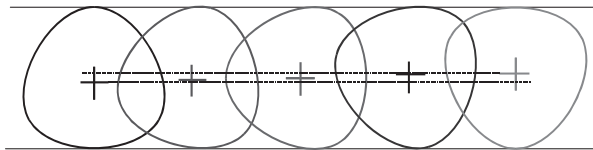


Figure 11 Diameter measurement can't be used to measure odd lobe geometry errors, because the method suffers from harmonic filtration, i.e., the method can not separate the odd lobe geometry error from the error motion of the rotating axis.

Since the sixties several methods and algorithms are presented to measure the roundness profile of a rotating workpiece with an error motion of the rotating axis. The most common methods are variants of multi point methods (Ozono 1974), where the roundness is calculated from weighted sensor signals in a given configuration around the rotor. Some roundness measuring methods and devices are patented, for instance (Gebel et al. 1976, Bellwood 1990), but in this research field there are numerous scientific articles on different roundness measuring methods and algorithms by e.g. Chetwynd and Siddall (1976), Moore (1989), Gao et al. (1996, 1997a, 1997b), Muralikrishnan (2004), Zhao et al. (2006). Some of these methods have previously been evaluated by the research group.

2.3.3.1 Hybrid-method measuring device

Hybrid-method (Väänänen 1993, Kuosmanen and Väänänen 1996) is a combination of a multipoint method presented by Ozono (1974) and a 2-point method for a precise diameter measurement. The hybrid measuring system can be realized with either a floating measuring frame with supporting rollers, or with a fixed measuring frame, as shown in Figure 12. The fixed frame utilizes four measurement sensors to measure both the roundness profile and error motion of the rotational axis. The floating frame follows the rotational axis by taking support from the roll surface. With this measuring arrangement the information of the error motion of the rotational axis is lost.

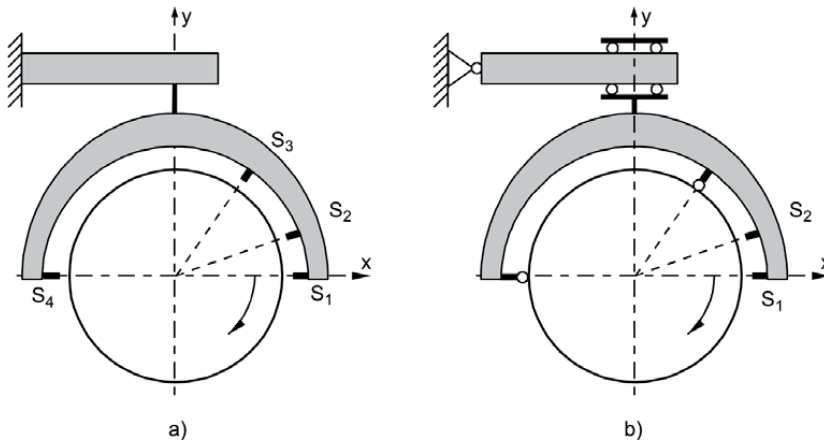


Figure 12 Utilization of the four point method. The measuring frame can be a) fixed or b) floating depending on a number of measuring elements S_i . (Väänänen 1993).

The method is used in roll grinding machines and mostly with the fixed frame arrangement. Most common sensors used in this device are length gauges with a measuring principle of photoelectrically scanning an incremental scale. The contacting measuring method works with most roll surfaces when the rotating speed is approximately the same as in grinding, i.e. 1...10 rpm.

Measuring frame is manufactured using laminated carbon fiber and epoxy resin. Some of the advantages with carbon fiber are good stiffness to weight ratio for easy handling and a 20 times lower thermal expansion coefficient than aluminum. The latter plays an important role in a typical roll shop without a temperature controlled environment.

This setup can be used to measure roundness, cylindricity and rotational error motion in addition to traditional workshop measurements. The cylindricity can be measured either as a continuous spiral measurement or stepwise one cross-section after another.

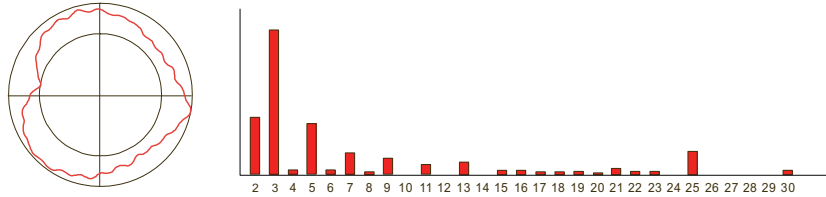


Figure 13 Roundness profile and its amplitude terms of Fourier series measured from a reference disc (Väänänen 1993).

The roundness can be expressed with Fourier series amplitude and phase terms. In Figure 13, the first 30 amplitude (p-p) terms of a heart shaped profile are shown. This illustrates the geometry and its undulation per revolution content very informatively, because the second term corresponds to ovality, third term to triangularity, fourth to squareness, etc. The roundness profile can be reconstructed using the amplitude and phase terms. An error motion of the rotational axis is calculated from the roundness profile data and run-out data (Väänänen 1993).

More detailed presentation of the method is in the Chapter 3.1.3 Roundness on page 64.

2.3.4 Thermal effects on roll geometry

W. Wirtz (2002) has made a short review on different aspects on designing a modern heated roll minimizing the unwanted thermal effects.

Thermo rolls i.e. heated rolls are manufactured mostly from chilled cast iron that has good wear resistance. Yet, chilled cast iron has reached its limits in most recent applications. Practically, the use of material is limited by heating capacity of close to 150 kWm^{-1} ; beyond that more advanced materials, such as forged steel, have to be used. The thermal behavior of the roll material has a direct influence on the runnability of a paper machine and paper quality.

Wirtz mentions half-critical speed as a consequence of material homogeneity. For example, chilled cast iron consist of layers of materials (white iron, gray iron and an intermediate layer in between) which have different material properties, such as tensile strength, the modulus of elasticity and the coefficient of thermal expansion. Varying layer thickness with different material properties causes deformations in operating conditions.

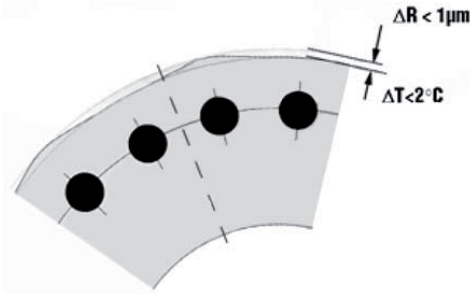


Figure 14 Heating of the peripherally bored roll leads to polygon effect under operating load (Wirtz 2002).

Peripherally bored thermo rolls are deforming, because of the heat load of the roll and the geometry is affected by the number of holes, as shown in Figure 14. While the reported temperature difference is less than 2°C, the radial deviation in geometry is less than 1 μm. It is shown that this geometry error is a causing barring vibration in calenders. Wirtz also states that the dynamic deflection of chilled cast thermo rolls is increasing when the roll is heated. In a case study, the roll temperature was heated up to 150°C, and a run-out deviation of 160 μm was measured. The deflection is reported to be a function of temperature, as shown in Figure 15. Wirtz reports that not only a displacement of the roll center occurred, but there is also a deviation from the ideal geometry.

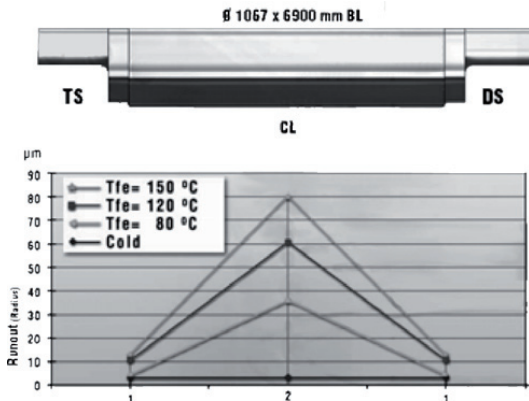


Figure 15 Run-out behavior of a heated chilled cast iron roll as a function of operating temperature. (Wirtz 2002)

The geometry deviation observed in the edge areas of the roll, as shown in Figure 16, is caused by heating flux differences along the length of the roll. Wirtz states that the difference at the ends of the roll is caused by the journal connections.

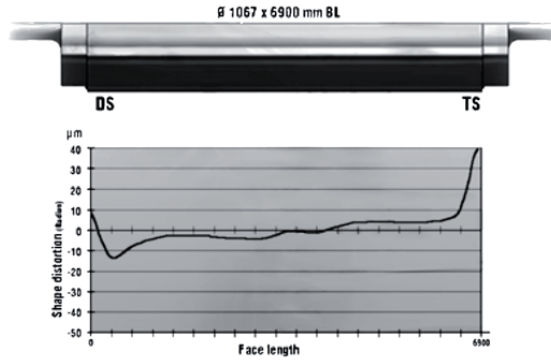


Figure 16 Radial deformation of a thermo roll at operating conditions.
(Wirtz 2002)

Widmaier et al. (2010) have analyzed the thermal effects of chilled cast iron thermo rolls and their tendency to deflect under thermal load. Widmaier created a FE model with two iron layers. The model is based on the results of an ultrasonic wall thickness measurement of a thermo roll. The thickness variation is interpreted as iron layer thickness variation. FE model is used to analyze the deflection at operating temperature. The results are in accordance with the studies of Wirtz.

3 Research methods and equipment

In this chapter the most important methods, devices and algorithms to measure and analyze all data used in this thesis are presented.

3.1 Measurement and analysis methods

3.1.1 Fourier analysis

A measuring device e.g. a displacement sensor gives a signal in a time domain. A physical signal has a value with a real number continuously over time. When the signal is sampled with digital computer systems, separate instants form a finite sample and the signal is discrete.

The signal can also be expressed in a frequency domain which is used to describe the content of a signal with respect to a frequency rather than time. A given signal can be converted between time and frequency domains using mathematical means. Commonly used tools for these conversions are Fourier transform to convert the signal from the time domain to the frequency domain, while inverse Fourier transform converts the frequency domain signal back to the time domain.

In the analysis of measurement signals, it is often relevant to decompose a measurement signal into its harmonic components. A measurement signal can be composed using a sum of an infinite set of cosine functions, for instance. This is based on the studies of J. Fourier, who showed that general functions may be represented by sums of simpler trigonometric functions. In engineering, this operation is called Fourier analysis, and several mathematical methods of performing the analysis exist.

The Fourier analysis for periodic functions can be carried out by using Fourier series. Any periodic function $f(x)$ with a period 2π can be expressed

$$f(x) = a_0 + \sum_{n=1}^{\infty} \left(a_n \cos \frac{n\pi}{L} + b_n \sin \frac{n\pi}{L} x \right) \quad (13)$$

where the a_0 , a_n and b_n are derived from Euler equations

$$a_0 = \frac{1}{2L} \int_{-L}^L f(x) dx, \quad (14)$$

$$a_n = \frac{1}{L} \int_{-L}^L f(x) \cos \frac{n\pi x}{L} dx \text{ and} \quad (15)$$

$$b_n = \frac{1}{L} \int_{-L}^L f(x) \sin \frac{n\pi x}{L} dx, \quad (16)$$

where $n=1, 2, \dots, N$.

In practice, the function has finite duration and therefore a limited number of Fourier series coefficients.

For calculations Fourier series can also be expressed as a sum of complex exponential functions

$$f(x) = \sum_{n=-\infty}^{\infty} c_n e^{inx} \quad (17)$$

for all integers n where the Fourier coefficients c_n are given by

$$c_n = \frac{1}{2\pi} \int_0^{2\pi} f(x) e^{-inx} dx \quad (18)$$

where $n=0, \pm 1, \pm 2, \dots$

Fourier analysis and Fourier series have been commonly used for assessing roundness.

3.1.2 Synchronous averaging

A technique called time domain averaging (Braun 1975) or time synchronous averaging TSA (McFadden 1987) is a powerful and well-adopted signal processing technique which enable periodic signals to be extracted from noisy signals. It is used in vibration analysis of rotating components such as gearboxes to separate a single harmonic component from the vibration of the complete system.

The technique is based on a trigger signal which is phase locked with an angular position of a rotating component. In a complex system with several rotating shafts, a triggering signal in every shaft is a powerful tool for separating the cause for vibration. Typically, a tachometer is used for one pulse per revolution signal. An optical encoder with several pulses per revolution is used for better angular resolution.

The averaging process is presented assuming a signal $x(t)$ to consist of the sum of a periodic signal $f(t)$ and additive noise $n(t)$

$$x(t) = f(t) + n(t). \quad (19)$$

When summing up subsequent x the repetitive part of the signal f will add coherently, and the noise uncoherently. After N summation

$$x(t_i) = Nf(t_i) + \sqrt{N}n(t_i) \quad (20)$$

and the signal to noise ratio is enhanced by a factor of \sqrt{N} . Braun also states that an appropriate sampling rate together with pre-filtering to reject the frequencies above the Nyquist frequency can drastically reduce the required number of averagings N to reduce the broadband noise to a certain level.

The method works also for attenuating narrow band noise and harmonic signals. To estimate the necessary N in order to achieve a specific attenuation of interfering signal Braun derived equation

$$N > \frac{\alpha}{\pi^2 F} \quad 21$$

where α denotes the required attenuation and F is defined as a non-dimensional variable

$$F = \frac{f}{f_i} - K, \quad K=0, 1, 2, 3. \quad 22$$

where f_i is called the synchronizing or the triggering frequency. For attenuation of $\alpha = 100$ (40 dB) and $F = 0.01$, number of averagings $N > 1000$ is required.

Hochmann and Sadok (2004) have analyzed the synchronous averaging in more detail and they agree that for non-coherent components the amount of attenuation is related to the reciprocal of \sqrt{N} , but is not representative for the non-synchronous terms. The signal $f(t)$ consist of synchronous coherent term $S(t)$, non-synchronous coherent term $N(t)$ and non-synchronous and non-coherent term $T(t)$.

$$f(t) = S(t) + N(t) + R(t) \quad 23$$

The attenuation factor α can be expressed as

$$\alpha = \frac{C \sin(\pi\alpha N)}{N \sin(\pi\alpha)} \quad 24$$

for all coherent terms; C denotes the Fourier amplitude term of the coherent component.

Hochmann observed that large number of averages in effect creates a bandpass filter that is so sharp that unless acquired data is gathered

perfectly with respect to the constant speed or tachometer, the filtering process is itself causing variance by attenuating signals that are close to the base period. In case of using an external clock for triggering and timing the perfect data acquisition requirement is met.

Some more advanced algorithms have also been introduced (Bonnardot 2005, Combet and Gelman 2007) for cases where it is impossible to attach a speed sensor to the rotating shaft. They introduce two methods; a spline angular sampling and a tacho pulse recovery for an angular sampling of the rotor angular position. They propose a methodology for the estimation of the TSA without a speed sensor, which requires only an *a priori* estimation of the shaft speed and e.g. the number of teeth of the meshing gears. The methodology forms an automated scheme which can be useful for condition monitoring applications where speed measurement cannot be used. Obviously, one drawback of the method is that the angular reference is lost for the localization of a single fault. Mark et al. (2010) suggest a new frequency-domain damage detection algorithm by analyzing the harmonic content of the measured signals under a wide range of operating conditions i.e. multiple tooth contact, for instance.

Halim et al. (2008) propose a different approach to the same application, called time domain averaging across all scales, which combines time synchronous average and wavelet transformation to extract the periodic waveforms at different scales from noisy signals. The strength of the developed technique lies in the way it preserves the frequency domain information while performing the average, and captures the deterministic part of the periodic signal for one period removing the stochastic part efficiently.

Shao et al. (2007) present another variant of the time domain synchronous averaging analysis method for cases where the speed of a rotary machine varies with the fluctuation of voltage and load. Standard period based synchronous averaging suffers from fluctuation of rotating speed because of the phase errors accumulation from the errors of round-off and frequency estimation. The method is based on instant speed i.e. frequency per rotation using Fast Fourier Transform-Fourier Series. First, the FFT is used to analyze the input signal, and then another Fourier Transform is applied to increase the frequency resolution. Shao et al. conclude that the modified algorithm has good results even if the signals include the frequency fluctuation and random noise.

McFadden (2000) presents an application of synchronous averaging on rolling element bearings taking into account the different components of a rolling element bearing.

3.1.3 Roundness

In the literature one of the first numerical methods for assessing roundness is presented by Ozono (1974). The roundness profile is determined by measuring run-out $s_1(\theta)$, $s_2(\theta)$ and $s_3(\theta)$ from three different angles denoted γ_1 , γ_2 and γ_3 . In practice, the first angle is set as $\gamma_1=0$.

The sampling function $m(k)$ is denoted as

$$m(k) = s_1(\theta) + w_2 s_2(\theta) + w_3 s_3(\theta) \quad (25)$$

where $k = 0, 1, 2, \dots, N-1$. The weighting factors w_2 and w_3 are got from conditions

$$\sin \gamma_1 + w_2 \sin \gamma_2 + w_3 \sin \gamma_3 = 0 \text{ and} \quad (26)$$

$$\cos \gamma_1 + w_2 \cos \gamma_2 + w_3 \cos \gamma_3 = 0. \quad (27)$$

If these conditions are met, the center point motion is eliminated and signals S_2 and S_3 will measure the center point motion and signal S_1 measures run-out. Kato *et al.* (1990) have developed a numerical method to optimize the measuring angles:

$$\begin{aligned} \gamma_1 &= 0^\circ, \\ \gamma_2 &= 38^\circ \text{ and} \\ \gamma_3 &= 67^\circ. \end{aligned} \quad (28)$$

The selection and the sensitivity of chosen angles are presented also by Väänänen (1993). As a function of observation angles the weighting factors w_2 and w_3 can be expressed

$$w_2 = \frac{-\sin \gamma_3}{\sin(\gamma_3 - \gamma_2)} \text{ and} \quad (29)$$

$$w_3 = \frac{\sin \gamma_2}{\sin(\gamma_3 - \gamma_2)}. \quad (30)$$

The roundness profile is typically presented in polar coordinates, but for analytic purposes a more relevant presentation is the use of Fourier series terms as described earlier. For roundness characterization only terms with $n \geq 2$ are significant, because the term $n = 0$ denotes the offset of the signal and the term $n = 1$ stands for the eccentricity of the roundness profile. Therefore the results in this research include only the terms $n \geq 2$.

The roundness $r(\theta)$ profile can then be expressed as

$$\begin{aligned}
r(\theta) &= \sum_{n=2}^N A_n \cos(n\theta) + B_n \sin(n\theta) \\
&= \sum_{n=2}^N C_n \cos(n\theta - \varphi_n)
\end{aligned} \tag{31}$$

where amplitude term C_n and phase term φ_n are

$$C_n = \sqrt{A_n^2 + B_n^2} \text{ and} \tag{32}$$

$$\varphi_n = \tan^{-1}\left(\frac{B_n}{A_n}\right). \tag{33}$$

From an observation angle ϕ_i the run-out s_i consists from the roundness profile component $r(\theta)$ and the error motion of the rotational axis, given in Cartesian coordinates $y(\theta)$ and $x(\theta)$.

$$s_i(\theta) = r(\theta + \phi_i) + y(\theta) \sin \phi_i + x(\theta) \cos \phi_i \tag{34}$$

where $i=1, 2, 3, \dots$

Väänänen has analyzed that the sensitivity of the algorithm is at the best with no major harmonic filtration when the number of lobes per revolution is below 35.

The roundness algorithm used in this study has been derived from a 2-point diameter measurement method and the 3-point Ozono-method. A fourth sensor is introduced at the opposite to the sensor S_1 i.e. the fourth sensor angle $\gamma_4=180^\circ$. The measurement results from the opposing sensors give reliable results on measuring the even lobe geometry components i.e. oval, 4-lobe etc. geometries where $N=2, 4, 6, \dots$. With this setup, the harmonic filtration of even lobes is minimized. For roundness calculation, the least squares method is used. For convenience, the amplitudes of the harmonic components of a roundness profiles are expressed as peak-to-peak values for easier comparison with the roundness values, which is defined by two concentric circles enclosing the profile with minimum radial distance t apart that is a peak-to-peak amplitude of the profile.

There are several other variants of a multi-point method in the literature. Gao et al. (1996) present a method where one displacement sensor is replaced by an angle sensor at one of the remaining sensors. Gao concludes that the presented method can separate the roundness profile and the spindle error completely, and it is well suited for measuring profiles that include high frequency components. Gao develops the method further (1997) using an error separation method with the information from one displacement sensor and one angle sensor.

3.2 Measurement data acquisition

The measurement system is a device based on a PC. The basics of a computer based data acquisition can be studied from numerous references such as Doebelin (1990). General data acquisition principles e.g. the sampling frequency, the Nyquist theorem and aliasing are not presented.

Measurement device uses five principal sensors i.e. four displacement sensors to measure the run-out from four different directions, and a rotational encoder to position each measurement on the coordinate system.

The data acquisition hardware has changed during the years, but the signal analysis has followed the same principles during the development.

3.2.1 Rotary pulse encoder

The angular position is measured using a rotary pulse encoder (e.g. Heidenhain ROD 420) of either 256 or 1024 pulses per revolution depending on a measurement setup. The pulse encoder produces six square wave signals: A , B and I and their inverse functions \bar{A} , \bar{B} and \bar{I} .

Signals A and B have 90° phase shift that is used for observing the angular direction. The \bar{A} , \bar{B} and \bar{I} can be used to minimize the effects of noise i.e. the output changes only when both the signal and its negation change. The index is used to fix a zero angle of the roll. Typically this zero angle was positioned so that there is a permanent marking on the roll that would be used for indexing later operations.

The main function for the rotary pulse encoder was being used as an external clock. One measurement point from each sensor was digitized at each tick of the external clock. The advantage of this principle is that each measurement with the same rotational angle index is measured actually from the same point. This might have importance when using triangular laser beam displacement sensors, because of the laser speckle effect described in Chapter 3.6.4.

3.2.2 Displacement sensor

The amplified analog displacement signals from the transducer are passed through a dedicated amplifier which is set to minimum signal processing. It was chosen that the low-pass filtering is carried out in a separate hardware component to be aware of the signal behavior in the filtering process. The Matsushita Nais LM300/R30 uses visible class 2 red laser with a response speed of 5 kHz when two sensors are attached to the unit (20 kHz with one sensor head). The internal data acquisition frequency of the sensor is 50 kHz. A measuring distance of 30 ± 3 mm gives a small safety range when

attaching, adjusting and using the measuring system. The resolution of the device is $0.2\ \mu\text{m}$. The announced accuracy using matte white ceramic target has no value for this study, because the typical surface for backing rolls is light absorbing black rubber.

A Nais LM300 2-channel triangular beam diffusive reflective type laser displacement sensor was selected as the best all-round performer. The selection process is described in the Chapter 3.6.3 and experimental uncertainty evaluation of the sensor is presented in the Chapter 3.7.



Figure 17 The 2-channel laser displacement sensor unit Matsushita Nais LM300/R30 uses diffusive reflective triangular laser beam technology.

3.2.3 Low pass filtering board

A programmable 8-channel low pass filtering board (Alligator AAF-3) was used for anti-aliasing. The board can be configured using 2-channel separate modules for filtering and gain. Linear phase filtering modules were chosen to make it easy to correct the signal amplitude and phase in the pass band, if the distortion in filtering need to be taken into account. Gain modules were required for differential measurement for each measurement channel.

The filter board was programmed to change its cut-off frequency as a function of the rotating frequency to maintain a constant ratio between the rotating frequency and the cut-off frequency. Therefore, the form of the signal passing through the filtering board is not changing as the speed is increasing.

There would have been other possibilities to carry out the same task. The data acquisition frequency and cut-off frequency could have been chosen to be high enough not to distort the low frequency signal components at the

required operating frequency range. Then digital filtering could have been applied for further processing of the signal.

3.2.4 Data acquisition board

Requirements for the data-acquisition system can be met with many of the current data acquisition boards. A few models have been used in this study the first one being a Data Translation DT 3831, which was later displaced by Microstar DAP board for some onboard digital signal processing.

In a basic measuring setup the data acquisition was carried out by using an external clock to maintain a constant signal length for each revolution.

In a typical measurement to study the low frequency components from dynamic geometry changes, the data acquisition using 256 samples per revolution is enough. To present a sine wave signal about ten points are required to get the form accurately enough. The studied components in this research are mainly second and third harmonics of the base rotating frequency so there is more than enough points to analyze the geometry. Other vibration phenomena might require higher data sampling frequency.

Differential measurement was used instead of single ended measurement for greater accuracy.

3.2.5 Measurement signal processing

The signals from laser sensors are passed through the amplifier with a minimum internal signal processing. The reason is that the main unit uses a moving average algorithm for filtering the signal and therefore a fixed delay in the signal should be taken into account. The signals are low-pass filtered in the anti-alias filtering board with adjustable cut-off frequency. This is used to keep the signal component content amplitude and phase independent of the rotating frequency of the studied rotor.

The triggering signal from the rotary pulse encoder is used to fix the phase of the measurement signal to a known angular position of the shaft. The clock signal of the pulse encoder is used as an external clock for sampling to ensure that each measurement at a certain rotational index is taken from the same angular position of the rotor even if the speed is fluctuating. Each of the four laser sensor signal is cut into signals with one full revolution and these samples are averaged.

The roundness calculation and processing conform to the methodology presented in Chapter 3.1.3 Roundness on page 64.

3.3 Experimental uncertainty of measurement

In experimental studies, the uncertainty of measurement is to be calculated according to the Guide to the expression of uncertainty in measurement GUM. The principle is originally presented in GUM:1995 and its revised version ISO/IEC 98-3:2008. The Joint Committee for Guidance in Metrology later published a revised version (JCGM 100:2008) with minor corrections. An alternative to the evaluation of uncertainty in measurement is using a Monte Carlo method described in (JCGM 101:2008). European co-operation for Accreditation has also published guides for the expression of the uncertainty of measurement in calibration (EA-4/02) and quantitative testing (EA-4/16). The following presentation is based on these references mostly. In the literature, there are numerous papers for application and extensions of these documents and guidelines. Some relevant application references have been included in this study.

Uncertainty of a measurement is a parameter associated with the results of a measurement that characterizes the dispersion of the values that could reasonably be attributed to the measurand. When carrying out measurements, the *true value* is out of reach. With a systematic approach a *correct value* can be obtained. Even that requires the best available instruments according to the state of the art technology. Still, some unknown systematic errors might be present preventing us to reach the true value.

Without any efforts in error estimation, the measurement result contains both known and unknown systematic errors as well as unknown random errors. Fixed errors and variable but deterministic errors are referred as bias errors. With correct measurement procedures and sufficient measurement devices it is possible to reach the desired accuracy of the measurement. Still the error analysis and uncertainty consideration play a major role in designing experimental research.

In this study, the principles of error analysis and uncertainty analysis are presented. In calculations, spreadsheet computation is used.

Evaluation of standard uncertainty requires a classification of input estimates to either *Type A* or *Type B* method of evaluation. The *Type A* evaluation is a method of evaluating the uncertainty by the statistical analysis of a series of observations. In this case, the standard uncertainty is the experimental standard deviation of the mean that follows from an averaging procedure or an appropriate regression analysis. The *Type B* evaluation is the method of evaluating the uncertainty by means other than the statistical analysis of a series of observations. In this case the evaluation of the standard uncertainty is based on some other scientific knowledge.

In calibration a measurand i.e. output quantity Y depends on a number N of input quantities X_i .

$$Y = f(X_1, X_2, \dots, X_N) \quad (35)$$

An estimate of a measurand Y i.e. the output estimate y is obtained using input estimates x_i for the values of the input quantities X_i .

$$y = f(x_1, x_2, \dots, x_N). \quad (36)$$

The standard deviation associated with the output estimate or measurement result $u(y)$ is the standard deviation of the measurand Y .

$$u(y) = \sqrt{u_1^2(y) + u_2^2(y) + \dots + u_N^2(y)} \quad (37)$$

$$u_i(y) = c_i u(x_i) \quad (38)$$

$$c_i = \frac{\partial f}{\partial x_i}. \quad (39)$$

The partial derivatives c_i , often called sensitivity coefficients, describe how the output estimate y varies with the changes in the values of the input estimates. Sometimes these sensitivity coefficients c_i are determined experimentally measuring the change in output by changing one particular input quantity X_i at a time. The knowledge of sensitive coefficients is useful in the determination of the most efficient target for developing the measurement system further. In this study, the sensitivity coefficient factors were not determined.

Type B uncertainty, which is typically received from a calibration certificate, a manufacturer's specification or a handbook, states the expanded uncertainty of measurement U .

The standard uncertainty u of measurement is obtained using the coverage factor k , which is explained in the next chapter.

Type A method is used if the input quantity X is observed several times and different values are found. The value of \bar{x} is the arithmetic mean of the observations

$$\bar{x} = \frac{x_1 + x_2 + \dots + x_N}{n} \quad (40)$$

The standard uncertainty of a measurement is calculated by equation

$$u(\bar{x}) = \sqrt{\frac{(x_1 - \bar{x})^2 + (x_2 - \bar{x})^2 + \dots + (x_N - \bar{x})^2}{n(n-1)}}. \quad (41)$$

GUM suggests that at least 10 measurements should be determined for statistical reliability. It should be noted that uncertainty u is not an absolute upper bound on the error.

3.3.1 Expanded uncertainty of measurement

The standard uncertainty of a measurement is not suited to prove conformity of a measured value. It indicates the quality of a measurement results, but proof of conformity requires a range that covers a high fraction of values consistent with the measurement conditions. Therefore the expanded uncertainty of measurement U is derived from the standard uncertainty u for industrial purposes.

$$U = k \cdot u(x), \quad (42)$$

where k is the coverage factor. The coverage factor is also referred to as coverage probability. The most used uniform coverage probability of 95 % gives a coverage factor $k = 2$. The result of a measurement is expressed as $Y = y \pm U$ i.e. the best estimate of the value attributable to the measurand Y is y and that $y - U$ to $y + U$ is an interval where most of the measured values should be expected.

The estimation of a measurement uncertainty is derived from a model for evaluating the results. The model should include all available knowledge about the measurement. For the roundness measurement device, the model should include uncertainties affecting the measurement e.g. displacement measurement uncertainty, alignment accuracy of sensors and frame as well as the algorithm that is used for calculating the results from each sensor.

In this research, the uncertainty of the roundness measurement includes the definition of the uncertainty of the laser triangulation sensors.

3.3.2 Uncertainty interval

To apply the GUM for practical purposes, it is necessary to understand the meaning of the result of the analysis: whether the measured values are within the limits or not i.e. the proof of conformity of a value within a specification. Figure 18 represents the characteristics of an uncertainty interval. It should be noted that a manufacturer of a product has to attest the conformance i.e. the values measured in quality control has to be within an upper and a lower limit of conformance. Again, the customer has to accept the values also within the uncertainty range, but can complain in case of non-conformance.

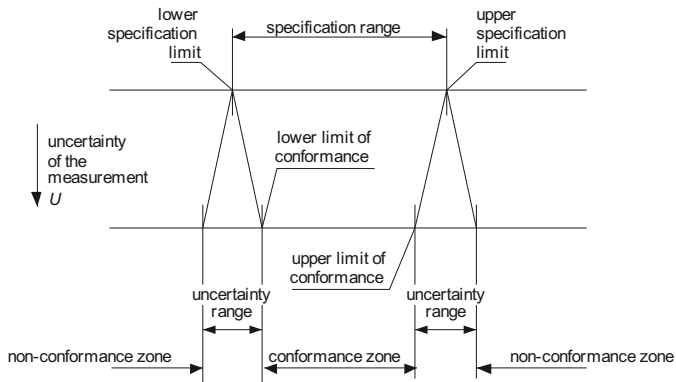


Figure 18 Ranges of conformity and non-conformity of a measured value with a specification range.

3.3.3 Error separation

By using an error separation method the measurement result can be more accurate than the accuracy of the measuring instrument alone. Whitehouse (1976) has presented some principles of both multi-orientation and multi-probe techniques to remove systematic and variable errors. Characteristic to the error separation is that the measurement is repeated several times after moving or repositioning the target or the measuring device. In the studied case, the method utilizes a multi-point method, but also other error separation techniques can be considered. The requirements for error separation are:

- mathematical model including the measuring target and the measuring device,
- good repeatability of a measurement, and
- knowledge of the error sources in the measurement.

Applications of the error separation method are published for laboratory measurements of straightness and roundness as well as for calibration of 2D-standards. For example an error separation technique (Li 1996) is described for *in-situ* measurement of the straightness of a workpiece without an accurate instrument datum. The goal in the presented method is to alleviate the deficiencies of the traditional sequential-two-point method and the sequential-three-point method. The new method is established by extending a multi-probe Discrete Fourier Transform (DFT) based roundness measurement method. The aperiodic nature of straightness measurements, which makes the use of DFT inappropriate, is remedied by a

numerical search scheme which corrects those data points affected by this limitation. The results of computer simulations and measurement experiments show that this method is a very good one for short workpiece straightness measurement in an ultra-precision diamond turning lathe.

3.3.4 Roundness measurement uncertainty

There are several approaches and standards to the evaluation of uncertainty of measurement and calibrating a roundness measurement device.

One typical method for the calibration of measuring instruments is the usage of nearly perfect roundness standards. In an international comparison of roundness profile measurements Frennberg and Sacconi (1996) used three roundness standards which were commercially available artefacts (a glass hemispherical roundness standard by Rank Taylor Hobson Ltd, and silicon nitride and zirconium oxide $\varnothing 30$ mm spheres with holding mounts). Two of the artefacts have roundness of approximately 40 nm, and the roundness of the third standard is less than 1 μm which is used for revealing problems in transducer calibration. The challenge in this setup is to reveal the attenuation of any frequency component. Although the filtering and other measuring parameters were fixed, some variation in the measurement results was observed. Similar results have been published by Haitjema et al (1996) receiving a standard deviation in each data point of less than 2 nm.

Nielsen and Malburg (1996) state that commercially available patented (U.S.Pat 4,429,464) calibration specimen, "flick" standard is a cylindrical artefact with a nominally flat or slightly concave area, as shown in Figure 19. This type of calibration can be used to evaluate the dynamic response of a measuring system and to verify the filtering and the software. The challenge using this flick standard is that it has a continuous undulations per revolution content i.e. the frequency spectrum is wide. The higher frequency components are cut off and the form of the flick shape at the corners changes as the filtering is changed. In the paper Nielsen and Malburg present a new method for the calibration of flick standards for roundness measuring instruments by using circular fits and the convolution of the standardized probe geometry.

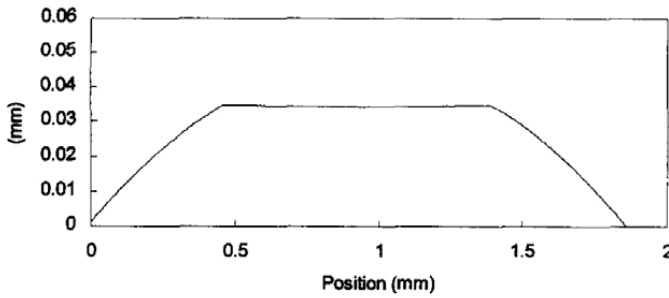


Figure 19 Profile of a flick standard at a cut sector (Nielsen and Malburg 1996).

Schneider and Hübner (1992) constructed a single frequency wave standard using only one undulation component which is a step forward for dynamic calibration, but analysis of the ability to measure the different waveforms is still limited.

The most advanced calibration standard for purposes of this research is presented by Jusko and Lüdicke (1999). They realized the need for a standard which embodies several superimposed sinusoidal waves on a cylindrical surface, as shown in Figure 20. The profile consists of only certain selected frequency components i.e. 5, 15, 50 and 150 undulations per revolution. The disc is manufactured by turning with a fast tool servo and ultra-precision milling.

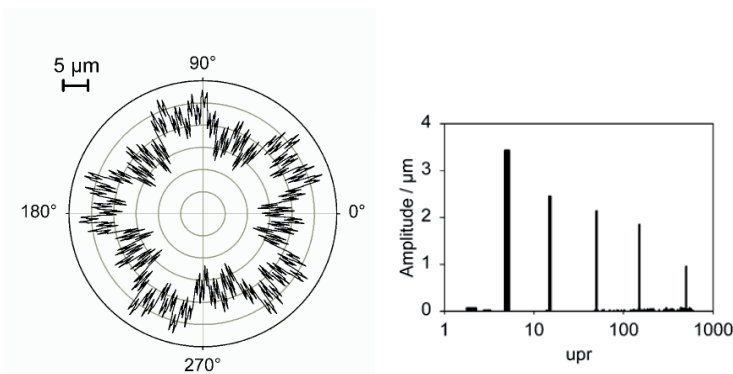


Figure 20 Form profile and spectrum of a multi-wave roundness standard (Jusko and Lüdicke 1999)

Thalmann (2006) describes the usage of different types of roundness standards. The nearly perfect or ideal geometry standards are used mainly for spindle error evaluation and multi-wave roundness standards are used

for the uncertainty analysis of probe magnification. In general, the roundness measuring device accuracy is assessed by

- the determination of spindle error using error separation techniques
- a traceable calibration of the probe,
- noise and the bandwidth of electronics,
- the stability of the instrument, and
- the validation of software.

For this research the uncertainty of measuring roundness components is derived using a multi-wave standard. The geometry of the manufactured disc is mathematically defined using Fourier series amplitude and phase terms. The chosen geometry includes harmonic roundness error components from 2-lobe (oval) to 30-lobe geometry component. The phases of the terms were chosen to minimize the roundness error of the profile.

There are also methods to define an unknown geometry of a flat or a sphere using three specimens with unknown geometries. The technique is based on unknown geometries of three discs assembled on the same shaft and an unknown rotational error motion of the shaft. The discs are measured in at least two separate setups in which one disc is flipped around to have one more equation with no extra unknowns. The difference is measured as follows. Let us denote the unknown geometry profiles with $A(\theta)$, $B(\theta)$ and $C(\theta)$ and the unknown rotational error motion as $r(\theta)$. The four unknowns are solved from the following equations.

$$C(\theta) - A(\theta) = \Delta R_1(\theta) + r(\theta) \quad (43)$$

$$C(\theta) - B(\theta) = \Delta R_2(\theta) + r(\theta) \quad (44)$$

$$B(\theta) - A(\theta) = \Delta R_3(\theta) + r(\theta) \quad (45)$$

$$B(\theta) - A(-\theta) = \Delta R_4(\theta) + r(\theta) \quad (46)$$

where ΔR_i are the respective measurement results. The difference between the last two measurements is that the profile of $A(-\theta)$ is measured in a reverse direction. The challenge in this method is to obtain the same rotational error after disassembling and reassembling one of the discs although methods to assess the uncertainty estimation for multiposition methods by Estler et al. (1997) for instance can be used. For practical measurement calibrations a standard with a known profile is recommended to avoid the repositioning of the disc.

For developing the measuring device further a more advanced approach utilizing the error analysis will have to be carried out. A systematic analysis of the measuring system and the determination of all error sources and their significance have to be carried out to find out the most efficient focus areas of further development.

3.4 Test roll

During the years manufacturing methods and materials of backing rolls have changed due to increasing demands on dynamic behavior and cost effectiveness. The most typical materials for the shell are carbon steel and cast iron. In this research, four different roll structures have been studied in the experimental measurement section.

There are several types of welded structures used for steel plate roll shells depending on the available manufacturing equipment. The bent plate is welded axially by one seam or two seams. There are also circumferential seams when two or three cylinders are welded together end-on-end. In some cases it has been found that nip rolls for other unit processes have been modified for use in a backing roll position. These rolls are often very thick walled compared with the 20...50 mm range of typical backing rolls.

In the 90's the material and manufacturing process was changed to cast iron roll shells which required internal machining to achieve required quality.

The end plates and their attachment to the roll shell have varied also during the years. Some end plates are welded together from two parts; the shaft and the end plate can be attached to the shell by a bolt connection or by welding. Recently a typical structure has a steel shaft fixed to a cast iron end plate which is bolted to the roll shell.

The laboratory test roll is a full-sized backing roll that has formerly been used in a paper mill. The rubber roll cover has been removed for the study as seen in Figure 21. The principal dimensions of the roll are presented in Table 4. Spherical roller bearings are used.

Table 4 Laboratory test roll.

<i>Diameter</i>	1450 mm
<i>Nominal wall thickness</i>	40 mm
<i>Length of the roll shell</i>	8200 mm
<i>Bearing distance</i>	9400 mm
<i>Mass</i>	18 000 kg



Figure 21 The test roll at the laboratory grinding machine. White painted stripes were used in testing for better surface quality in the laboratory measurements to test a possible improvement in a performance of laser sensors.

The roll is manufactured from steel and it is welded together from two parts. The shafts are fixed to the end plates using shrink-fitting. The thickness of the end plates is 200 mm and they are fixed to the roll shell by welding. The holes in the end plates, seen in Figure 21, are for balancing purposes. In this backing roll balancing masses (steel rods of 50 mm in diameter and maximum length of close to 700 mm) had been used. For this generation of backing rolls there is no internal machining, hence the internal surface geometry initiates from the bending process of the steel sheet.

3.5 Ultrasonic measurement of wall thickness

The ultrasonic measurement can be used for different purposes to analyze material structure. Ultrasonic systems are commonly used for non-destructive testing (NDT) to find material or manufacturing defects such as cracks or pores. Welds are often checked by ultrasonic measurements. Ultrasonic measurement is used to control cutting depth to ensure equal wall thickness of a thin walled cylinder attached to a three-jaw-chuck (Stoebener and Dijkman 2007). In addition, some mechanical properties, such as the strength and forming parameters, can be characterized using ultrasonic measurements to some extent (Thompson 1996).

Ultrasound is characterized as sound with frequency over 20 kHz. Precision ultrasonic thickness gages usually operate at frequency range from 0.5 to 100 MHz. Typically, lower frequencies are used to optimize penetration when measuring thick, highly attenuating, or highly scattering materials. For measuring the thickness of a paper machine roll made of

steel the applicable frequency range is about 1...10 MHz, which optimizes the resolution and penetration (Fowler et al. 1997).

A pulse-echo ultrasonic thickness gage determines the thickness of a part or a structure by accurately measuring the time required for a short ultrasonic pulse generated by a probe to travel through the thickness of the material, reflect from the back or the inside surface, and be returned to the probe (Figure 22).

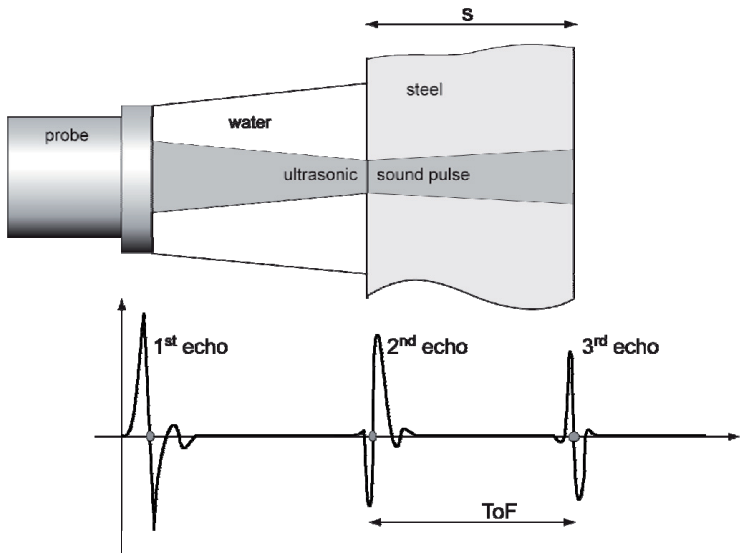


Figure 22 Typical echoes from an ultrasonic measurement with little damping in the material. The 1st echo is the sensor surface, the 2nd echo is the outer surface and the 3rd echo comes from the backside wall of the measured object.

The measured two-way time of flight (ToF) is divided by two to account for the down-and-back travel path, and then multiplied by the velocity of sound in the test material. The result is expressed as:

$$s = \frac{v \cdot t}{2}, \quad (47)$$

where s is the thickness of the work piece, v is the velocity of sound waves in the material and t is the measured time of flight. Continuous on-line ultrasonic thickness gauging is done by coupling the sound beam into the test piece through a water column generated by a squirter probe.

The best measurement accuracy is obtained when both the front and the back surfaces of the test piece are smooth and parallel. In this study, the back surface is fairly rough, therefore the returning echo may be distorted due to the multiplicity of slightly different sound paths seen by the transducer, and measurement inaccuracies will result.

When measuring curved surfaces, it is important that the transducer is placed approximately on the centerline of the part and held as nearly normal to the surface as possible. Also, tilting the transducer will distort echoes and cause inaccurate readings.

If the contact surface and back surface of the test piece are tapered or eccentric with respect to each other, the return echo will be distorted due to the variation in the sound path across the width of the beam. The welding seam of the roll shell might give false readings because the inner surface is not machined after welding.

There are several conditions found in certain engineering materials that can potentially limit the accuracy and range of ultrasonic thickness measurements:

Sound scattering - In materials such as cast stainless steel, cast iron, fiberglass and composites, sound energy is scattered into the material. Porosity in any material can have the same effect.

Sound attenuation or absorption - In low density plastics and rubber, sound energy is attenuated rapidly at the frequencies used for ultrasonic gauging. The maximum thickness that can be measured in these materials will often be limited by attenuation, for example soft roll covers might be hard to penetrate with ultrasound. In this study, the rubber cover was removed before measurements.

Velocity variations - An ultrasonic thickness measurement will be accurate only to the degree that material sound velocity is consistent with gauge calibration. For example cast iron used in some paper machine rolls exhibit significant variations in sound velocity from point to point (Widmaier et al. 2010). This happens due to the changes in grain and material structure that result from varied cooling rates in casting process, and the anisotropy of sound velocity with respect to grain structure. Many plastics and rubbers show a rapid change in sound velocity with the temperature. He (2001) has proposed a technique of simultaneous measurements of sound velocity and wall thickness using a pair of transmitters on the opposite sides of the measured tube and analyzing all reflected and transmitted pulses and their delays.

Phase reversal or phase distortion - The phase or polarity of a returning echo is determined by the relative acoustic impedance (density · velocity) of the boundary materials. In most cases, the test piece is backed by air which has lower acoustic impedance than metals, ceramics, or plastics. However, if one measures the thickness of a roll cover over a metal body this impedance relationship is reversed, and the echo appears phase reversed. To maintain accuracy in these cases it is necessary to change the detection polarity.

3.5.1 Measurement device and setup

Wall thickness measurements were carried out by Krautkrämer USPC2100 ultrasonic board, which is attached to a PC. The probe Krautkrämer H5KF is shown in Figure 23. A squirter is used for coupling the sound beam from the front face of the gage into the test piece through a water column. In the test setup, a cutting fluid of the grinding machine was used. The sensor operates at 5 MHz, which gives acceptable penetration and resolution.



Figure 23 *Krautkrämer H5KF probe (left) and with squirter attached (right).*

The measurement system is illustrated in Figure 24. The measurement system comprises position sensing devices. The rotational angle of the roll was measured by an incremental rotary encoder Heidenhain ROD450, which outputs four sine-wave functions A and B and their inverse functions \bar{A} and \bar{B} . Functions A and B are shifted by 90° to determine the rotational direction of the roll.

The axial position of the ultrasonic sensor was measured by another ROD450. The motion of the rotary encoder was converted into linear displacement measurement by using a wheel on the encoder axis. The wheel with a known diameter was pressed against the slideways of the roll grinding machine.

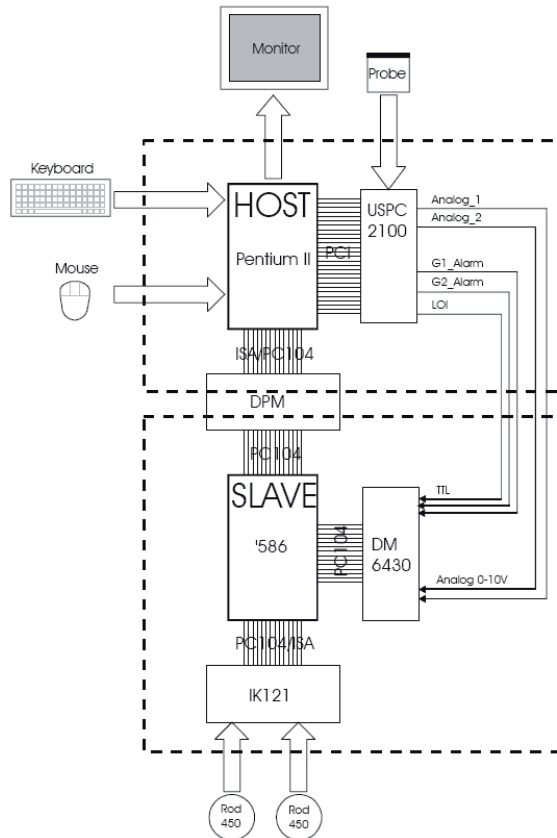


Figure 24 Ultrasonic measurement system consist of two computers. Host computer is used for setting up the measurement and ultrasonic measurement unit while the slave computer is saving the ultrasonic and position data. (Uski 1999)

In this study, the measurement is carried out in a grinding machine as shown in Figure 25. Ultrasonic measurement probe is installed on the carriage using cutting fluid as shown in Figure 26. The transducer is aligned perpendicular to the measured surface and the setup is steady during the measurement.

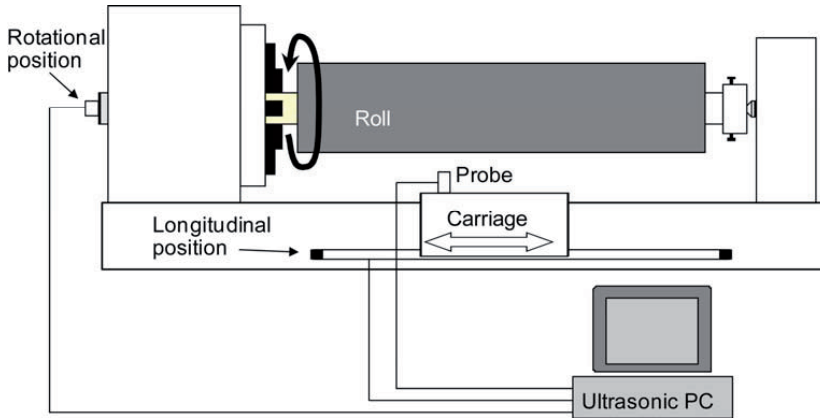


Figure 25 Ultrasonic measurement system consists of an ultrasonic probe, a computer with ultrasonic measurement unit and two position encoders to map the data.



Figure 26 The thickness map of a rotating roll is measured using a ultrasonic squirter probe in which the cutting fluid transmits the sound waves from the transducer to the measured object.

Wall thickness variation is measured as a spiral measurement. With a pitch of 10 mm/rev the measured matrix is 1024 x 690 points, hence a total of 720 000 measured points are acquired.

3.5.2 Measurement uncertainty

The ultrasonic probe is calibrated by setting the sound velocity with respect to the material being measured.

The most important source for systematic error is the sound velocity in the material, which can be determined with a steel gauging block with known thickness values. The nominal wall thickness of the test roll was 40 mm, hence a block with thicknesses ranging from 38.9 mm to 41.0 mm

was used in the calibration procedure. The block is machined with 0.1 mm thickness steps, the total number of steps is therefore 22. To determine the uncertainty of the block thickness values each block step was measured ten times. The calibration block is shown in Figure 27.



Figure 27 The calibration block consists of 22 thickness steps ranging from 38.9 mm to 41.0 mm.

The measurement was carried out in ten separate sequences starting from the 39.0 mm block step. The uncertainty of the thickness value is received from measurements according to GUM, where a precision micrometer Tesa micromaster 25-50mm IP54 is used. The calibration certificate indicates that the uncertainty of the micrometer is calculated as

$$U_{95\%} = (2 + 6L)\mu\text{m} . \quad (48)$$

The calibration certificate indicates the mean and maximum differences to be 0.0 micrometers in the range of 37.9...42.6 mm. The uncertainty of the precision micrometer is therefore neglected in further analysis.

Ten separate measurement series were carried out. The measurement was carried out in a temperature controlled room and temperature was 19.7°C during the measurements. The calibration block measurement results are given in Table 5.

Table 5 Thickness measurement [mm] results of the calibration block.

Step [mm]	Measurement #									
	1	2	3	4	5	6	7	8	9	10
38.9	.876	.893	.879	.882	.883	.884	.885	.880	.885	.878
39.0	.984	.999	.977	.986	.991	.989	.990	.986	.990	.987
39.1	.090	.097	.088	.086	.091	.090	.089	.087	.091	.087
39.2	.195	.200	.186	.186	.194	.186	.191	.187	.193	.191
39.3	.305	.306	.292	.293	.304	.299	.301	.295	.299	.295
39.4	.404	.410	.394	.398	.409	.399	.404	.402	.404	.400
39.5	.507	.509	.497	.502	.505	.501	.505	.503	.505	.499
39.6	.618	.613	.599	.612	.609	.604	.605	.605	.604	.602
39.7	.721	.713	.704	.714	.711	.707	.708	.708	.709	.710
39.8	.823	.810	.807	.814	.814	.809	.810	.809	.810	.813
39.9	.925	.914	.914	.920	.914	.916	.914	.915	.910	.911
40.0	.037	.017	.018	.017	.019	.018	.015	.017	.018	.010
40.1	.132	.120	.122	.121	.123	.121	.116	.122	.122	.121
40.2	.238	.223	.224	.224	.225	.225	.226	.227	.229	.224
40.3	.338	.328	.328	.326	.329	.329	.330	.328	.334	.328
40.4	.439	.427	.432	.429	.429	.431	.427	.430	.432	.428
40.5	.549	.534	.535	.536	.536	.540	.539	.535	.539	.535
40.6	.649	.643	.641	.638	.640	.642	.637	.640	.644	.639
40.7	.749	.741	.738	.740	.742	.739	.741	.739	.740	.742
40.8	.848	.838	.837	.839	.839	.842	.839	.840	.836	.839
40.9	.944	.929	.929	.933	.934	.933	.931	.936	.932	.932
41.0	.034	.023	.027	.025	.026	.022	.025	.026	.023	.022

Ultrasonic calibration measurements were carried out using the ultrasonic device. A calibration block target was measured. The block was immersed in water during the measurements and wall thickness readings were recorded on a spreadsheet shown in Table 6.

Calculation of measurement uncertainty is carried out using GUM principles. For each thickness level a mean value and standard uncertainty values were calculated as well as the expanded uncertainty with a coverage factor $k = 2$ for the coverage probability of approximately 95 %.

The results are presented in Table 7. The columns \bar{L}_{ref} and \bar{L}_{US} show the mean average values of ten separate measurements of the calibration block measurement with the precision micrometer and the ultrasonic measuring device, respectively. The expanded uncertainties U_{Lref} and U_{LUS} are calculated. The difference between reference measurement and ultrasonic measurement is presented as ΔL

$$\Delta L = \left| \bar{L}_{US} - \bar{L}_{ref} \right|. \quad (49)$$

Table 6 Ultrasonic thickness measurement [mm] of the calibration block

Nominal value [mm]	Measurement #									
	1	2	3	4	5	6	7	8	9	10
38.9	.913	.919	.925	.926	.925	.925	.925	.938	.919	.918
39.0	.024	.027	.026	.027	.027	.024	.027	.033	.023	.063
39.1	.125	.122	.124	.128	.125	.128	.124	.123	.128	.121
39.2	.234	.226	.226	.228	.234	.227	.227	.230	.235	.230
39.3	.331	.338	.333	.334	.339	.337	.340	.338	.333	.335
39.4	.436	.435	.435	.437	.436	.437	.444	.434	.444	.440
39.5	.538	.535	.537	.541	.537	.538	.537	.542	.539	.540
39.6	.650	.641	.640	.646	.644	.642	.641	.643	.640	.643
39.7	.749	.748	.740	.748	.746	.747	.751	.745	.741	.746
39.8	.845	.851	.852	.850	.851	.849	.857	.848	.849	.847
39.9	.950	.958	.952	.951	.955	.960	.955	.960	.955	.950
40.0	.051	.055	.051	.055	.055	.057	.055	.058	.060	.056
40.1	.164	.160	.154	.160	.157	.154	.159	.161	.160	.166
40.2	.270	.262	.258	.263	.260	.257	.262	.269	.261	.263
40.3	.363	.365	.361	.365	.364	.362	.362	.368	.364	.365
40.4	.463	.463	.466	.472	.472	.470	.464	.469	.468	.471
40.5	.568	.571	.568	.576	.573	.569	.577	.577	.576	.576
40.6	.668	.678	.669	.675	.675	.670	.675	.676	.677	.677
40.7	.776	.774	.773	.781	.779	.771	.772	.773	.779	.777
40.8	.871	.869	.876	.875	.875	.868	.870	.872	.878	.873
40.9	.968	.965	.972	.978	.974	.970	.967	.966	.976	.967
41.0	.055	.051	.058	.064	.063	.061	.063	.059	.065	.063

The measurement result is analyzed (Figure 28) for systematic errors such as gain error and offset. The used speed of sound wave in the studied material is a good approximation, because there is little gain error of 0.2 %. The offset can be corrected in measurements and the offset corrected mean average value of the wall thickness measurement is presented as ΔL_{OC} . Also, a gain correction ΔL_{OGC} is applied, but no significant improvement can be observed in the studied measurement range.

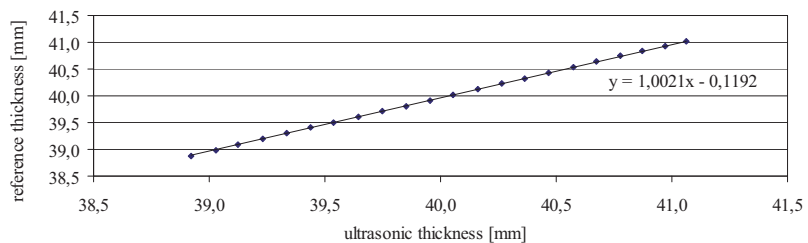


Figure 28 Ultrasonic measurement vs. reference measurement.

Table 7 Calibration block thickness mean value and expanded uncertainty of the reference instrument (\bar{L}_{ref}, U_{Lref}) and the ultrasonic device (\bar{L}_{US}, U_{LUS}). The difference between ultrasonic measurement against the reference measurement is analyzed by using uncorrected values ΔL and corrected values ΔL_{OC} and ΔL_{OGC} which can be evaluated against the combined uncertainty of the measurement U_{Δ} .

L mm	\bar{L}_{ref}	U_{Lref}	\bar{L}_{US}	U_{LUS}	ΔL	ΔL_{OC}	ΔL_{OGC}	U_{Δ}
38.9	38.883	0.0030	38.923	0.0042	0.041	0.004	0.003	0.0052
39.0	38.988	0.0036	39.030	0.0075	0.042	0.006	0.005	0.0083
39.1	39.090	0.0020	39.125	0.0016	0.035	0.001	0.002	0.0025
39.2	39.191	0.0030	39.230	0.0022	0.039	0.002	0.002	0.0037
39.3	39.299	0.0032	39.336	0.0019	0.037	0.000	0.000	0.0037
39.4	39.402	0.0031	39.438	0.0023	0.035	0.001	0.001	0.0039
39.5	39.503	0.0023	39.538	0.0013	0.035	0.001	0.001	0.0027
39.6	39.607	0.0037	39.643	0.0020	0.036	0.001	0.000	0.0041
39.7	39.711	0.0030	39.746	0.0022	0.036	0.001	0.000	0.0037
39.8	39.812	0.0029	39.850	0.0021	0.038	0.002	0.003	0.0035
39.9	39.915	0.0027	39.955	0.0024	0.039	0.003	0.004	0.0037
40.0	40.019	0.0044	40.055	0.0018	0.037	0.000	0.002	0.0047
40.1	40.122	0.0025	40.160	0.0024	0.037	0.001	0.003	0.0035
40.2	40.227	0.0028	40.263	0.0027	0.036	0.000	0.001	0.0038
40.3	40.330	0.0022	40.364	0.0013	0.034	0.002	0.000	0.0026
40.4	40.430	0.0022	40.468	0.0023	0.037	0.001	0.003	0.0032
40.5	40.538	0.0028	40.573	0.0024	0.035	0.001	0.001	0.0037
40.6	40.641	0.0022	40.674	0.0023	0.033	0.004	0.001	0.0032
40.7	40.741	0.0019	40.776	0.0022	0.034	0.002	0.001	0.0029
40.8	40.840	0.0021	40.873	0.0021	0.033	0.003	0.000	0.0030
40.9	40.933	0.0027	40.970	0.0028	0.037	0.001	0.004	0.0039
41.0	41.025	0.0022	41.060	0.0028	0.035	0.002	0.002	0.0036

Correction terms for ultrasonic measurements are

$$L_{OC} = L_{US} - \frac{1}{N} \sum_1^{10} (L_{ref,n} - L_{US,n}) = L_{US} - 0.0364 \text{ and} \quad (50)$$

$$L_{OGC} = 1.0021 \cdot L_{US} - 0.1192. \quad (51)$$

The reported expanded uncertainty of measurement is stated as the standard uncertainty of measurement multiplied by the coverage factor $k = 2$, which for a normal distribution corresponds to a coverage probability

of approximately 95 %. The standard uncertainty of measurement has been determined in accordance with EAL Publication EAL-R2 using the uncertainty evaluation principles.

Comparing the expanded uncertainty of measurement values U_{Δ} with values of uncorrected values ΔL and corrected values ΔL_{OC} and ΔL_{OCG} it can be seen that

- the maximum experimental measurement uncertainty in the ultrasonic thickness measurements is calculated to be approximately 0.004 mm i.e. $U_{US} \approx 0.004$ mm,
- the expanded uncertainty U_{Δ} is smaller than the difference between the reference value and the measured value. Therefore, a correction is required to eliminate systematic errors from the measurement, and
- the expanded uncertainty U_{Δ} is larger than the corrected values ΔL_{OC} and ΔL_{OCG} . After the correction the mean average of the measurement is within the uncertainty limits of the reference measurement.

3.6 Dynamic behavior measurement of large rotating cylinders

Most paper mills and roll shops have some measuring systems to control their manufacturing and maintenance quality. Common measurement systems include a geometry measurement of a roll at grinding speed. The purpose of these measurements is to verify the machining accuracy to be within tolerances. Until recently the tolerances were described as conventional geometric tolerances such as straightness, roundness and form error. A typical measurement of a paper machine roll is carried out by measuring the roundness profile with a device using a 2-point or a multipoint method from three cross-sections of a slowly rotating roll. The 2-point method can't measure the true roundness profile, only the even lobes of a roundness profile. In addition, an axial diameter profile is measured by the 2-point method while the roll is not rotating. The tolerances for these measurements have typically been in the range of $\pm 5 \dots \pm 20 \mu\text{m}$. In addition to these measurements on a grinding machine, the dynamic behavior of a roll is sometimes measured on a balancing machine. If the unbalance forces exceed the limits, the roll is balanced according to the procedure described in Chapter 2.2.3.1. Should the dynamic deflection be minimized, a three plane balancing procedure is carried out by either counter weights or centring according to the balancing of flexible rotors, as described in Chapter 2.2.3.2.

To achieve high operational accuracy, when the operating conditions of paper machine rolls are far from workshop conditions, more advanced measuring technology must be used to verify the dynamic behavior of a roll.

The major differences between the machine workshop condition and operating condition in a paper machine are running speed, mechanical load and thermal load. These are different phenomena and therefore must be dealt separately. The focus in this study is on the effect of running speed although in the literature study the effects of mechanical loads and thermal loads are discussed briefly.

A new measurement system to measure the dynamic geometry of a paper machine roll was developed.

The run-out measurement in this study means radial run-out measured by a distance gauge or a displacement sensor. The radial run-out of a roll is described as a movement of the surface of the roll in the direction perpendicular to the rotating axis of the roll. A typical realization of this measurement is carried out by a clock gauge.

3.6.1 Dynamic geometry measurement principle

The geometry measurement of a paper machine roll is studied by several researchers during the last two decades. Väänänen (1993) developed a new method for measuring the geometry of paper machine roll by combining the traditional 2-point method and the 3-point method presented originally by Aoki and Ozono (1966) and Ozono et al. (1974). The roundness measuring algorithm used in this study is the one presented by Väänänen.

3.6.2 Measurement setup

The developed measurement system is based on commercial equipment for measuring systems. The setup consists of displacement sensors fixed in a measuring frame, sensors or indicators for the both rotational angle and axial position of a single run-out measurement and a PC for data acquisition and analysis. Later, the commercial realizations of the original measurement system also include the control of machine speed and the axial position of the measurement frame.

The backing roll at the laboratory was setup on a test bed which can be used for both grinding research and dynamic behavior studies. The test bed consist of separate beds for the roll and machining and measuring systems. One system setup is shown in Figure 29.

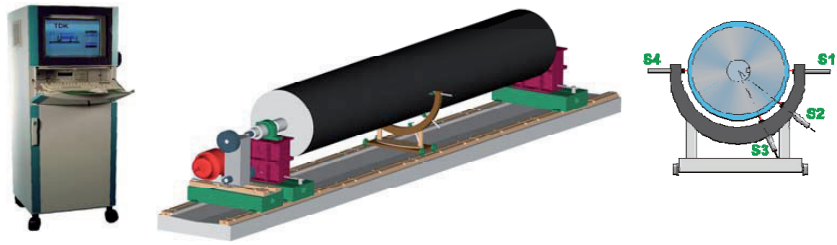


Figure 29 The measuring data acquisition system is built into an industrial cabinet (left). The measuring frame can be set on a carriage underneath the roll. The four sensors S1...S4 are set in relative angles at 0, 38, 67 and 180 degrees. The rotational angle is measured using a rotary pulse encoder.

During the research, new data acquisition hardware was tested and the system was gradually updated.

3.6.3 Displacement sensors

Requirements for the displacement sensors include a demand for sufficient accuracy, suitability to measure all materials used for paper machine rolls and roll covers, and insensitivity to the material errors such as welds and surface roughness. Sufficient measuring speed was a matter of course. The selection is based on the basic information of sensors in literature (Doebelin 1990, Slocum 1992) and manufacturers' data sheets.

The first selection was done between contacting and non-contacting sensors. Experience from previous studies on run-out measurements had shown that there had been many problems with contacting sensors as the tangential speed of the measured surface increases. Frictional heat and vibrations, such as stick-slip, caused erroneous readings. Both basic principles for the contacting element, either sliding or rolling, had its own drawbacks. Kiviluoma (2009) has studied a sliding contact probe for measuring the run-out of paper machine rolls in operating conditions. For general purpose and especially for the case of backing rolls contacting sensors were neglected from further studies.

The final selection was done among the following sensor types:

- capacitive displacement sensor,
- eddy-current displacement sensor,
- laser displacement sensor (diffuse reflective),
- laser displacement sensor (specular reflective),
- laser vibrometer (Doppler interferometer) and

- laser interferometer (Heterodyne interferometer).

Some devices of different sensor types were tested in the laboratory with the real application. Some sensor types were neglected by literature study because the sensor does not fulfill the basic requirements on measured material or surface quality. The following chapters introduce the operation principle of sensors and a short summary of the applicability in the studied case.

3.6.3.1 Capacitive displacement sensors

The capacitive displacement sensor is based on the principle of a plate capacitor. Two electrodes are formed by the sensor and the target surface. A constant alternating current goes through the sensor and the amplitude of the voltage on the sensor is proportional to the spacing of the capacitor electrodes.

With a single-plate sensors target surface characteristics have influence on the results. A curved or rough surface will need to be calibrated and the result still refers to an average gap between the sensor and the target. Surface shape also influences the homogeneity of the electric field and thereby the measurement linearity.

Precision measurement requires minimizing environmental influence. When using capacitive sensors cleanliness, constancy of temperature and humidity during the measurement are essential.

Depending on a sensor type the effective measurement beam is quite large and therefore surfaces with holes or sharp indents cannot be measured.

The capacitive sensor is rejected due to restrictions in environmental requirements and a relatively large measurement beam.

3.6.3.2 Triangular laser displacement sensors

The triangular laser displacement measurement method is based on measuring the position of intensity maximum on a detector of diffusive reflected or specular reflected monochromatic light from a laser diode (Figure 30). The method is insensitive on surface roughness and scattered light to some extent. Surface characteristics may have an effect on readings as explained in more detail in Chapter 3.6.4. The measuring beam is typically in the range from tens of micrometers to less than a millimeter, and therefore grooved surfaces can be measured.

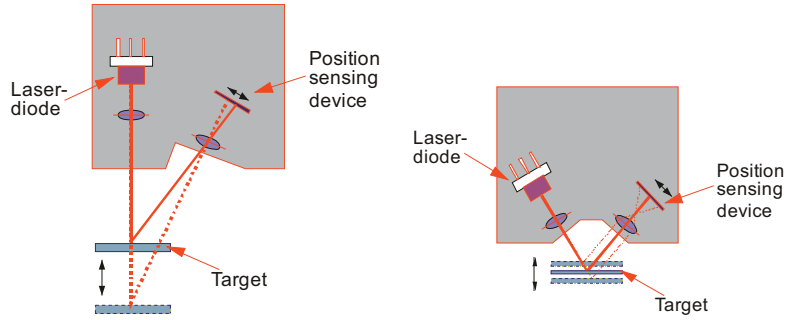


Figure 30 Triangular laser beam displacement sensors have different operating principles for diffusive reflective surfaces (left) and specular reflective surfaces (right). The distance between the target and the sensor taken from the intensity maximum on the position sensing device.

The specular reflective sensor requires a mirror like surface finish which is not the case with most of the roll surfaces. The diffusive reflective sensor fulfills most of the requirements and therefore it is selected for further evaluation.

3.6.3.3 Confocal laser beam sensor

One method of using laser is a confocal principle, which is based on measuring the focal length of an accurately focused lens and a target. The laser beam is focused automatically on the target surface with a fast moving lens. While the lens is moving the reflected light is passed onto a pinhole plate through a dichroic mirror. The light passes through the pinhole, when the beam is fully focused on target. The position of a moving lens is read after the detector has observed the signal. The position of the lens is directly proportional to the distance of the target.

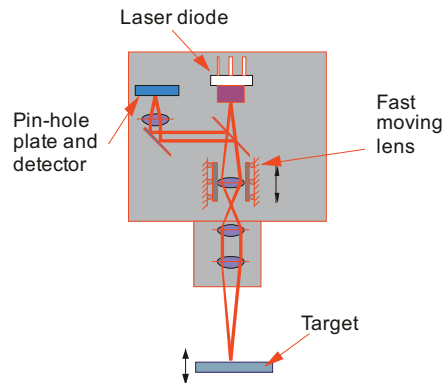


Figure 31 Confocal laser beam displacement sensor consist of fast moving lens and detecting when the beam is fully focused on the target.

This is an interesting displacement sensor, but no sample could be obtained for further evaluation.

3.6.3.4 Laser interferometers

There are many different measuring methods and devices called interferometers that utilize the interference of light to measure displacement, straightness or angular displacement. A common feature to these methods is observing the beat frequency (Figure 32) or phase difference of either one or two laser beams.

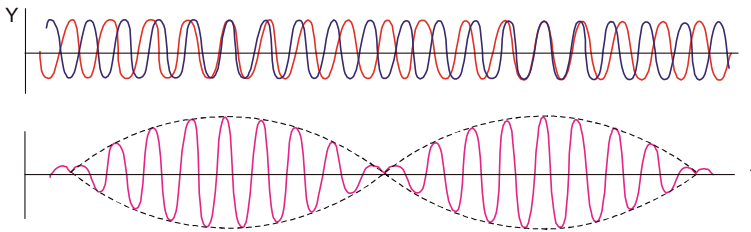


Figure 32 Two laser signals with a frequency shift cause a beat frequency. The effect is used in some of the laser interferometers.

Many interferometers are based on a common path of the measurement and reference beams as long as possible. This requires the usage of polarized light with 90° angle between the measurement and reference beams, as shown in Figure 33. Different optic components can be used to reflect, split or twist without interfering with each other.

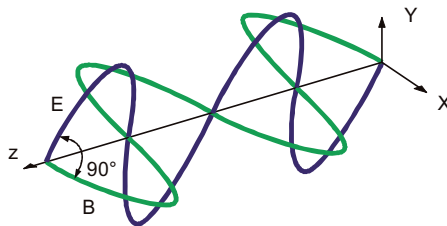


Figure 33 In interferometers the measurement and reference beams are separated by 90° angle.

Most of the sensors require special optic components for measuring and surfaces with arbitrary roughness cannot be measured. Some manufacturers, such as Sios, have introduced an interferometer (Figure 34) to measure vibrations of rotating components with arbitrary surface roughness, but according to the manufacturer these sensors can only be used for axial vibrations measured from the axial center point where there is practically no surface velocity.

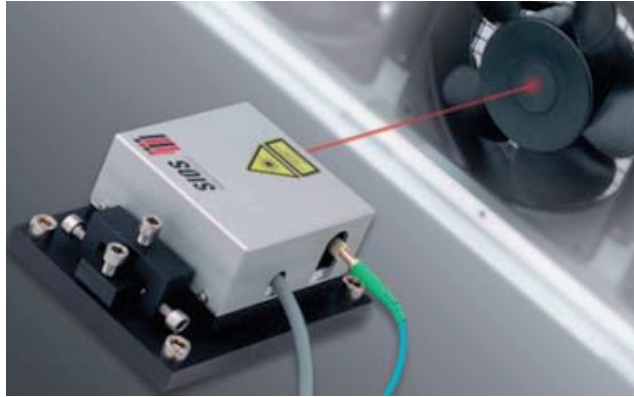


Figure 34 *Laserinterferometric vibrometer from SIOS Meßtechnik GmbH can be used for displacement measurements of surfaces with arbitrary roughness (www.sios.de).*

Doppler-laser is based on the change of frequency between the emitted beam and the reflected beam, therefore it can be used to measure moving targets only.

The requirement for small vibration amplitude of a few micrometers at relatively slow rotating speed (about 0.2 Hz) was found to be a very difficult challenge for a Doppler vibrometer, which can also be deduced from the specifications given by the manufacturer. One model was tested briefly in the laboratory and the results were not satisfying.

3.6.3.5 Selection of the displacement sensor

As discussed above the diffusive reflective laser triangulation displacement sensor is the most versatile sensor of the sensors available for further testing. In the middle of 90s there were four vendors in Finland that provided samples for testing. An unpublished review revealed two equally performing displacement sensors which were technically on the same level: Keyence LC2430 and Matsushita Nais LM300/R30. The Nais LM300 was available as a 2-channel version while Keyence LC2430 had only one channel per head unit which made the price-performance ratio of the Nais LM300 better. The selected sensor type has been used for over a decade in this research. There are new and perhaps better sensors available on the market, but testing of those is excluded from this study.

3.6.4 Speckle pattern effect

The laser triangulation measuring principle and its uncertainty in distance measuring has been studied by Dorsch et al (1994). Uncertainty in the distance measurement of laser triangulation sensors and other coherent sensors is limited by speckle noise. Speckle arises because of the coherent

illumination in combination with rough surfaces. This uncertainty is a function of the wavelength, the observation aperture and the speckle contrast in the spot image. They introduce uncertainty principle connecting lateral resolution and distance uncertainty. Design criteria for a sensor with minimum distance uncertainty are determined: small temporal coherence, small spatial coherence, and a large observation aperture.

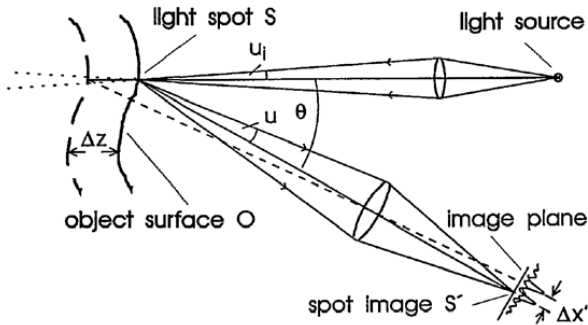


Figure 35 Principle of laser triangulation (Dorsch et al. 1994).

According to the experiments with a planar ground glass, the uncertainty of a measurement shows the independence of the spot size. While the glass is displaced in the lateral direction, the apparent location of the spot image varies although its true position is constant at the reticle position. The true position is concealed from the observer because of the microtopology that varies locally.

Dorsch et al conclude that distance measurements by laser triangulation suffer from a fundamental uncertainty that speckle introduces. Theory and experiments show that the uncertainty comes mainly from the observation aperture, the speckle contrast and the angle of triangulation. For short-range macroscopic applications the distance uncertainty is in the range of a couple of micrometers to more than 10 μm . The uncertainty does not depend on the size of the projected light spot as long as this spot is larger than the observed subjective speckle. For sufficiently rough surfaces the uncertainty can be reduced more than twice by low temporal coherence illumination. The introduction of low spatial coherence offers a significant improvement.

These results hold for an ideally rough object such as ground glass. Technical surfaces usually display a much greater distance error. As an example, they replaced the ground glass with a scratched copper substrate. The results show - the larger the spot size the more local reflection errors are collected; thus uncertainty increases with a large spot size.

3.7 Calibration procedure and measurement uncertainty

The measurement system accuracy can be estimated by different means, such as error budgeting which is very useful in the research and development of a measuring equipment. With these methods overall uncertainty is deducted from several single error sources and calculated by mathematical means. It may be difficult to evaluate the magnitude of an error from a single source and therefore it is crucial to validate the measurement uncertainty using a calibration method which is traceable to the international standards.

3.7.1 Measurement uncertainty of laser displacement sensors

Laser sensors were initially tested briefly before selecting the sensor type and the model used in this study. The triangular laser beam displacement sensor was the all-purpose sensor with fewer restrictions for measurement surfaces and structures. A NAIS LM300 unit with two sensor heads is selected.

The laser sensor is calibrated on a rig with a precision micrometer and a target surface similar to a typical roll surface. In manufacturers' specifications, white ceramic is used for the characterization of laser sensors, but roll surface characteristics with arbitrary surface roughness affect the uncertainty of measurement.

The determination follows the same workflow that was used in the determination of uncertainty of ultrasonic measurements in Chapter 3.5.2.

The measurement procedure was carried out with static measurements using minimum amount of filtering in the Nais LM300 head unit. The measurement range was from -1.5 mm to +1.5 mm in 0.5 mm increments and the reading of the precision micrometer was set at a value within 1 μm at each measuring step. The measurement series was repeated at least fourteen times in the whole range, and in the center of the measuring area a few more measurements were made. Individual results are not reported.

The results of laser displacement measurement versus the reference measurement are shown in Figure 36. The fitted linear regression curve and the correction function are calculated using MS Excel least squares fitting curve function.

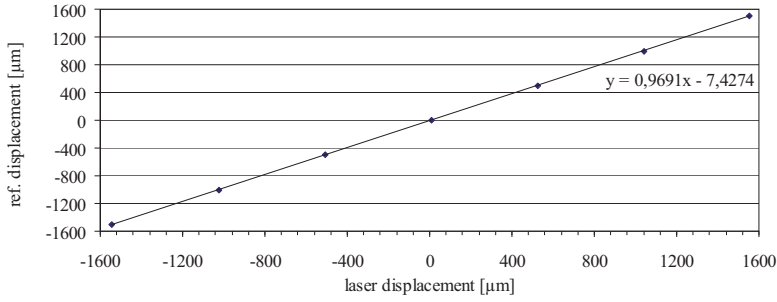


Figure 36 Laser displacement measurement vs. reference measurement. The fitted linear regression curve shows the correction function for laser measurements.

In Table 8 the mean \bar{S}_{LSR} and experimental expanded uncertainty of measurement $U_{S_{LSR}}$ are presented at each of the measured displacement steps. There is a gain error of 3 % in the laser sensor measurement which is corrected in \bar{S}_{LSRC} .

Table 8 The mean \bar{S}_{LSR} and expanded experimental uncertainty of measurement $U_{S_{LSR}}$ of laser sensors in static calibration. The analysis of the difference between ultrasonic measurement against the reference measurement is carried out by using uncorrected difference values ΔS and corrected values ΔS_C which can be evaluated against the combined uncertainty of the measurement U_{Δ} . The value \bar{S}_{LSRC} shows the corrected value of measurement.

\bar{S}_{ref} [μm]	\bar{S}_{LSR} [μm]	$U_{S_{LSR}}$ [μm]	ΔS [μm]	\bar{S}_{LSRC} [μm]	ΔS_C [μm]	U_{Δ} [μm]
-1500	-1543.0	2.03	-43.0	-1502.7	-2.7	2.26
-1000	-1025.6	2.69	-25.6	-1001.3	-1.3	2.87
-500	-505.2	2.01	-5.2	-497.0	3.0	2.25
0	11.3	2.13	11.3	3.5	3.5	2.35
500	524.2	2.86	24.2	500.5	0.5	3.03
1000	1039.6	2.63	39.6	1000.0	0.0	2.81
1500	1552.4	3.33	52.4	1497.0	-3.0	3.48

Comparing the expanded uncertainty of a measurement values U_{Δ} with the uncorrected values ΔS and the corrected values ΔS_C , it can be seen that:

- The experimental measurement uncertainty in the laser displacement measurements is calculated to be less than 3.5 μm in the practical

measurement range without any signal conditioning i.e. $U_{LSR} \leq 3.5 \mu\text{m}$. The expanded uncertainty U_{Δ} is smaller than the difference between the reference value and the uncorrected measured value ΔS . Therefore a correction is required to eliminate systematic errors from the measurement.

- The deviation between measured value \bar{S}_{LSR} and the reference value \bar{S}_{ref} comes mainly from the gain error of approximately 3 %.
- The expanded uncertainty U_{Δ} is larger than the corrected values ΔS_c . After the correction the measurement uncertainty is within the uncertainty limits of the reference measurement.

3.8 Finite element models

Two finite element FE models of a roll are created in order to evaluate the significance of geometry errors due to normal wall thickness tolerances. The first model was built for another case study with dryer cans and the second cylindrical FE model was built to analyze the backing roll case study.

3.8.1 Cross-section model

The cross-section FE model used in this study does neither take into account the measured wall thickness distribution nor the end plate support. The wall thickness variation is simplified by the allowed tolerances of the inner wall roundness. FE analysis is done only for the cross-sections. The FE model is not end supported and the inner surface profile is assumed to be the same for the whole cylinder.

The cross-section of the outer surface of a cylinder is an ideal circle ($D=2188 \text{ mm}$) with nominal wall thickness $t=30 \text{ mm}$. The material of the cylinder is cast iron ($E=150 \text{ GPa}$, $\nu=0.33$, $\rho=7000 \text{ kg/m}^3$). The analysis is performed by the variation of surface velocity (0, 1200, 1500 and 1700 m/min) and inner surface profile errors for harmonics 2, 3 and 4 one at a time with amplitudes $A_{2H}=0.5, 1.0$ or 2.0 mm , A_{3H} and $A_{4H}=0.25, 0.5$ or 1.0 mm , as shown in Figure 37. In the model the cross-section rotates around the geometric center of the outer surface. The centrifugal forces are distributed according to the mass distribution and corresponding rotation radius. The stiffness of the ring is taken into account. Each analysis consists of one harmonic of the inner surface profile only (A_2, A_3 or A_4). The run-out profile of the outer surface is therefore the roundness profile.

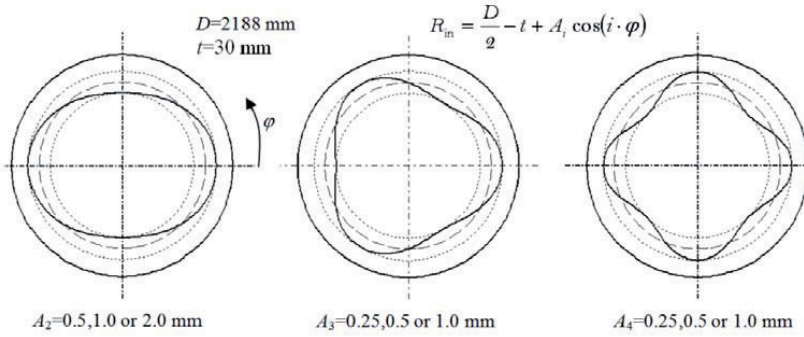


Figure 37 Cross-section verification model with varying amplitudes of 2nd (left), 3rd (middle) and 4th (right) harmonic components of wall thickness variation. (Juhanko et al. 2010)

The FE analysis is performed using conventional 24 degrees of freedom 8-node brick elements. Mesh consists of 64 elements in hoop and 3 elements radially in the cross-section resulting in 512 nodes, 192 elements and 1536 degrees of freedom. The FE model is constrained on the plane of the cross-section. The analysis is performed in Matlab 6.1 using code based on linear structural FEM-FEA. (Juhanko et al. 2010)

3.8.2 Cylindrical finite element model

A finite element model was created to simulate the effect of manufacturing accuracy as a function of a rotating speed of the roll.

The cylinder is modeled by Forsberg (2006) using Elmer FE software, and the model is verified using another finite element model built with Abaqus FE software. In verification, only the main components of wall thickness variation are modeled (Figure 38).

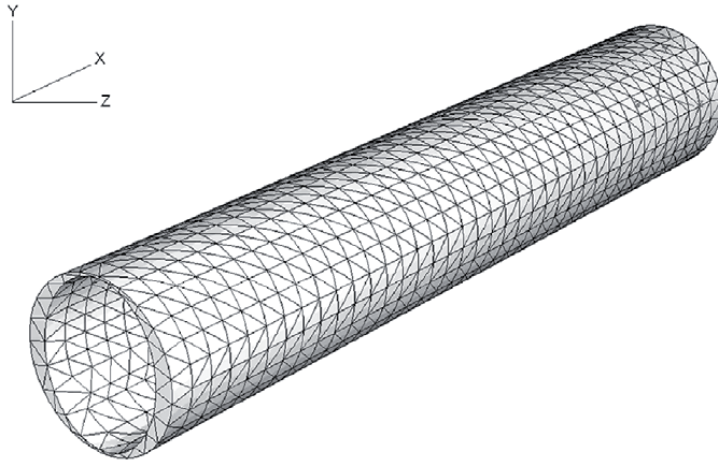


Figure 38 Cylindrical verification model with only 2nd harmonic component of wall thickness variation. (Forsberg 2006)

Forsberg studied the effect of element type and the number of elements. The nodes defining the outer surface of the cylinder are modeled as perfect cylinder geometry. The measured wall thickness variation defines the inner surface nodes. This applies well for the actual manufactured geometry, because the outer surface has been either turned or ground within the tolerance that is only a fraction of the wall thickness tolerance.

The program uses the measured wall thickness that defines mesh coordinates based on Lagrange interpolation. The program writes element, node and boundary condition together with header files for the Elmer FE software. In this study, the analysis is carried out by tetrahedral elements. The following assumptions and simplifications are used in the modelling:

- the end plates are fixed,
- Young's modulus of the shell material is constant, including the welding seam,
- the outer surface geometry is a perfect cylinder,
- the spiral measurement result matrix is taken as an orthogonal matrix,
- the eccentricity of the shaft is neglected, and
- the load is applied as volume forces on elements.

3.9 Measurement of coating quality variations

Paper quality variations are measured with a Tapio PMA paper machine analyzer by Tapio Technologies Ltd. The presentation is based on the papers of Makkonen (U.S.Pat. 4,773,760), Perento (1999), Hilden and

Perento (2000) and Ghosh (2001) and the personal discussions with the analysts.

Tapio PMA measures both the cross direction (CD) and the machine direction (MD) paper samples with high resolution. The device measures several properties of paper such as caliper and gloss among others.

Typical sample length in machine direction analysis is 5000 m and can be as long as 7 km. With this measurement range the unit is able to cover the whole range of variation spectrum ranging from the long term (0.003 Hz) to the very short term (40 000 Hz).

Tapio PMA consists of the analyzer unit, sensors and a computer. The analyzer includes the transportation mechanism of paper, measurement and control electronics. Different sensor positions in the analyzer are corrected. This ensures that the user always knows how the measured values compare with one another at any point during the measurement.



Figure 39 Tapio PMA is used for analysis of both machine and cross direction samples of paper. (Fig: Tapio PMA for CD Applications. Tapio Technologies Oy).

Quality variations of coated paper are revealed best by gloss, grammage and ash variation analyses. The gloss measurement is the most sensitive feature, because many machine related problems affect the glossiness. The sensor measures the reflected light from both sides of the paper web. The grammage sensor is based on the attenuation of beta-radiation in paper.

Tapio PMA has a wide variety of analysis options both in time and frequency domain, some of which are shown in Table 9. The frequency domain is generated from the measured wavelength and the machine speed data that is given to the analyzer by the user.

Usually the machine direction (MD) sample rolls are obtained at the winder or re-winder from close to the ends of a reel. The length of the

sample should be 2500...5000 m to get a proper wavelength ("frequency") resolution to separate the rotating machine elements from each other. In addition, the roll positions, the paper grade and the speed of the paper machine are documented.

Table 9 Basic machine direction analyses and options of Tapio PMA with some detailed analysis and results.

	<i>Analysis</i>	<i>Further analysis</i>	<i>Result</i>
<i>Machine direction samples</i>	Data graph	Filtered signal	Signal in machine direction
	Limits (min. max)		Data stability
	Spectrum	Diagnosis SOS-analysis Stability of the spectrum	Machinery problems in machine direction MD
	Characteristics		Statistical information
	Zoom		Detailed analysis of machine component frequencies
	Distribution (=floccule analysis)	Distribution Cumulative distribution	Floccule analysis and average flock size

For this study 5000 m long samples were taken to analyze the effect of each backing roll, the diameters of which can be close to one another.

3.9.1 Analysis in machine direction

The measurement results can be expressed in a time domain which is typically used to get a general impression of the signal content. Mean, deviation, minimum and maximum values and range are used to characterize the whole measurement or a data sample.

A spectrum is calculated using FFT-algorithm by first splitting the whole data sample into smaller length samples. The amplitude spectra are averaged. Selected parameters include the starting point, the number of samples, resolution and the number of separate spectra used in analysis. In the basis weight spectrum, shown in Figure 40, only one sample is used in the calculation of FFT.

Spectra can be analyzed by the rotating frequency components of machines and devices; the database can include base rotation frequencies of rolls, pumps, felts and wires. When a peak is selected in the variation spectrum, the program lists the components that a base frequency or its multiple matches the selected peak.

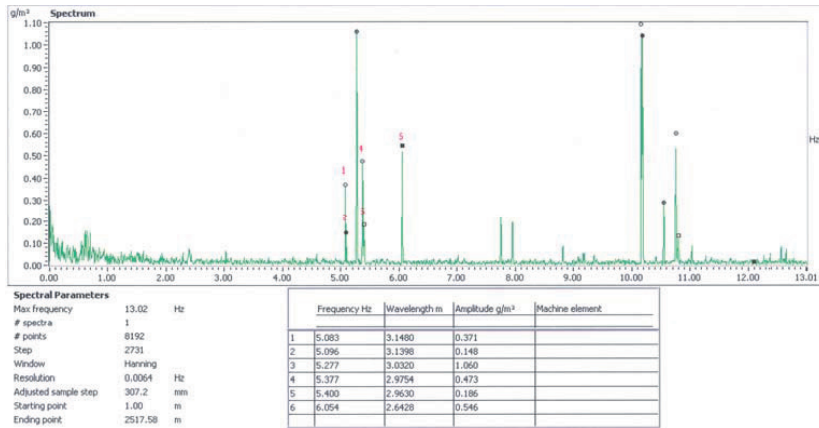


Figure 40 Tapio spectrum analysis reports the peak frequencies and possible matching devices in the database.

Tapio sos-analysis is used to find the relative portion of the total quality variation of the measured quantity caused by a certain device. The result is presented in a time domain and in polar coordinates, in which the graph is drawn using one full revolution of the studied device. In Figure 41 it can be seen that the gloss variation component twice per revolution of the studied device is a significant cause for gloss variation (0.34 %), thus 51 % of the total gloss variation of 0.67 % is caused that device including base frequency and its multiples.

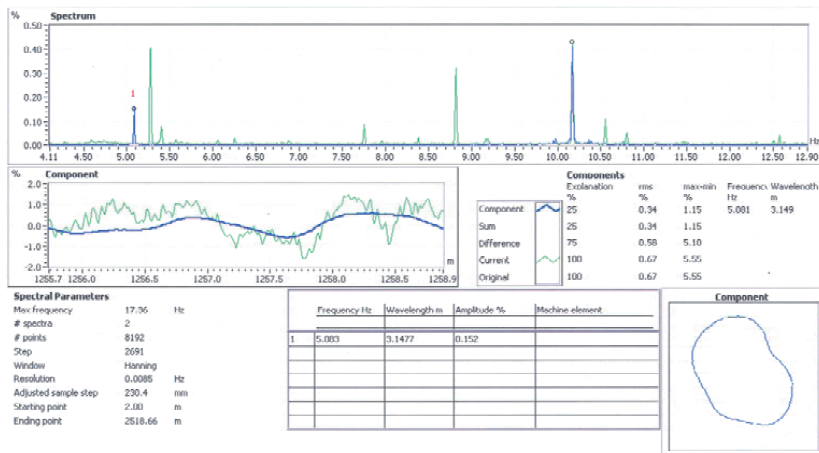


Figure 41 Tapio sos-analysis is used to analyze the portion of a single source in total variation of the measured quantity.

Also, the total quality variation caused by a single device can be calculated. The variation can be presented also in a time domain to give the form of variation. The analyses are used to study the error sources for variations in the machine direction. Typical application is the analysis of

the coating grammage variation which is synchronous to the backing roll of a coating station. With the *sos*-analysis the effect of the backing roll is analyzed. In addition, the improvement of paper quality can be estimated if the backing roll behavior can be improved.

3.10 Survey of backing rolls in industrial use

During the research the dynamic behavior of several backing rolls were investigated.

The measurements for the survey were carried out in several locations in Finland and abroad. Most of the measurements in industry were carried out in a workshop condition e.g. using a balancing machine, as shown in Figure 42 (left). Some measurements were done in operating conditions at a coating machine as shown in Figure 42 (right) to study also the other effects that exist in a paper machine.



Figure 42 Measurement setup at a roll workshop (left) and at a coating station of a paper machine.

The manufacturing method of rolls varies according to a manufacturing unit and year. Different welded steel shell structures and cast iron shell structures are included in this study.

3.11 Roll maintenance

During the years since starting the research several backing rolls have undergone a renewal process to minimize the dynamic geometry error. In this thesis, the renewal processes are not explained in detail, but the methods are presented as alternative choices for improving the dynamic behavior of current rolls instead of purchasing completely new rolls. The presented methods are stiffening of the roll shell, internal grinding, added counterweight method and 3 D grinding.

4 Results

The results chapter is divided into eight sections. The first chapter presents the initial FE analysis which was performed to find out the importance of wall thickness variation on dynamic geometry effects at typical operating conditions of a paper machine.

Second chapter describes the measurement results from the ultrasonic measurements for wall thickness evaluation and for further FE analyses.

Third chapter shows the results of the FE analysis utilizing the wall thickness measurement results presented in the second chapter. As a result of this FE analysis, a dynamic roundness behavior of a laboratory roll is characterized.

The fourth chapter presents the results of verification and validation of the developed dynamic roundness measuring device. In chapter five uncertainty analysis of the measuring device is followed by detailed measurement results of the laboratory roll, which is the same that was used in ultrasonic measurements and FE analysis.

For evaluation of the importance on the studied behavior in paper industry, a survey of the roll behavior is presented in chapter six. Dynamic behavior of backing rolls measured during the past few years is presented.

In chapter seven the coating quality variation measurement results of one industrial case are presented.

In chapter eight, some roll renewal methods are presented. Some of the methods were initiated in the research projects and some are developed by the companies participating in the projects. The analysis of the methods is not detailed including all of the necessary calculations and models – more like presenting the basic ideas and principles.

4.1 Finite element analysis of cross-section model

The cylinder tube is analyzed using shell thickness variation component values derived from the thickness measurement data and web speeds of operating speed range up to 1700 m/min. The results are shown in Figure 43. Each graph consists of the simulated data from three analyzed amplitudes of the harmonic error components of thickness variation.

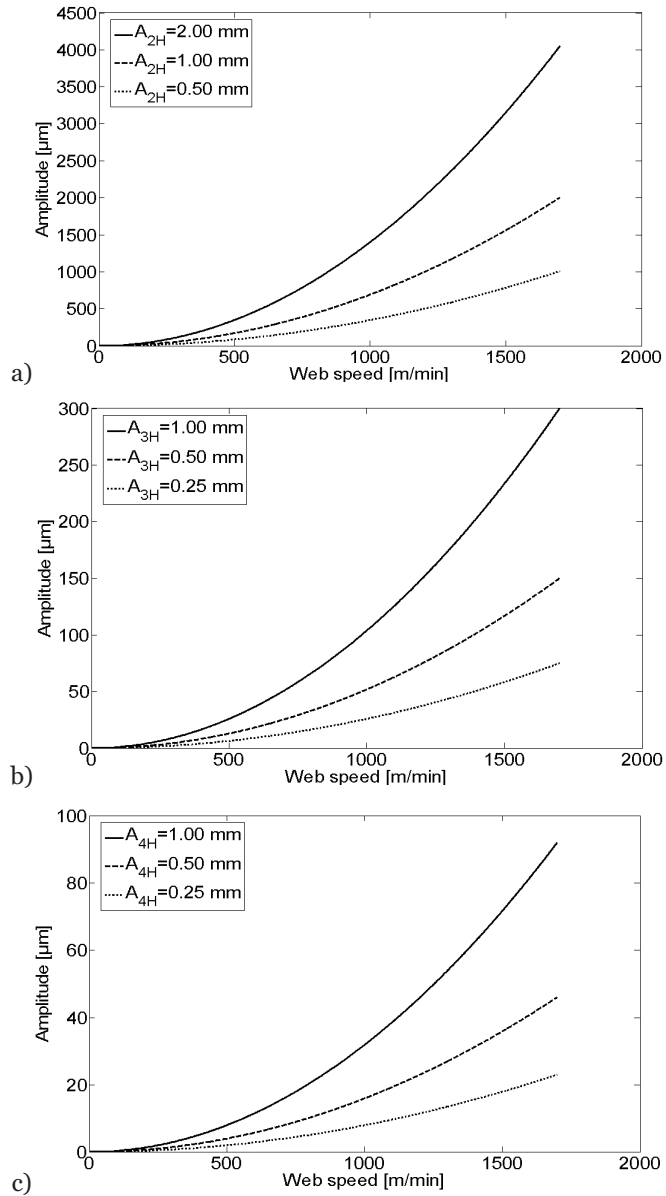


Figure 43 The effect of the wall thickness variation on the dynamic roundness of a paper machine roll. The 2nd (top), 3rd and 4th (bottom) harmonic components of the varying wall thickness variation and matching run-out harmonics of the outer surface.

For example, 1 mm of systematic thickness variation component at 2nd harmonic (oval inner geometry) results in the dynamic geometry change of about 2 mm at the speed of 1700 m/min, as seen in Figure 43. The dynamic

geometry changes for 3rd and 4th harmonic variation components are 0.3 mm and 0.09 mm, respectively.

4.2 Wall thickness of cylinder

The thickness map of a rotating roll is measured using an ultrasonic squirter probe in which the cutting fluid transmits the sound waves from the transducer to the measured object. A total of 720 000 measured points are acquired. Low-pass filtering is used to remove some high frequency noise and peaks. The result is shown in Figure 44.

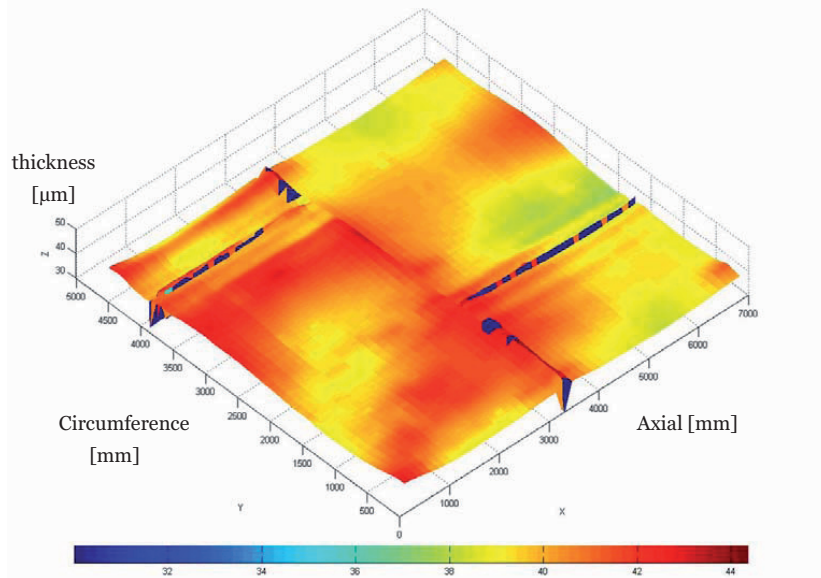


Figure 44 Wall thickness of a measured cylinder varies in the range of 37...43 mm. The values measured at welding seams are excluded. The measuring length of the cylinder shell is 7000 mm and 4700 mm in perimeter.

The measured thickness values are in the range 37...43 mm. The values measured at welding seams are excluded. The back wall echo is scattered at welding seams, hence it is hard to determine the material thickness accurately.

The roll is welded from two rolled cylinders with one radial welding seam close to the lengthwise center of the roll. Also, there are two axial welding seams on the opposite sides of the roll shell. The welding seam positions can be seen in Figure 44 and the positions are shown in Figure 45.

The roundness of the outer surface is typically less than 20 μm, hence the wall thickness variation comes from the inner surface geometry. The most

prominent component in the wall thickness variation is the second harmonic component, i.e. oval geometry. The FFT analysis shows that the average value of 2nd harmonic component is about 2 mm. The other harmonic components are smaller.

4.3 Finite element analysis using measured wall thickness

When the structure and the measured wall thickness of a cylinder are used in FE analysis at a rotating speed of 5.6 Hz, the result is a deformed profile, shown in Figure 45.

The midsection roundness from the linear quasi-static FE analysis of the cylinder shell deforms similarly like the simple cross-section model, and the main component is ovality. The ends remain unchanged because of the used boundary conditions. In the FE analysis, the centrifugal forces and shell stiffness are linked together with finite element formulations of solid elements.

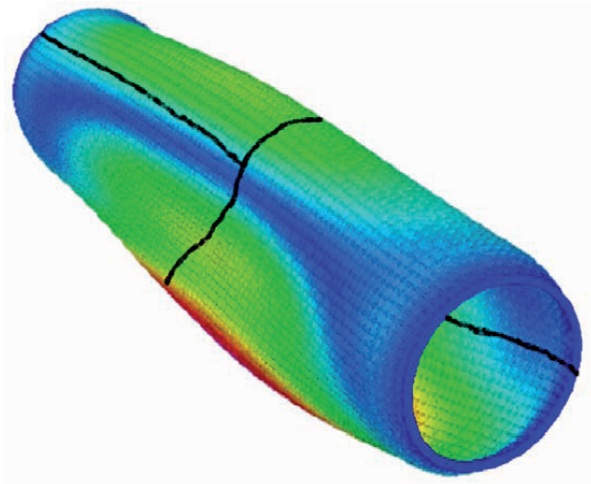


Figure 45 Simulated dynamic geometry of the cylinder at rotating speed of 5.6 Hz. The roundness at the middle cross-section is 196 μm . Black lines show the position of welding seams. (Forsberg 2006)

The dynamic roundness profile changes clearly as a function of rotating speed, as shown in Figure 46. At the speed of 0.2 Hz the roundness is less than 40 μm . An increase in the rotating speed has a clear effect on the dynamic geometry. At the maximum speed of 5.6 Hz the major component in the roundness profile is the 2nd harmonic component i.e. the profile is oval.

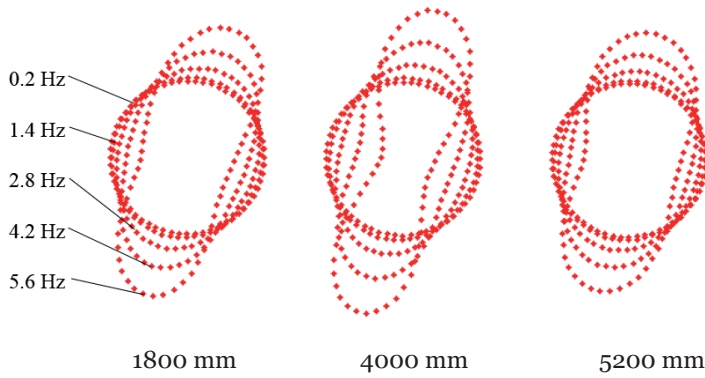



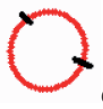













Figure 46 Simulated dynamic roundness of the middle cross-section of the cylinder at rotating speeds of 0.2, 1.4, 2.8, 4.2 and 5.6 Hz. The roundness error increases from 37 μm to 196 μm . (Forsberg 2006)

The roundness values were calculated only for the center cross-section and two cross-sections at 1800 mm and 5200 mm from the drive side end of the shell. The roundness values are presented in Table 10.

Table 10 Roundness profiles and dynamic roundness values in analyzed cross-sections as a function of running speed. Positions of the welding seams are shown with black cross-hairs.

rotating speed [Hz]	Roundness [μm] at a cross-section (c-s) from drive side		
	c-s 1800 mm	c-s 3500 mm	c-s 5200 mm
0.2	 57.1	 37.2	 41.8
1.4	 62.5	 45.7	 45.9
2.8	 80.5	 74.1	 64.6
4.2	 116.3	 123.7	 96.0
5.6	 168.9	 196.3	 142.4

4.4 Roll measurement device

The measurement algorithm and basic setup for measuring sensors were used as developed in earlier research projects. The author replaced the front-end of the measuring system with different types of sensors and signal conditioning and analysis prior to the roundness measuring algorithm. In this study, the development of the method itself is excluded; therefore the uncertainty of measurement is restricted in verification of the results using a calibration reference measurement.

4.4.1 Calibration disc

Measurement uncertainty is evaluated by using a calibration disc which geometry is traced by an official accreditation agency. In literature, calibration discs typically have a perfect geometry or the geometry is a

perfect circle with a sector cut off on one side. Advanced geometries for roundness standards are also developed, as is presented in Chapter 3.3.4.

Table 11 Geometry of the calibration disc is formed using Fourier series amplitude of 10 μm and selected phase terms for each undulation per revolution (upr) component from 2 to 30.

<i>upr#</i>	<i>1</i>	<i>2</i>	<i>3</i>	<i>4</i>	<i>5</i>	<i>6</i>	<i>7</i>	<i>8</i>	<i>9</i>	<i>10</i>
phase [deg]	-	9	200	253	20	55	2	137	1	161
<i>upr #</i>	<i>11</i>	<i>12</i>	<i>13</i>	<i>14</i>	<i>15</i>	<i>16</i>	<i>17</i>	<i>18</i>	<i>19</i>	<i>20</i>
phase [deg]	212	24	200	245	188	16	11	75	211	294
<i>upr #</i>	<i>21</i>	<i>22</i>	<i>23</i>	<i>24</i>	<i>25</i>	<i>26</i>	<i>27</i>	<i>28</i>	<i>29</i>	<i>30</i>
phase [deg]	165	81	104	59	91	44	157	91	321	161

The roundness profile of the calibration disc is generated using Fourier series terms from 2 to 30, as shown in Table 11. The amplitude of each undulation term is chosen to be 10 μm (p-p). The phase of each term is optimized to find a relatively small value for the roundness error using the solver function of Microsoft Excel 2002 SP3. The solver algorithm uses generalized reduced gradient nonlinear optimization code¹. The calculated geometry profile of the calibration disc is shown in Figure 47.

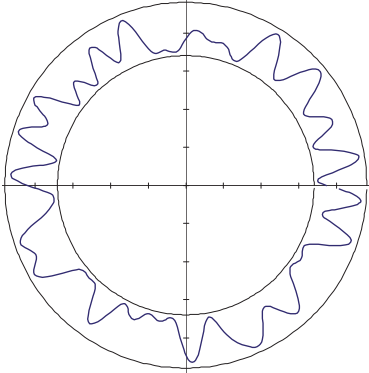


Figure 47 Mathematically determined calibration disc profile.

4.4.1.1 Manufacturing of the disc

The disc diameter is chosen to be large enough to be used in the calibration of industrial measurement devices and small enough to be

¹ algorithm developed by Leon Lasdon, University of Texas at Austin, and Allan Waren, Cleveland State University). <http://www.frontsys.com>.

handled easily and measured in Mikes (Centre for Metrology and Accreditation). The diameter of 503 mm and the width of 54 mm resulted in the mass of approximately 50 kg. The material is cold-work tool steel Uddeholm's Rigor (AISI A2). The basic geometry was machined before hardening and annealing with sub-zero treatment.

The chosen geometry was machined using a 3D grinding machine of a Finnish paper mill, as shown in Figure 48 (left). The machining accuracy was checked after the machining using the measuring instrument of the grinding machine. The amplitude, the phase and the direction of the measured profile, shown in Figure 48 (right), is not scaled to correspond to the determined profile shown in Figure 47. The undulation per revolution (not shown) seemed to be close to the desired 10 μm amplitude for the lobes from 2 to 30.

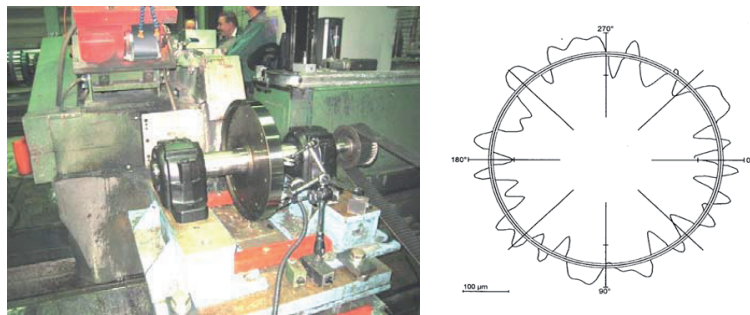


Figure 48 The grinding of the desired geometry was done at a Finnish paper mill (left). The measured roundness profile is shown on the right.

4.4.1.2 Reference measurement of the calibration disc

The calibration disc was measured at Mikes using a coordinate measuring machine Mitutoyo Legex 9106 which is installed in vibration and temperature controlled environment. The disc was installed on the measuring bed of the device and the rotational position of the disc was adjusted according to the reference mark on the disc, as shown in Figure 49.

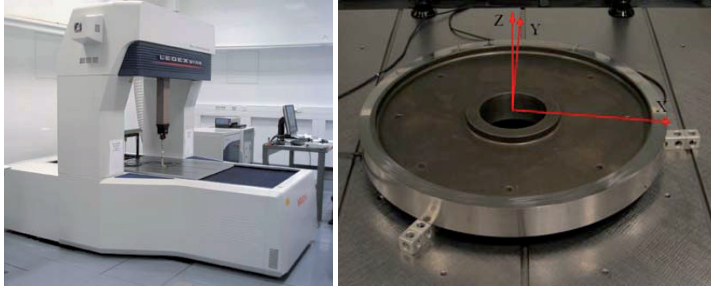


Figure 49 The reference measurement was carried out with Mitutoyo Legex 9106 coordinate measuring machine at Mikes.

The measurement uncertainty of the device is presented as a maximum permissible error for a length measurement MPE_e:

$$\text{MPE}_e = (0.35 + L/1000) \mu\text{m}, L = \text{mm and} \quad (52)$$

When this is applied for the dimensions of the disc we get

$$\text{MPE}_e = 0.85 \mu\text{m} \quad (53)$$

According to the DIN EN ISO 10360 MPE defines a maximum value that a measuring deviation is not allowed to exceed. The standard uncertainty of measurement u_{ref} is calculated in this study with a coverage factor $k=3$ (99.73 % probability)

$$u_{\text{ref}} = 0.28 \mu\text{m}. \quad (54)$$

The values from the reference measurement are given in cartesian coordinates. The amplitudes of the harmonic components i.e. undulations per revolution (upr) shown in Figure 50 are calculated after transformation into amplitude and phase terms (polar coordinates).

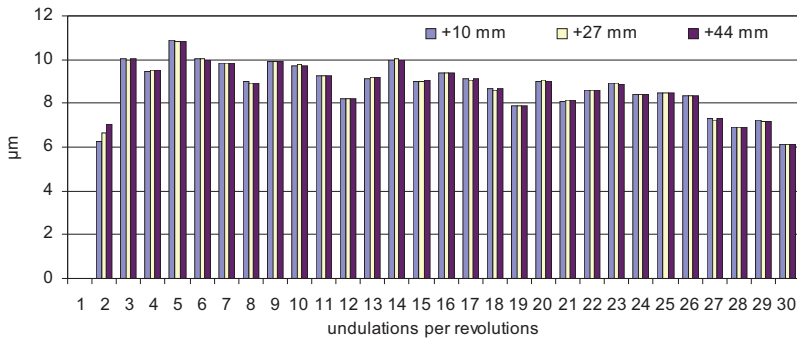


Figure 50 The harmonic components of the reference disc at different cross-sections 10 mm, 27 mm and 44 mm.

The amplitude values of the reference disc are close to what is the original aim for 10 μm amplitude for each component. The 2nd harmonic is

surprisingly low, and the alignment of the disc during the measurement is not confirmed. If the measurement plane is misaligned, the results would be seen in the 2nd harmonic component. The 2nd harmonic component differs from the targeted value that might indicate uncertainty in that measurement. The 2nd harmonic was 9.3 μm in the previous measurement carried out with the measurement device at the paper mill.

Further measurements and comparisons are carried out mostly close to the +27 mm cross-section; hence the measured harmonic component amplitudes in that cross-section are given in Table 12.

Table 12 The measured reference amplitudes of the calibration disc.

<i>upr#</i>	<i>1</i>	<i>2</i>	<i>3</i>	<i>4</i>	<i>5</i>	<i>6</i>	<i>7</i>	<i>8</i>	<i>9</i>	<i>10</i>
<i>amp</i> <i>[μm]</i>	-	6.6	10.0	9.5	10.9	10.0	9.8	8.9	9.9	9.8
<i>upr #</i>	<i>11</i>	<i>12</i>	<i>13</i>	<i>14</i>	<i>15</i>	<i>16</i>	<i>17</i>	<i>18</i>	<i>19</i>	<i>20</i>
<i>amp</i> <i>[μm]</i>	9.3	8.2	9.2	10.0	9.0	9.4	9.1	8.6	7.9	9.0
<i>upr #</i>	<i>21</i>	<i>22</i>	<i>23</i>	<i>24</i>	<i>25</i>	<i>26</i>	<i>27</i>	<i>28</i>	<i>29</i>	<i>30</i>
<i>amp</i> <i>[μm]</i>	8.1	8.6	8.9	8.4	8.5	8.4	7.3	6.9	7.2	6.1

4.4.2 Measuring device calibration measurements

The dynamic roundness measuring device calibration measurements are carried out at the same rotational frequencies as the laboratory roll is measured to determine the measurement uncertainty with relevant measurement parameters and conditions.

The calibration disc is setup up in a measuring rig as shown in Figure 51. The calibration disc is fixed to the shaft using SKF Concentra element SHL100. The same component is used for bearing assembly; SKF 1222 bearings are assembled in SNL522-619 housings. The disc can be attached to any axial position in the bearing span.

A rotational pulse encoder is attached to the end of the shaft, as shown in Figure 52. The index of the encoder is adjusted according to the reference mark on the calibration disc.

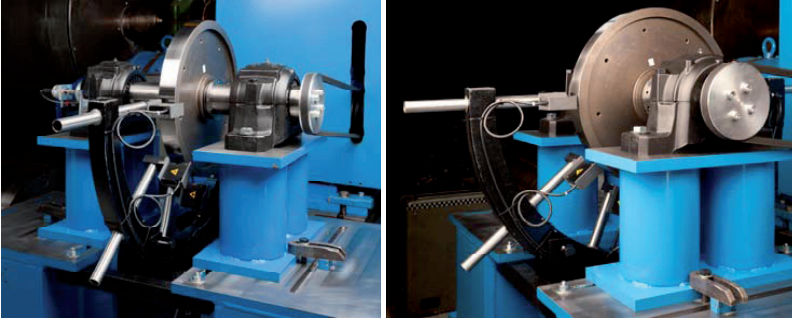


Figure 51 Measurement setup for determination of measurement uncertainty of the device.

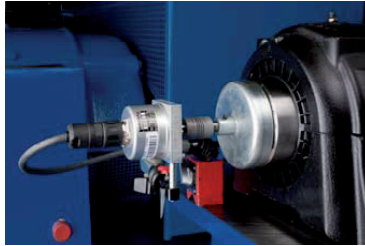


Figure 52 A rotary pulse encoder is fixed to the end of the shaft for timing the measurement.

All sensor angles are set within ± 0.1 degrees using an inclinometer with a digital readout. The measuring frame is aligned against the rotational axis within the same accuracy of ± 0.1 degrees. The center point of the measuring frame is set within ± 0.5 mm of the rotational center point of the disc. According to Väänänen (1993) this accuracy is more than enough for required accuracy of the measuring system.

The zero index is positioned within accuracy of ± 0.3 degrees to the index mark on the calibration disc. The parts of SKF Concentra fittings are also marked for reference angles. Asynchronous bearing error motion is attenuated by time synchronous averaging.

Sensors are repositioned between measurement sets. The frame remains in its initial position until deliberately moved for further analysis.

In analysis of even and odd lobes it must be noted that the algorithm uses different functions for the calculation of even lobe components.

Calibration measurements are carried out in several test setups. The list of tested parameters is shown in Table 13. Each measurement is repeated ten times; thus the total number of experimental uncertainty evaluation measurements is 490.

Table 13 Measurement parameters in experimental uncertainty analysis.

Set #	Rotating speed [Hz]	Revolutions N	Filtering cut-off factor	Axial position [mm]	Frame eccentricity [mm]
1	0.22, 1.46, 2.93, 4.39, 5.85	100	100	27	0
2	5.85	1, 10, 20, 50, 100, 200, 500	100	27	0
3	5.85	100	15, 30, 50, 100	27	0
4	5.85	100	100	10, 27, 28, 29, 30, 31, 32, 44	0
5	5.85	100	100	28	-3, -2, -1, 0, +1, +2, +3
6	0.2, 1, 2, 3, 4, 5, 6, 7, 8, 9, 10, 11, 12, 13, 14, 15, 16, 17	100	100	28	0

The selected rotating speeds at the test set #1 are the same rotating speeds that are used in backing roll measurements. The further presentation of this measurement set is combined with the test set #6, which is carried out for wider speed range coverage.

The revolutions parameter in the test set #2 is used to set the number of revolutions N used for time synchronous averaging. The filtering cut-off factor sets the cut-off frequency of anti-alias filtering board according to the rotating speed e.g. a rotating frequency of 2 Hz with a cut-off factor of 100 results in a cut-off frequency of 200 Hz. The test set #3 is used to analyze the amplitude attenuation behavior around the cut-off frequency.

The axial position of the measuring frame is changed in the test set #4, because the surface characteristics have been mentioned as a source for error with laser sensors as the surface roughness and speckle patterns change. Also, along the axis there is some difference in the roundness profile of the calibration disc that was observed in reference measurements at Mikes.

The effect of eccentric position of the measuring frame is checked with the test set #5. The original analysis of the frame positioning error is carried out by Väänänen (1993) and there should not be significant error within the tested parameter range. The frame is displaced horizontally within ± 3 mm, but in practice the frame can be easily centered within ± 0.5 mm.

The test set #6 is a general test over a wide rotating frequency range. This test is to verify the usability of the measuring device for faster rotating rolls i.e. rolls with a smaller diameter in a faster paper machine.

4.4.3 Effect of synchronous averaging

The effect of time synchronous averaging is tested on a series of measurements where the number of revolutions included in the measurement is increased from 1 revolution i.e. no averaging up to 500 revolutions. The results are shown in Figure 53. There is a slight change in the amplitudes on some harmonic components of roundness as the number of revolutions in the averaging increases. The largest changes are at the 2nd and 3rd harmonic components. There are some individual deviations from the mean as can be seen e.g. in the 9th, 13th and 25th components.

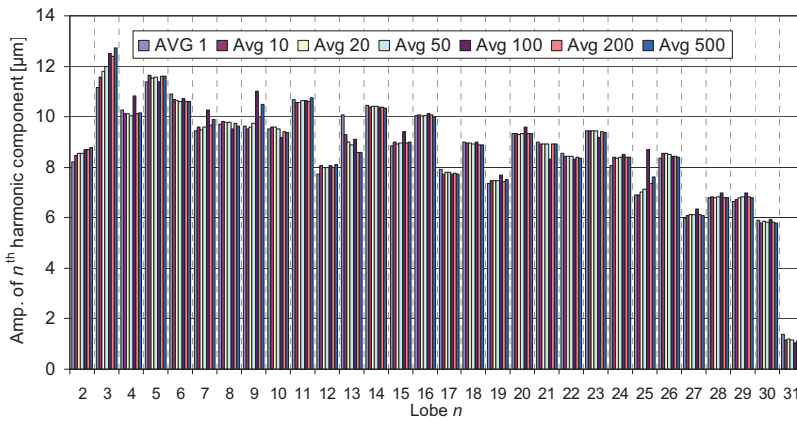


Figure 53 The effect of time synchronous averaging on the amplitudes of the 2nd... 31st harmonic component of the roundness profile.

The more important phenomenon can be seen in Figure 54, where the expanded uncertainty of measurement U is plotted against the number of revolution N used in the time synchronous averaging. Without averaging the uncertainty of measurement U is approximately 1 μm , and U decreases rapidly when the number of averagings increases.

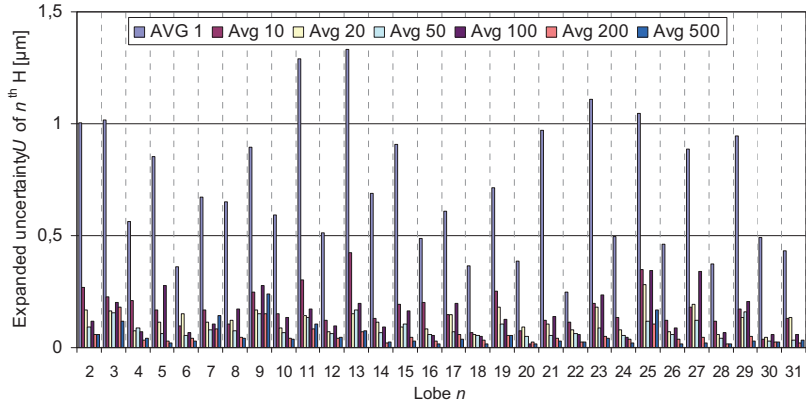


Figure 54 The effect of time synchronous averaging on the expanded uncertainty U of the 2nd... 31st harmonic components of the roundness profile.

4.4.4 Effect of cut-off frequency

The effect of cut-off frequency is measured using a series of measurements with four different set values. The set value is a multiplying factor k_{co} which sets the cut-off frequency f_{co} of the filtering board $f_{co} = k_{co} \cdot f_r$, where f_r is the rotating frequency of the roll. By definition the amplitude should be attenuated by 3 dB at the cut-off frequency.

The mean values of the measurement results are shown in Figure 55.

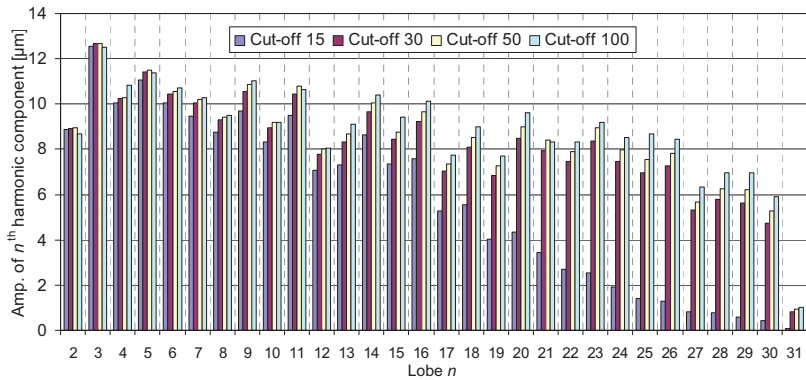


Figure 55 The effect of cut-off frequency on the amplitudes of the 2nd...31st harmonic components of the roundness profile.

The measurement results at lower components are in a good agreement with each other. The cut-off frequency behaves as expected and the values of higher components are attenuated. There is also a slight attenuation in all signals in the pass band that could be corrected in the calculation routine.

The power of a correctly chosen filtering parameter can be seen in Figure 56. The unwanted harmonic components and noise are attenuated effectively with lower cut-off frequency.

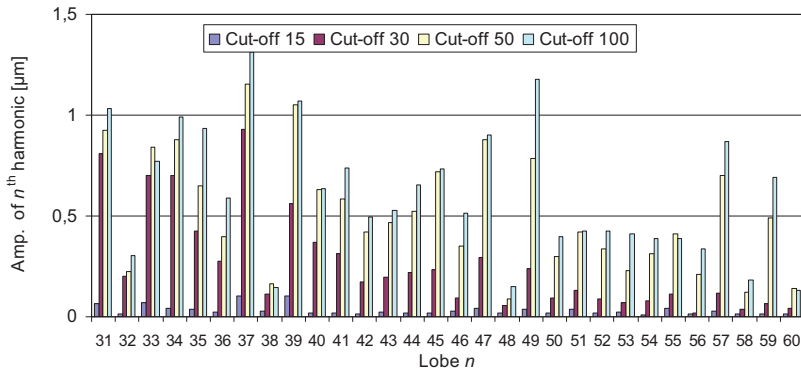


Figure 56 The effect of the cut-off frequency on the amplitudes of the 31st... 60th harmonic components of the roundness profile.

4.4.5 Effect of measuring axial position

This measurement setup is to reveal the effect of the measuring surface and minor changes in surface characteristics. Although the calibration disc has a ground metal surface the structure under the laser beam might reveal phenomena reported as an effect of speckles (Dorsch 1994). Actually, there are some visible differences because of a typical ground surface of the disc. Those differences are very hard to characterize from one location to another as a standard surface roughness measurement doesn't see the difference. There is some visible difference in the individual components, as can be seen in Figure 57. The calculated expanded uncertainty of the measurement vary depending on the axial position of the measurement and the values range from less than 0.1 μm to over 0.6 μm.

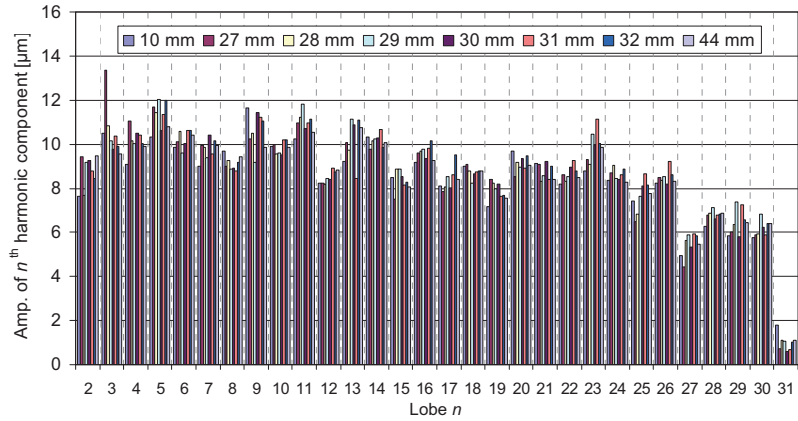


Figure 57 The effect of the axial position of the measuring frame on the amplitudes of the 2nd... 31st harmonic components of the roundness profile.

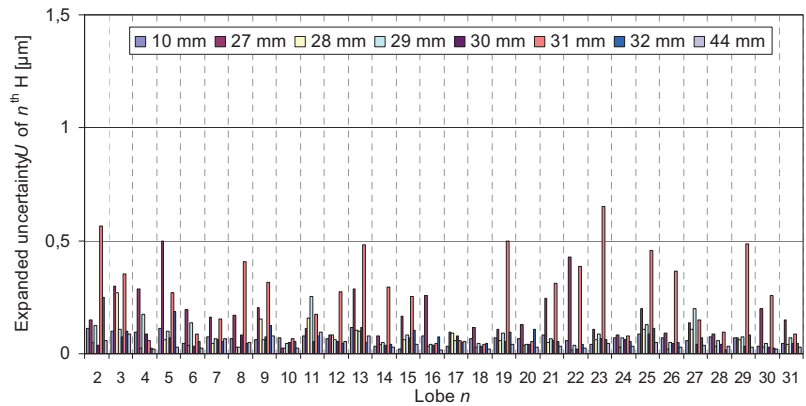


Figure 58 The effect of axial position of the measuring frame on the expanded uncertainty U of the 2nd... 31st harmonic components of the roundness profile.

4.4.6 Measuring frame eccentricity

The effect of measuring frame eccentricity is tested by varying the position of the frame relative to the rotational axis of the disc. The displacement is done in the horizontal axis only; hence the even lobe undulations should have no change due to the displacement, because the opposing sensors would measure the same diameter profile. This setup gives a reference if there is a difference in the characteristics of even and odd lobe undulations.

The frame is displaced in the range of -3...+3 mm in 1 mm steps where 0 mm represents the perfect centering of the frame. The movement of the frame is done without a linear motion unit so the absolute positions of the laser beams on the disc are expected to vary a little.

The measured roundness values are shown in Figure 59. All values are within $\pm 1 \mu\text{m}$ and there are no clear ascending or descending trends in even or odd lobe undulations. There are single measurements with harmonic components that deviate clearly from the mean value.

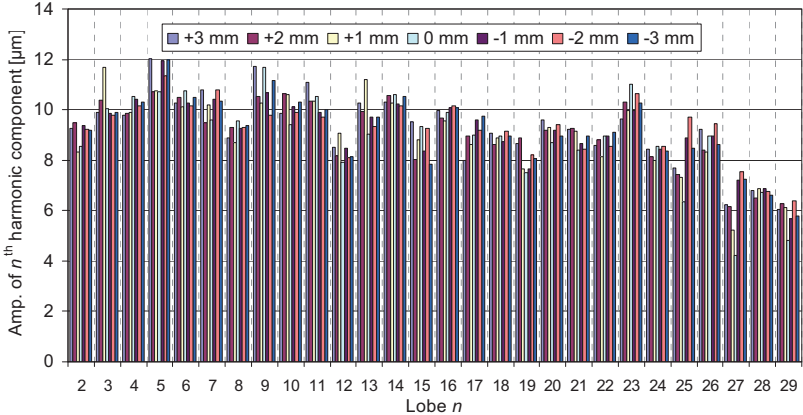


Figure 59 The effect of the measuring frame eccentricity on the amplitudes of the 2nd... 31st harmonic components of the roundness profile.

The expanded uncertainty of each of the ten measurement series is shown in Figure 60. For each measurement series the uncertainty is less than $0.1 \mu\text{m}$. The measuring frame has been fixed during each of the measurement series, and the repeatability of the measurement is good.

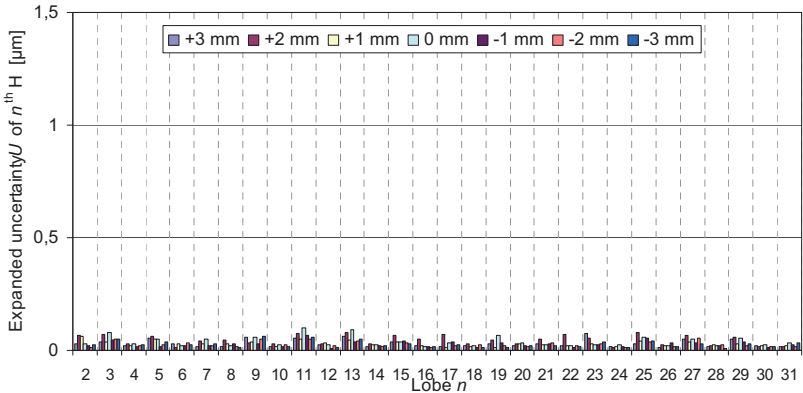


Figure 60 The effect of the measuring frame eccentricity on the expanded uncertainty U of the 2nd... 31st harmonic components of the roundness profile.

4.4.7 Rotating speed range test

In this measurement series the speed is increased from 0.2 Hz to 17 Hz. The amplitudes of the 2nd... 31st harmonic components of the roundness profile are presented in Figure 61. The values of each component are approximately within 1 μm .

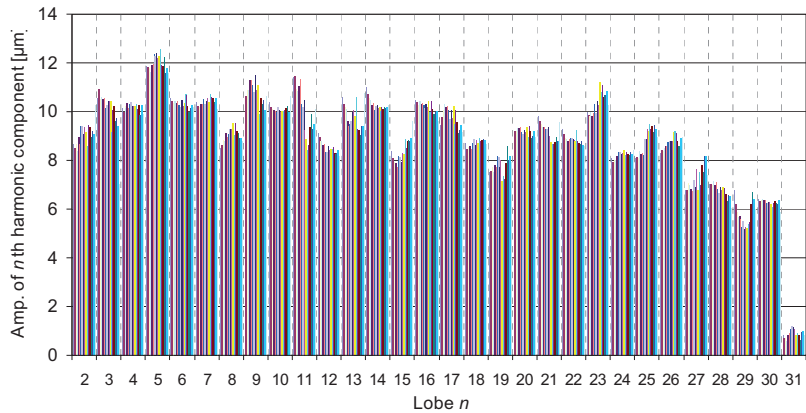


Figure 61 The effect of the rotating speed from 0.2 Hz to 17 Hz on the amplitudes of the 2nd... 31st harmonic components of the roundness profile.

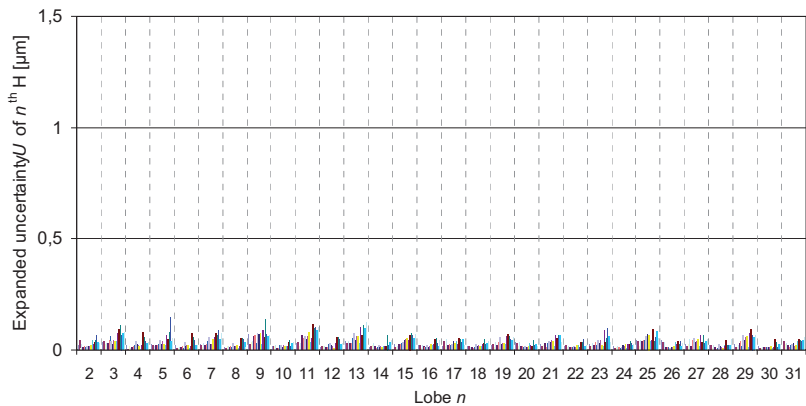


Figure 62 The effect of the rotating speed from 0.2 Hz to 17 Hz on the expanded uncertainty of measurement U of the 2nd... 31st harmonic components of the roundness profile.

The effect of rotating speed on the uncertainty of measurement can be seen in Figure 62. There seems to be a tendency that the uncertainty of a measurement increases for each harmonic component as the speed increases.

4.5 Laboratory measurements of test roll

Laboratory measurements of the test roll are carried out at 13 cross-sections. Each cross-section is measured at constant rotating speeds starting from 50 m/min which is a typical jogging speed of a paper machine. The range from 100 to 1600 m/min is measured at 100 m/min steps. The measurement speed is given as m/min, because the program outputs the figures in a quantity that is commonly used in paper industry. For convenience and scientific purpose, Table 14 presents the used measurements speeds in a more common SI unit, Hertz [Hz].

Table 14 Interpretation of web speed [m/min] in SI-units [Hz] in the following software printouts.

<i>web speed [m/min]</i>	<i>rotating speed [Hz]</i>
50	0.2
100	0.4
200	0.7
300	1.1
400	1.5
500	1.8
600	2.2
700	2.6
800	2.9
900	3.3
1000	3.7
1100	4.0
1200	4.4
1300	4.8
1400	5.1
1500	5.5
1600	5.9

4.5.1 Roundness at measured cross-sections

Roundness measurement results are presented using only the lowest harmonic components (2...4) of the measured roundness profile. In the literature, these components are often referred as undulations per revolution upr. Any systematic changes in these components can be observed.

The measurement result is also shown as a dynamic change which is calculated from the roundness component vectors by subtracting the static measurement vector from the result that is measured at higher speed. These values can be compared with the values from the FE analysis. A detailed presentation of results is limited to five measured cross-sections

although the results of all 13 measured cross-sections are used for further analyses.

4.5.1.1 Dynamic roundness at cross-section #1

Cross-section #1 is measured at 100 mm from the drive side (DS) end of the roll shell. Therefore, the measurement takes place at the end plate area. Figure 63 shows the lowest harmonics of all roundness profile measurements as a function of running speed. It can be seen that no major changes are present.

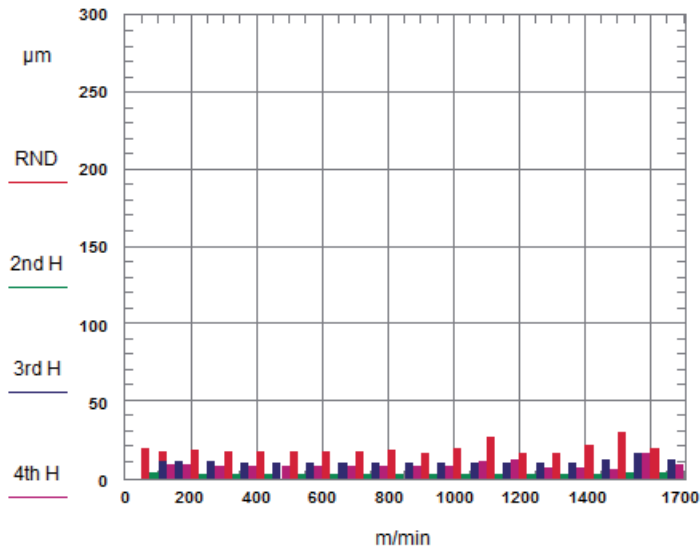


Figure 63 The roundness (RND), ovality (2^{nd} H), triangular (3^{rd} H) and four-lobe (4^{th} H) components are shown as a function of running speed at the cross section#1 100 mm from the drive side end plate.

The dynamic change in the measured speed range is very little and within the uncertainty limits of the measurement i.e. the geometry is practically constant, as shown in Table 15. The dynamic change is two micrometers or less. With low amplitudes under two micrometers, the phase has no significant meaning and therefore is not reported.

Table 15 Amplitude (μm) and phase of the dynamic change in roundness components (*upr*) as a function of running speed at cross-section #1.

<i>upr</i>	amplitude and phase							
	400 m/min		800 m/min		1200 m/min		1600 m/min	
	amp [μm]	phase [$^\circ$]	amp [μm]	phase [$^\circ$]	amp [μm]	phase [$^\circ$]	amp [μm]	phase [$^\circ$]
2	0	-	0	-	0	-	1	-
3	0	-	0	-	1	-	1	-
4	0	-	1	-	2	39	1	-

4.5.1.2 Dynamic roundness at cross-section #4

Cross-section #4 is measured at 2050 mm from the drive side (DS) end of the roll shell. Figure 64 shows the lowest harmonics of all 17 roundness measurements as a function of the running speed. It can be seen that the roundness (RND) is increasing from 17 μm to 210 μm as a result of the increasing 2nd harmonic from 6 μm to 203 μm .

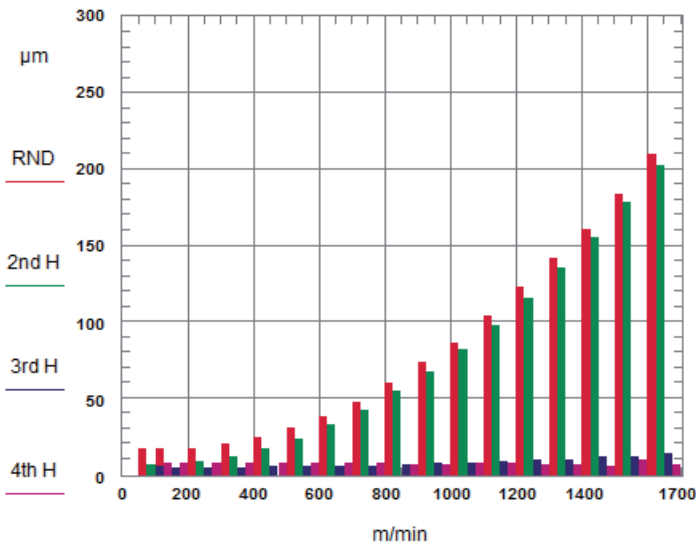


Figure 64 The roundness (RND), ovality (2nd H), triangular (3rd H) and four-lobe (4th H) components are shown as a function of running speed at the cross section #4 2050 mm from the drive side end plate.

The change in the 2nd harmonic is evident and the amplitude is increasing up to 197 μm at 1600 m/min, as shown in Table 16. The dynamic changes of the components 3 and higher are less. The maximum change is less than 9 μm for the 3rd component and less than 2 μm for the other components.

The phase of the 2nd harmonic stays at approximately 111°. This indicates the deformation increases in the same direction.

Table 16 Amplitude (μm) and phase of the dynamic change in roundness components (upr) as a function of running speed at cross-section #4, 2050 mm from DS.

upr	amplitude and phase							
	400 m/min		800 m/min		1200 m/min		1600 m/min	
	amp [μm]	phase [$^\circ$]	amp [μm]	phase [$^\circ$]	amp [μm]	phase [$^\circ$]	amp [μm]	phase [$^\circ$]
2	11	113	49	111	110	111	197	111
3	0	-	2	101	5	99	9	94
4	1	-	1	-	1	-	2	73

4.5.1.3 Dynamic roundness at cross-section #7

Cross-section #7 is measured at the middle cross-section of the roll shell. Figure 65 shows the lowest harmonics of all 17 roundness measurements as a function of the running speed. It can be seen that the roundness (RND) is increasing from 20 μm to 267 μm as a result of the increasing 2nd harmonic from 9 μm to 258 μm .

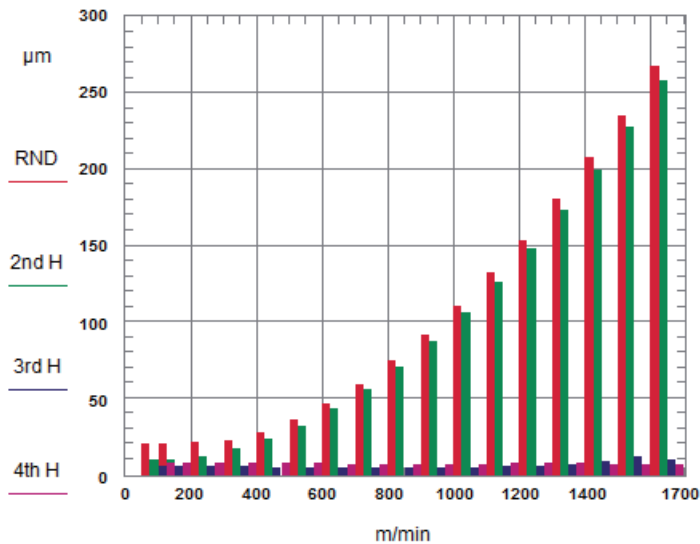


Figure 65 The roundness (RND), ovality (2nd H), triangular (3rd H) and four-lobe (4th H) components are shown as a function of running speed at the middle cross-section.

The change in the 2nd harmonic is significant, as can be seen in Table 17, and the amplitude is increasing up to 249 μm at 1600 m/min. The dynamic

changes of the components 3 and higher are very little. The maximum change is 6 μm for the 3rd component. The phase of the 2nd harmonic stays at 107° indicating the deformation increases in the same direction.

Table 17 Amplitude (μm) and phase of the dynamic change in roundness components (*upr*) as a function of running speed in the middle cross-section.

<i>upr</i>	amplitude and phase							
	400 m/min		800 m/min		1200 m/min		1600 m/min	
	amp [μm]	phase [°]	amp [μm]	phase [°]	amp [μm]	phase [°]	amp [μm]	phase [°]
2	14	108	62	107	140	107	249	107
3	1	-	2	14	3	62	6	104
4	0	-	1	-	2	52	1	-

4.5.1.4 Dynamic roundness at cross-section #10

Cross-section #10 is measured at 5950 mm from the drive side (DS) end of the roll shell. Figure 66 shows the lowest harmonics of all 17 roundness measurements as a function of running speed. It can be seen that the roundness (RND) is increasing from 28 μm to 202 μm as a result of the increasing 2nd harmonic from 20 μm to 191 μm .

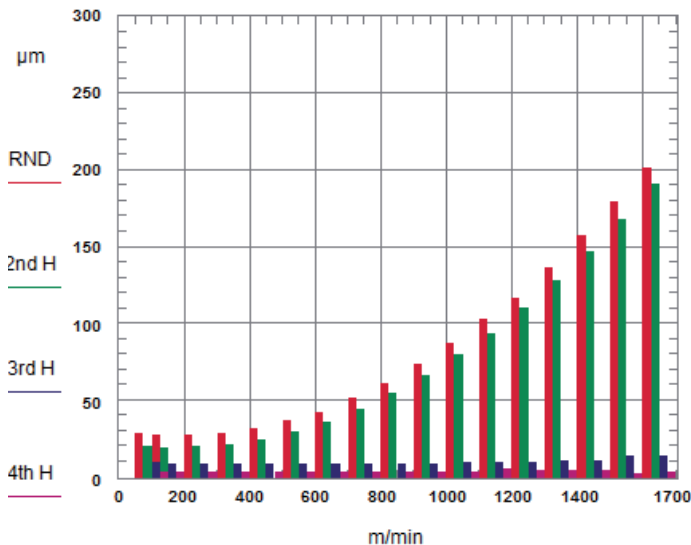


Figure 66 The roundness (RND), ovality (2nd H), triangular (3rd H) and four-lobe (4th H) components are shown as a function of running speed at the cross section #10, 5950 mm from the drive side end plate.

The change in the 2nd harmonic is significant, as shown in Table 18, and the amplitude is increasing up to 175 μm at 1600 m/min. The dynamic changes of the components 3 and higher are considerably less. The maximum change is 5 μm for the 3rd component. The phase of the 2nd harmonic rotates slightly from 122° to 104°.

Table 18 Amplitude (μm) and phase of the dynamic change in roundness components (upr) as a function of running speed at cross-section #10, 5950 mm from DS.

upr	<i>Bending amplitude and phase</i>							
	<i>400 m/min</i>		<i>800 m/min</i>		<i>1200 m/min</i>		<i>1600 m/min</i>	
	<i>amp</i>	<i>phase</i>	<i>amp</i>	<i>phase</i>	<i>amp</i>	<i>phase</i>	<i>amp</i>	<i>phase</i>
	<i>[μm]</i>	<i>[$^{\circ}$]</i>	<i>[μm]</i>	<i>[$^{\circ}$]</i>	<i>[μm]</i>	<i>[$^{\circ}$]</i>	<i>[μm]</i>	<i>[$^{\circ}$]</i>
2	7	122	38	108	94	105	175	104
3	1	-	1	-	2	70	5	15
4	0	-	0	-	1	-	1	-

4.5.1.5 Dynamic roundness at cross-section #13

Cross-section #13 is measured at 7900 mm from the drive side (DS) end of the roll shell. Hence the measurement is taken at the tending side end plate area. Figure 67 shows the lowest harmonics of all 17 roundness measurements as a function of running speed. It can be seen that no major changes are present and the static roundness error stays approximately the same through the speed range.

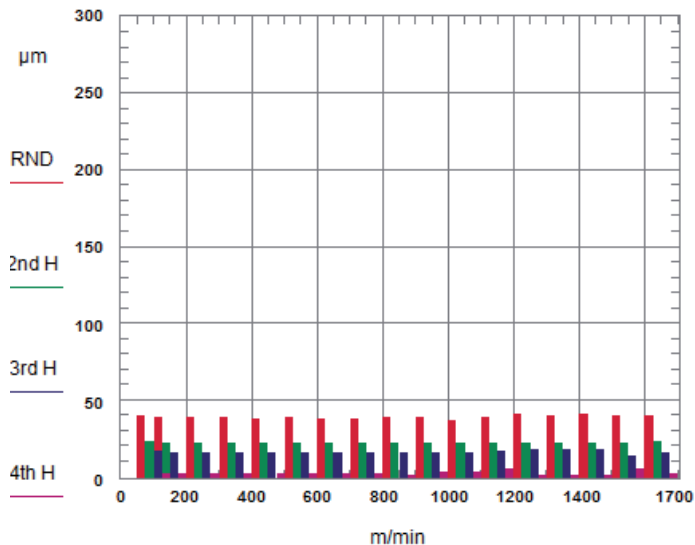


Figure 67 The roundness (RND), ovality (2nd H), triangular (3rd H) and four-lobe (4th H) components are shown as a function of running speed at the cross section #13, 7900 mm from the drive side end plate.

Practically no changes in the measured components (Table 19) can be seen. The dynamic change of the components is very little and within the uncertainty limits of the measurement. The maximum change is 1 μm or less.

Table 19 Amplitude (μm) and phase of the dynamic change in roundness components as a function of running speed at cross-section #13, 7900 mm from DS.

upr	Bending amplitude and phase							
	400 m/min		800 m/min		1200 m/min		1600 m/min	
	amp [μm]	phase [°]	amp [μm]	phase [°]	amp [μm]	phase [°]	amp [μm]	phase [°]
2	1	-	1	-	1	-	1	-
3	1	-	1	-	1	-	1	-
4	0	-	1	-	1	-	1	-

4.5.2 Dynamic bending

Dynamic bending results are shown as a reference to evaluate the importance of dynamic geometry in the dynamic behavior of a backing roll. Only three cross-sections are included in this section, because the dynamic bending analysis is not the focus point of this study.

The dynamic bending behavior is shown in Figure 68 for reference to see the relative effect of dynamic bending and dynamic roundness on the total erroneous behavior. Maximum bending values are at the drive side end, in the middle and at the tending side end $22\ \mu\text{m}$, $26\ \mu\text{m}$ and $16\ \mu\text{m}$, respectively. All measured dynamic bending values as a function of running speed are presented in Table 20.

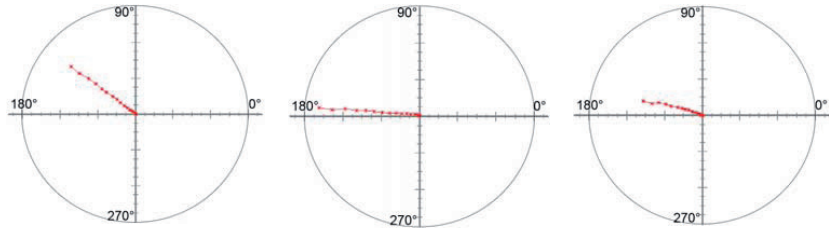


Figure 68 Dynamic bending of drive side end (left), the middle cross-section and at the tending side (right) is increasing as a function of running speed. The circle defines $30\ \mu\text{m}$ bending amplitude.

Table 20 Dynamic bending amplitude of the backing roll as a function of running speed.

speed m/min	Bending amplitude and phase at cross-section					
	100 mm		4000 mm		7900 mm	
	amp [μm]	phase [$^{\circ}$]	amp [μm]	phase [$^{\circ}$]	amp [μm]	phase [$^{\circ}$]
100	0	-	0	-	0	-
200	1	128	0	-	0	-
300	1	135	1	144	0	-
400	2	141	1	157	1	161
500	2	142	2	165	1	158
600	3	142	3	169	2	159
700	4	142	5	171	3	159
800	5	141	6	172	4	158
900	7	141	8	174	5	160
1000	8	141	10	174	6	160
1100	10	142	12	174	7	161
1200	12	142	14	173	9	163
1300	14	142	16	174	10	163
1400	16	141	20	174	12	163
1500	19	143	23	176	14	166
1600	22	142	26	175	16	166

4.5.3 Run-out

Run-out measurement results are presented only in three cross-sections, just to give an impression of the nature of the dynamic behavior in operating condition. This type of measurement is not designed for vibration analysis, because of quite large steps between the measured speed steps.

4.5.3.1 Drive side end

From the measurement in the horizontal direction at the drive side end, shown in Figure 69, it can be seen that two harmonics arise in the measured speed range; the 4th harmonic peak 120 μm close to 1100 m/min i.e. 4.0 Hz and 3rd harmonic of 90 μm at 1500 m/min i.e. 5.5 Hz indicating a resonance vibration.

The run-out behavior also shows the trend of the components over the speed range. The dominating error component is the first harmonic of 50 μm over the 2nd harmonic of 11 μm . The bending stiffness of the roll shell is higher than the stiffness of the roll shaft. Therefore the bending takes place either at the shaft or at the flexible supports. The measured cross-section is in the end plate area; therefore the shell stiffness at this cross-section is preventing large deformations.

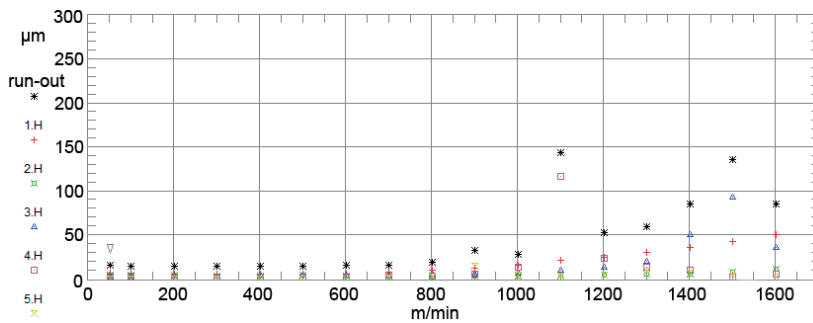


Figure 69 Horizontal run-out measurement at the drive side (DS 100 mm) end of the roll shell as a function of running speed. Two narrow band harmonics arise; the 4th harmonic peak at 1100 m/min and 3rd harmonic close to 1500 m/min.

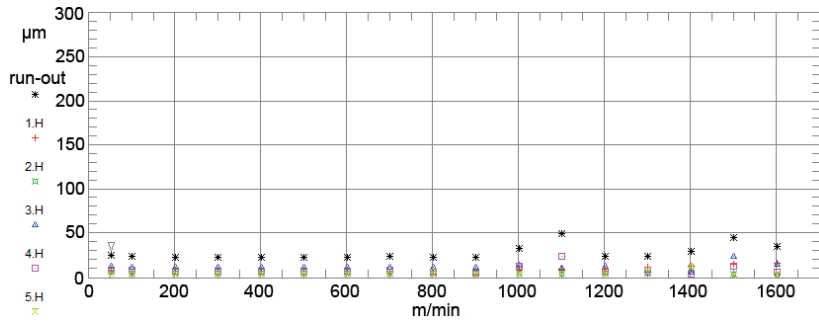


Figure 70 Vertical run-out measurement at the drive side (DS 100 mm) end of the roll shell as a function of running speed.

In the vertical run-out measurements, shown in Figure 70, the resonance vibration amplitudes are much lower than in the horizontal measurements at the same cross-section. The 1st harmonic is larger than the 2nd harmonic.

4.5.3.2 Middle cross-section

From the measurement in the horizontal direction at the middle cross-section (Figure 71) the run-out behavior shows significant change in the 2nd harmonic component, the value of which is increasing from 9 µm to almost 260 µm. At the same time, the first harmonic increases from 25 µm to 70 µm.

Two narrow band harmonics arise in the measured speed range; the 4th harmonic peak 120 µm close to 1100 m/min i.e. 4.0 Hz and 3rd harmonic of 90 µm at 1500 m/min i.e. 5.5 Hz indicating there is a resonance vibration close to that measured speed.

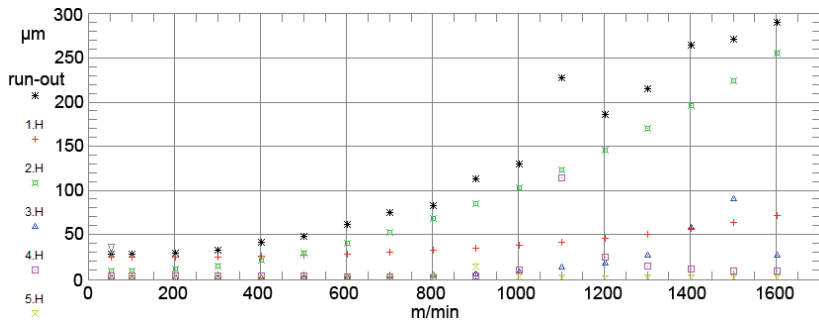


Figure 71 Horizontal run-out measurement at the middle cross-section of the roll as a function of running speed. The 2nd harmonic of run-out is dominating. Two narrow band harmonics arise; the 4th harmonic peak at 1100 m/min and 3rd harmonic close to 1500 m/min.

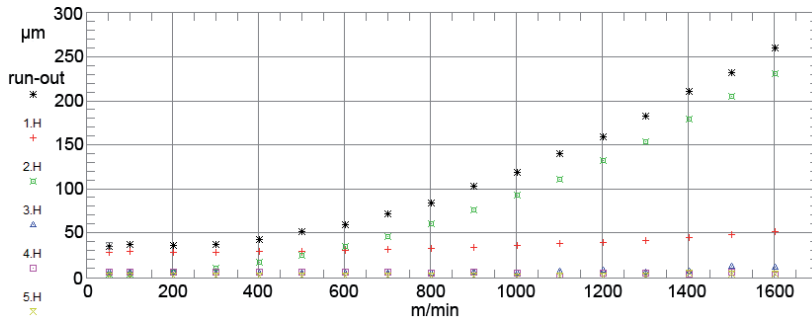


Figure 72 Vertical run-out measurement at the middle cross-section of the roll shell as a function of running speed.

In the vertical run-out measurements, shown in Figure 72, the resonance vibration amplitudes are practically non-existent. The 1st and the 2nd harmonic component behavior are similar to the horizontal measurement.

4.5.3.3 Tending side

From the measurement in the horizontal direction at the tending side (Figure 73) the run-out behavior shows a little change in the 1st harmonic component. Also, the narrow band harmonics arise in the measured speed range; the 4th harmonic peak 100 µm close to 1100 m/min i.e. 4.0 Hz and 3rd harmonic of 70 µm at 1500 m/min i.e. 5.5 Hz. The peak values are little lower than in the other cross-sections.

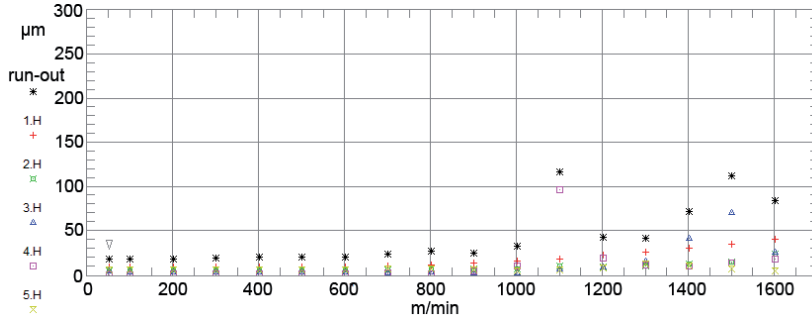


Figure 73 Horizontal run-out measurement at the tending side end of the roll shell as a function of running speed. A slight increase in the 1st and the 2nd harmonics can be seen. Two narrow band harmonics arise; the 4th harmonic peak at 1100 m/min and 3rd harmonic close to 1500 m/min.

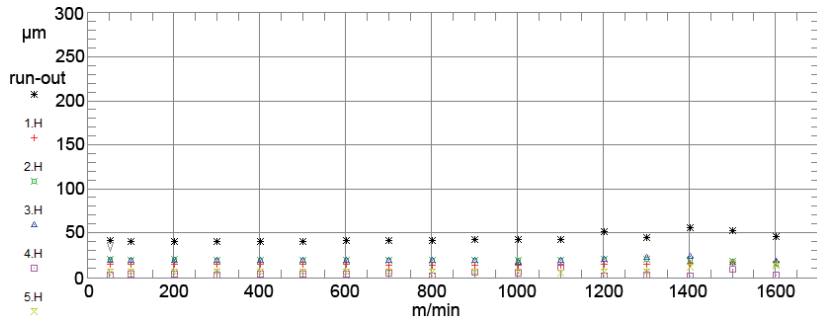


Figure 74 Vertical run-out measurement at the tending side end of the roll shell as a function of running speed.

In the vertical run-out measurements (Figure 74) the resonance vibration amplitudes don't exist and the change in the low harmonic components is small.

4.6 Survey of backing rolls in industrial use

In this chapter, the measurement results of several backing rolls are presented. These rolls are used in several paper mills in Finland and abroad. The manufacturing method of rolls varies according to a manufacturing unit and year. Different welded steel shell structures and cast iron shell structures are included in this study.

A summary of roll structures is presented in Table 21. Cast iron shell is used in class D rolls marked with '*'; the others are different steel structures, mostly.

Table 21 Backing rolls are classified by generations. Rolls marked with * have cast iron shell.

type	length (m)	diam. (m)	wall thickness (mm)	mfg year	notes	design speed (m/min)
A	≈7	≈1.2	<30	1970-	stiffening rings	1100...1200
B	≈8	≈1.2	≈40	1980-	no original internal machining	1400...1500
C	≈9	1.5	≈40	≈1990	no original internal machining	1400...1600
D*	≈10	1.5	≈35	≈2000	internal machining	≈2000

The dynamic roundness of the measured rolls at 1400 m/min is summarized in Figure 75. It can be seen that the class C rolls are prone to the dynamic roundness error. The results are expressed at the same surface

velocity (web speed) and the real operating speed might be higher or lower. Typical design speed for class B rolls is the used 1400 m/min and class C and D rolls are designed for higher service speeds, typically. Especially for class D rolls whose design speed is in the 2000 m/min region, the values are not representing the real operating conditions.

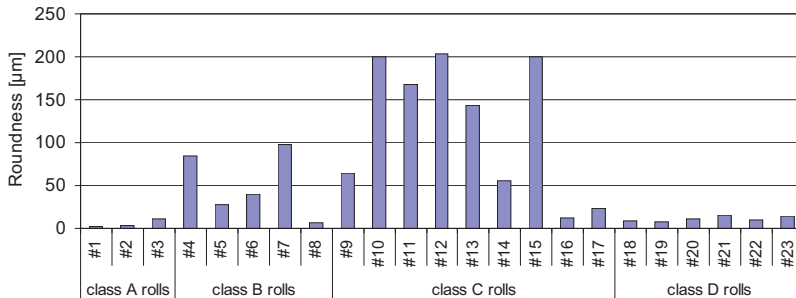


Figure 75 Dynamic roundness of backing rolls at a web speed of 1400 m/min. The rolls are grouped by generations.

Figure 76 presents the results of dynamic bending amplitudes of the same rolls. The rolls with a large diameter have high bending stiffness; hence the dynamic bending values are lower than the rolls with a smaller diameter. The dynamic bending values are in the same range under 25 µm. The shown values have to be multiplied by two for total run-out peak-to-peak values.



Figure 76 Dynamic bending of backing rolls at a web speed of 1400 m/min. The rolls are grouped by generations.

4.7 Coating quality variation

Paper samples were acquired just before and right after maintenance downtime during which some other measurements at a coating station were carried out. The approximately 5000 m samples were analyzed by the research staff of the paper mill.

TapiPMA analyzer was used to calculate the grammage variation values caused by four rolls used in two coating stations. The rolls were changed during the downtime and there might be some influence on the analysis

that whether the sample has been acquired before or after the scheduled maintenance break. The results are presented in Table 22.

Table 22 The grammage variation [g/m²] caused by backing rolls of two blade coating stations of a single coating machine. The samples were acquired from the middle (M) of the web and close to the edges (DS, TS). Total variation and four harmonic components are shown.

pos.	roll #3			roll #4			roll #5			roll #6		
	DS	M	TS	DS	M	TS	DS	M	TS	DS	M	TS
1 st H	0.07	0.09	0.17	0.03	0.26	0.09	0.11	0.60	0.12	0.37	0.87	0.31
2 nd H	0.11	0.74	0.36	0.12	0.17	0.17	0.36	0.28	0.06	0.48	0.88	0.27
3 rd H	0.30	0.15	0.11	0.05	0.03	0.04	0.32	0.16	0.15	0.08	0.11	0.06
4 th H	0.04	0.06	0.10	0.03	0.04	0.04	0.04	0.05	0.08	0.08	0.08	0.16
Tot.	0.9	1.7	1.2	0.4	0.7	0.5	1.4	1.6	0.7	1.6	3.1	1.0

The roll #6 is picked up for further comparison with separate run-out measurements. The grammage variation caused by a single backing roll is illustrated in Figure 77. The variation is strong in the middle of the paper web and the relation between the variation components is approximately the same.

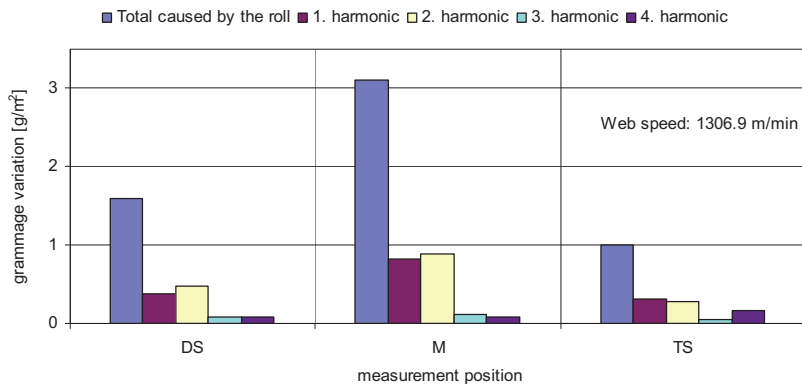


Figure 77 The grammage variation and its harmonics at different web positions caused by the backing roll #6.

4.8 Roll maintenance and renewal process

The measurement result and knowledge of the dynamic geometry change of backing rolls is followed by a need to improve the dynamic behavior. During the years since starting the research several backing rolls have undergone a renewal process to minimize the dynamic geometry error. The methods are presented in the following chapters as alternative choices for

improving the dynamic behavior of current rolls instead of purchasing completely new rolls.

4.8.1 Roll stiffening

The first renewal method was copied from an older backing roll structure . The roll shell is stiffened against deformations using stiffening rings inside the roll shell (Pullinen 1997 et al., Kuosmanen et al. 1998). The rings made from three sections each and they were welded inside the roll. The number of rings varied from five to eleven. Pullinen et al (1997) present that run-out in one case study decreased from 232 μm to 50 μm i.e. 80 % improvement was achieved using this method.

4.8.2 Internal machining

This is a procedure that was used for rolls which were not originally internally machined. The result depends on the quality of the centring of the roll shell. There is also a chance that possible internal stresses are affecting the geometry of the roll in the process conditions.

The unpublished results have been acceptable in some cases, but optimization for high speeds of modern paper machines usually requires more advanced methods. Some of these measurements were performed by the author.

4.8.3 Addition of counterweights

A method of adding counterweights on the inside surface of a roll has been used in industry. The mass is added along the length of the roll on the opposite sides of the shell. The amount of added mass is calculated using a FE model. The unpublished results have been satisfying if the mass required to compensate the geometry change is within reasonable limits. The challenge is to ensure that the added mass will be permanently fixed to the roll and the fixation does not affect the durability of the roll shell. This method can be used to fine tune the dynamic behavior after machining process.

4.8.4 3D grinding

A method that is used in some paper mills is referred as 3D grinding (Kuosmanen and Juhanko 2004, Kuosmanen 2004, Juhanko and Kuosmanen 2007). The method is based on the optimization of the geometry at the operating speed of a paper machine. The principle could be compared with the balancing of flexible rolls, for which the state of balance i.e. dynamic bending is minimized at one rotating speed. For the dynamic geometry optimization the dynamic roundness profile of the roll shell is

measured at several cross-sections. The measurement result is inverted and used in a grinding machine's control system to grind a geometry that is far from traditional workshop tolerances. The removed amount of material is so small that the dynamic geometry changing behavior is not altered. Therefore the roll still changes its geometry as a function of running speed and the geometry reaches its optimum at a desired operating speed. The principle of this method is presented in Figure 78. A more detailed presentation of this research is presented by Kuosmanen (2004).

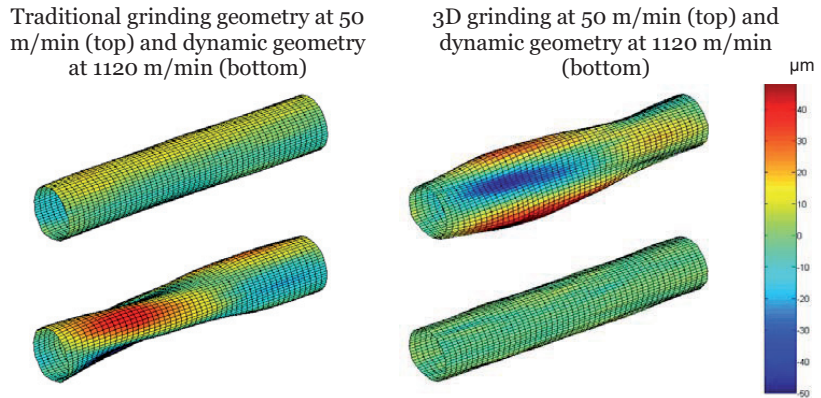


Figure 78 The principle of 3D machining of a backing roll to optimize the geometry at operating speed. On the left a traditional behavior is shown. The roll is manufactured to be cylindrical at workshop conditions. The 3D grinding (right) is used to optimize the geometry at operating conditions.

With 3 D grinding dynamic roundness improved from the original value of 76 μm down to 13 μm , and dynamic run-out decreased from 109 μm to 34 μm .

5 Discussion

In this research the dynamic roundness is assessed with several methods using experimental testing and mathematical models. The main tool for studying the original research problem has been experimental research using a developed and verified measuring device. The phenomenon is also analyzed with the finite element method using the experimental measurement results of a thickness measurement as an input data. The significance of the research is evaluated using a sample population of backing rolls and analysis of paper samples. Correlation between the manufacturing accuracy and the observed behavior is estimated as well as the effect of dynamic geometry change on paper quality variation.

5.1 Wall thickness

The wall thickness measurement of a paper machine roll showed significant systematic variation. The measured thickness values are in the range of 37...43 mm. The roll structure was determined easily from the results. The most important result was that the wall thickness variation is harmonic with one main component. The measured ovality of the inner surface geometry is in the range of millimeters instead of tens of micrometers that is the tolerance for outer geometry. In the case of the laboratory roll, the reason for the dynamic behavior is easily determined. The FFT analysis showed that the average value of 2nd harmonic component is about 2 mm. The other harmonic components are negligible.

In this study, only the mean value of the error component is used to find the initial values for the FE analysis. The welding seam is not modeled and therefore the effect of the welding seam is not analyzed. Because of the manufacturing technology the welding seam and the geometry of the roll might be related so that the basic harmonic components would be phase locked with the seam.

One challenge is that also the internally machined rolls show the dynamic geometry change behavior. The wall thickness maps of these rolls were not measured during this study, but the measured dynamic behavior suggests that there might still be a need for increasing the manufacturing accuracy of the internally machined roll shells to achieve the highest possible operating accuracy. In practice, this demand for new manufacturing tolerances would

increase the manufacturing costs exponentially, and therefore other solutions have been introduced, as presented in Chapter 5.7. The presented methods and their variations are applicable also for the manufacturing of new roll shells.

5.2 Finite element modeling

In the analyzed finite element cases, the outer surface deformation consists mainly of the harmonics of the inner surface profile. Centrifugal forces tend to rapidly increase the dynamic geometry error on the lowest harmonics ($upr = 2, 3, 4$) of the inner surface profile, as illustrated in Figure 79. The higher harmonics ($upr > 4$) of the inner surface profile have only little effect on the dynamic geometry under centrifugal forces.

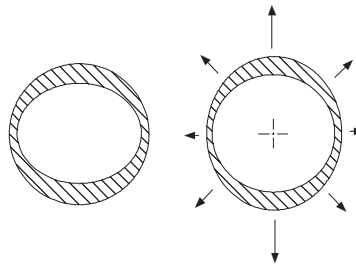


Figure 79 Uneven wall thickness distribution causes centrifugal forces and stiffness variation, and therefore dynamic geometry change on a rotating cylinder.

As the inner profile does not change without machining, the worst case is low inner surface harmonics with high amplitudes and a small wall thickness with increasing web speed. The normal engineering tolerance of the inner surface is run-out, which is not suitable solution for this kind of dynamic problem as it neither takes into account the harmonic content of the surface profiles nor the rotating speed. As the effect of centrifugal force on the roundness profile is dependent on the running speed to the power of two, the outer surface run-out harmonics may appear quite high at a normal production speed of a paper machine.

When a measured wall thickness variation is used in the FE modeling, the dynamic geometry characteristics are in accordance with the observations on the measurements in industry.

The FE analysis using the actual measured wall thickness data reveals the dynamic geometry change to be systematic with the maximum change in the middle section of the cylinder and less in the proximity of the fixed ends.

5.3 Measurement accuracy of the device

The measurement accuracy of the device is determined with several experimental tests to observe the effect of different signal processing parameters as well as some systematic changes in the measuring setup. When using laser triangular sensors, the surface quality and its characteristics with a coherent laser beam play a major role in the measurement uncertainty. Manufacturers determine the measurement accuracy using ground white ceramic targets. This is to minimize the effect of the surface quality characteristics that affect the measurement result.

In this research, the measurement accuracy was determined using the experimental uncertainty of a measurement according to "Guide to the expression of Uncertainty in Measurements" GUM principles. GUM is globally accepted and establishes general rules for evaluating and expressing uncertainty in measurement that are intended to be applicable to a broad spectrum of measurements.

The chosen approach to the uncertainty in measurement was experimental testing with repeats and a systematic design of experiments. The uncertainty of the measuring device was not determined by analyzing of error sources using model functions and error budgeting. These methods can be applied if the measurement device is further developed for the next generation dynamic roundness device series.

In the following chapters some tested measuring parameters and conditions are discussed.

5.3.1 Signal processing system

5.3.1.1 Synchronous averaging

The synchronous averaging is used for filtering out the transient components and those harmonic components that are not in synchronization with one full revolution. Thus any impacts and vibrations caused by e.g. bearing elements or surrounding machines should be eliminated. This is also true in practice. In the laboratory environment there is only a little benefit in increasing the number of revolutions beyond 20 in the time synchronous averaging. In industrial environment there are many vibrating machines and excitation sources; therefore a common practice has been adopted to use a synchronous averaging with 100 revolutions. Even higher value could be used, but the duration of the measurement increases linearly. With 100 revolutions a static measurement for a backing roll running at a jogging speed of 50 m/min would last for almost ten minutes. Increasing the number of revolution to 200 or 500 would increase the required measuring time up to 19 minutes and 47

minutes, respectively. It might be useful to increase the number of revolutions in averaging for very precise measurements.

Without synchronous averaging the maximum expanded uncertainty of measurement was $U_{\max} = 1.33 \mu\text{m}$ while the mean was $U_{\text{mean}} = 0.74 \mu\text{m}$. Using synchronous averaging the uncertainty improves rapidly when the number of samples is increased, as can be seen in Table 23. In this test series it can be seen that in the 100 revolution averaging test the values are considerably higher indicating maybe some increased vibration levels or transient impacts in the laboratory building.

Table 23 The effect of revolutions used in time synchronous averaging on the expanded uncertainty of measurement [μm].

<i># of avg</i>	<i>1</i>	<i>10</i>	<i>20</i>	<i>50</i>	<i>100</i>	<i>200</i>	<i>500</i>
U_{\max}	1.33	0.42	0.28	0.17	0.34	0.18	0.24
U_{mean}	0.74	0.19	0.14	0.10	0.16	0.06	0.06

5.3.1.2 Filtering cut-off frequency

The filtering cut-off frequency functions as expected. The amplitude of the harmonic content is attenuated according to the filtering principle. Depending on the needs of the measurement the cut-off frequency should be selected accordingly. For dynamic geometry changes which are present on low harmonic components of roundness only, it is not necessary to use higher cut-off frequencies than $15 \cdot f$, where f is the rotating frequency of the roll. If one is interested in harmonic content of the roundness profile up to 30 undulations per revolution, the cut-off should be set higher according to the attenuation of the signal.

The filtering has an effect on the phase also and the used linear phase filtering boards allow correcting the phase delay easily from the signals if necessary. In this study, the feature was not used, but some other applications require exact knowledge of the correct phases e.g. barring with a high number of lobes in the roundness profile.

5.3.2 Running speed

The observed experimental expanded uncertainty of measurement as a function of running speed is extremely low although there seems to be a little increase in the uncertainty values.

The increasing rotating speed increases the uncertainty of measurement, as shown in Figure 80. In a single measurement there are some exceptions in variation that could be explained by a change in vibration levels.

Typically, vibration in this frequency range increases as a rotating speed increases. There are some resonance vibrations that might increase the vibration level although the time synchronous averaging attenuates most of the frequencies that are not multiples of the rotating speed.

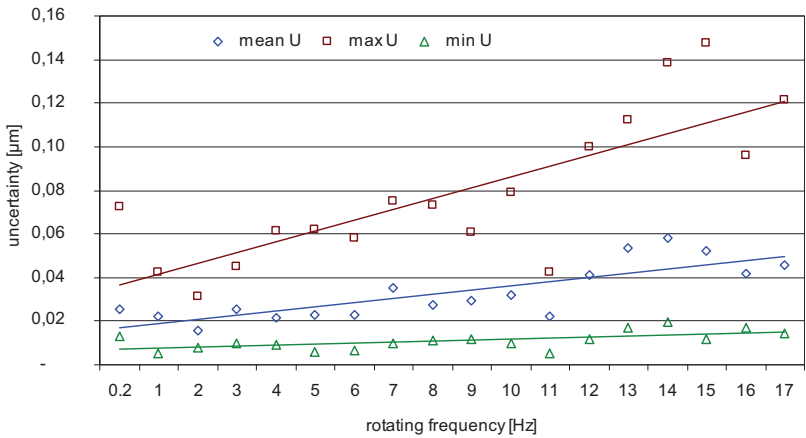


Figure 80 Mean, maximum and minimum values of expanded uncertainty of measurement of the 2nd ... 31st harmonic components of roundness as a function of rotating frequency.

Because the variation of the means of the repeated measurements over the speed range from 0.2 Hz to 17 Hz, a mean of these values is calculated for each roundness component and presented in Figure 81. The calculated experimental expanded uncertainty U has been added as error bars. The coverage factor $k = 2$ is used, which for a normal distribution corresponds to a coverage probability of 95 %. It can be seen that the expanded uncertainty of most components is very low, $U \leq 0.5 \mu\text{m}$. There are still some components with higher expanded uncertainty e.g. 3rd and 11th with $U \approx 1 \mu\text{m}$. It must be noted that expanded uncertainty of the odd lobe components is generally higher than the uncertainty of the even lobe components.

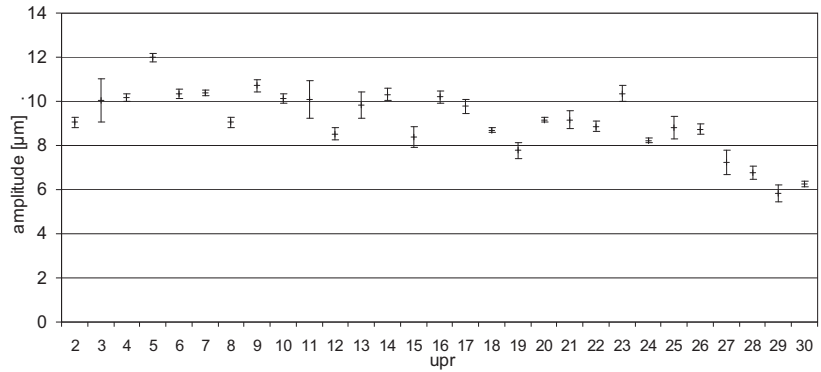


Figure 81 Roundness component mean amplitude and expanded measurement uncertainty in measurements over the frequency range from 0.2 Hz to 17 Hz.

To further improve the measurement device the measuring frame's sensitivity to the vibrations caused by external excitations has to be minimized. This could be done using different attenuation principles such as:

- addition of damping,
- semi-active or active vibration control,
- reducing the natural frequency of the that mode of the frame support below the interesting frequencies by using very flexible support, or
- measurement of vibration and subtracting the measured signal from the displacement measurement signal.

All of the above methods have their limitations, but possibly the most effective method that could be used in various measuring environments is to measure the movement of the displacement sensor with an accelerometer and correct the signal accordingly.

It has to be noted that the experimental measurement uncertainty as a function of running speed is adequate showing that basic data acquisition and signal processing system is satisfying. Yet, the measuring setup and the algorithm for odd number lobes could be improved, if the device is further developed.

5.3.3 Axial measuring position

Measurement results showed some variation of the mean values when the frame was displaced along the shaft axis. The reference measurement results of the calibration disc did not show any significant changes along the length of the disc, so good repeatability should be expected. The frame eccentricity was positioned according to normal tolerance within ± 0.5 mm. The values of the harmonic components varied within ± 1 μm with some exceptions e.g. one cross-section measurement showed high value for the 3rd harmonic component in the middle of the disc. There were some visual marks in that cross-section that might have come from earlier measurements with rolling and sliding contact sensors. In this study, this behavior was not analyzed further.

Because there is variation of the means of repeated measurements in each cross-section, a mean of these values is calculated and presented in Figure 82. The experimental expanded uncertainty U has been added as error bars. Coverage factor $k = 2$, which for a normal distribution corresponds to a coverage probability of 95 %.

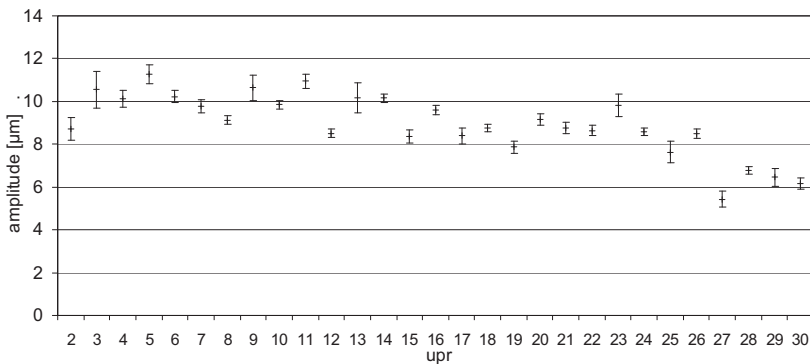


Figure 82 Roundness component mean amplitude and expanded measurement uncertainty of the axial repositioning of the measuring frame along the length of the shaft.

It is easily observed that the expanded uncertainty of the odd lobe components $U \approx 0.9$ μm is higher than the uncertainty of the even lobe components $U \leq 0.6$ μm . The explanation for this might be found in the algorithm which is precise for the even lobe components using direct the two-point measuring method with the opposing sensors. The odd lobe components are calculated using the weighing factors and approximate estimates. Further analysis of the reasons and the development of the algorithm are not included in this study.

5.3.4 Frame eccentricity

The expanded uncertainty in a measurement series was very good when the frame was fixed to a position, as shown in Figure 60. When the frame was displaced the mean value of harmonics changed, as could be seen in Figure 59, but the repeatability was still very good. Therefore, the very slight change in the axial measurement position caused systematic error. The mean of the mean values of separate measurement series are calculated and the harmonics of the roundness components are shown in Figure 83. The experimental expanded uncertainty U has been added as error bars using the coverage factor $k = 2$, which for a normal distribution corresponds to a coverage probability of 95 %. It can be seen that the expanded uncertainty for even lobe undulations 2, 4, ..., 30 are generally lower than for the odd lobe undulations. While the frame was displaced along the measuring line of these sensors, no error caused by frame positioning even should be present. Thus the low uncertainty value $U \leq 0.5 \mu\text{m}$ in measuring the even lobe undulations is natural.

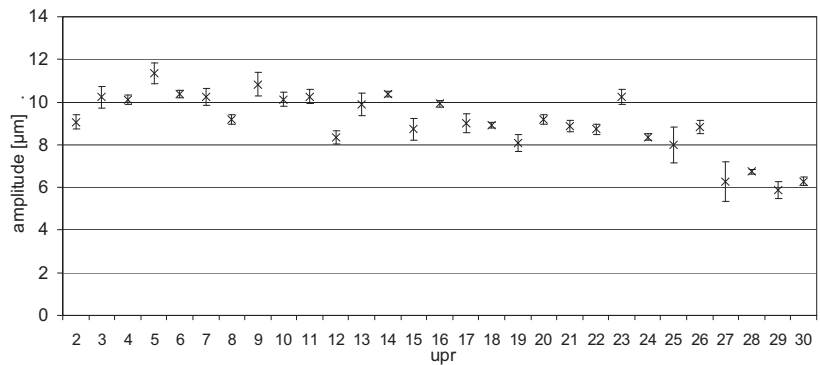


Figure 83 Roundness component mean amplitude and expanded measurement uncertainty of the horizontal frame eccentricity in the range $\pm 3 \text{ mm}$.

The odd lobe undulation components are affected by the frame displacement, because the observation angle changes and the line of the measuring beam moves away from pointing directly to the rotational axis. The uncertainty is $\pm 1 \mu\text{m}$ due to frame eccentricity.

It should be noted that when setting up the measurement the alignment of the frame can easily be adjusted within $\pm 0.5 \text{ mm}$.

5.3.5 Combined measurement uncertainty

The combined measurement uncertainty approach is carried out using the input quantities:

- X_i analysis of the speed parameter, which was measured in the same fixed position of the frame and only changing parameter was the rotating speed,
- X_j the analysis of the frame eccentricity, and
- X_k the analysis of the measurement surface characteristics in varying the axial position of the measuring frame.

The last two input quantities X_j and X_k are known to correlate to some extent i.e. they are dependent on each other. Both input quantities require the change of the frame position, and the measuring system is built that way it is impossible to reposition the frame exactly only in the studied direction.

To find a correlation of these repeated observations more attention should have been paid in building the test setup and transformations to new independent variables.

Because the degree of correlation is not known, it is useful to assess the *maximum influence* this correlation can have by an upper bound estimate for the standard uncertainty of the measurand using a general formula:

$$u^2 \leq \left(|u_1(y)| + |u_2(y)| \right)^2 + u_r^2(y) \quad (55)$$

where u_r contains the standard uncertainty of the rest of the uncorrelated input quantities. The standard uncertainties in measurement for the dynamic roundness measuring device are calculated and the results are presented in Figure 84 as expanded uncertainty in measurement U with a coverage factor $k = 2$, which for a normal distribution corresponds to a coverage probability of 95 %.

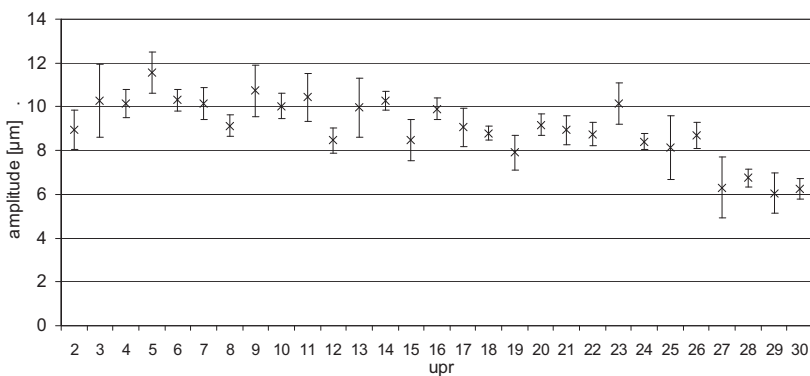


Figure 84 Roundness component amplitudes and combined expanded uncertainty of measurement of the dynamic roundness measuring device.

5.3.6 Measurement result versus certified value

To summarize the accuracy analysis of the measuring device the results are compared with the certified reference disc. Figure 85 presents the dynamic roundness measurement results and the certified measurement results of the calibration disc.

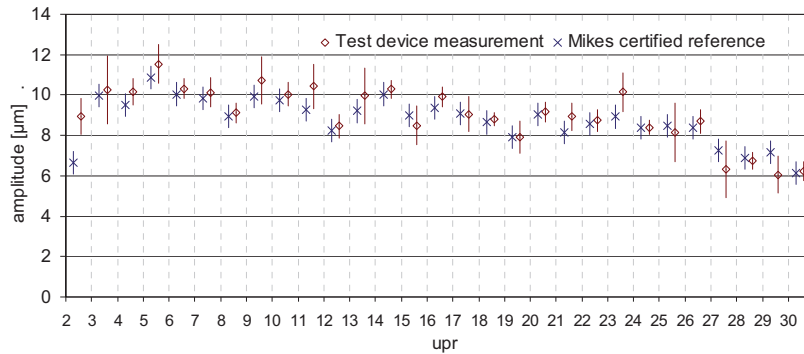


Figure 85 Roundness component amplitudes and combined expanded uncertainty of measurement of the dynamic roundness measuring device and the reference disc.

The similarity of the results is evident, but there are some deviations of which the most significant is the 2nd harmonic undulation component. The reference measurement result is 6.6 μm while the measurement result using the test device is 8.9 μm.

This behavior has emerged in other experiments with other measuring devices in the laboratory. Preliminary results indicate that the geometry of the disc changes when fixed to the shaft. The SKF Concentra adapter sleeve causes tension to the disc when tightened according to the instruction manual. Four measurement results are analyzed. The Mikes reference measurement was measured without the shaft and, therefore, no tension in the disc. When the disc was ground at a paper mill, the disc was measured using the measuring device of the grinding machine. The measurement device of the laboratory grinding machine at Helsinki University of Technology was used to measure the disc without the tension in the adapter sleeve. The measurement was repeated with the disc fixed to the shaft and tightened. The most significant variation was found in the 2nd harmonic component of the roundness profile and the results are shown in Table 24.

Table 24 The 2nd harmonic component of the roundness profile varies in different measuring setups. The tightening of the adapter sleeve cause a slight geometry change in the disc.

<i>upr</i>	<i>Reference measurement at Mikes</i>	<i>TKK 3D-measuring device</i>	<i>TKK 3D-measuring device</i>	<i>Paper mill grinding machine</i>	<i>Dynamic geometry measuring device</i>
<i>adapter</i>	open	open	fixed	fixed	fixed
<i>2nd H</i>	6.6 μm	6.0 μm	7.8 μm	9.3 μm	8.9 μm

It appears that the tightening of the adapter sleeve has an influence on the 2nd harmonic component of the roundness profile. The characteristics could be studied by rotating each of the components of the Concentra element one at a time trying different levels of tightening, and measuring the effect on geometry of the disc.

Most of the other harmonic components seem to be in the intended range, but the uncertainty in measurement is significantly larger. The comparison between the measurement results with the certified measurement is carried out using the principle by Linsinger (2005). The procedure is presented and applied for the calibration of the ultrasonic measuring device in Chapter 3.5.2. Table 25 summarizes the results of this analysis.

Table 25 Harmonic components mean value [μm] and expanded uncertainty [μm] of the reference instrument (\bar{A}_{ref}, U_{Aref}) and the dynamic geometry measuring device (\bar{A}_{DG}, U_{ADG}). The difference is analyzed by using uncorrected values ΔA and corrected value ΔA_c which is evaluated against the combined uncertainty of the measurement U_Δ .

<i>upr</i>	\bar{A}_{ref}	U_{Aref}	\bar{A}_{DG}	U_{ADG}	ΔA	ΔA_c	U_Δ
2	6.6	0.6	8.9	0.89	2.31	2.09	1.08
3	10.0	0.6	10.3	1.68	0.29	0.07	1.79
4	9.5	0.6	10.1	0.65	0.64	0.42	0.89
5	10.9	0.6	11.5	0.94	0.68	0.46	1.12
6	10.0	0.6	10.3	0.50	0.28	0.05	0.78
7	9.8	0.6	10.1	0.72	0.29	0.07	0.94
8	8.9	0.6	9.1	0.50	0.19	0.04	0.78
9	9.9	0.6	10.7	1.18	0.82	0.60	1.33
10	9.8	0.6	10.0	0.58	0.28	0.05	0.83
11	9.3	0.6	10.4	1.09	1.16	0.94	1.25
12	8.2	0.6	8.5	0.57	0.21	0.01	0.83
13	9.2	0.6	10.0	1.37	0.75	0.53	1.49
14	10.0	0.6	10.3	0.43	0.24	0.02	0.74
15	9.0	0.6	8.5	0.95	0.51	0.73	1.12
16	9.4	0.6	9.9	0.49	0.54	0.32	0.77
17	9.1	0.6	9.1	0.88	0.02	0.25	1.06
18	8.6	0.6	8.8	0.33	0.15	0.07	0.69
19	7.9	0.6	7.9	0.79	0.02	0.21	0.99
20	9.0	0.6	9.2	0.49	0.12	0.10	0.77
21	8.1	0.6	8.9	0.68	0.79	0.57	0.91
22	8.6	0.6	8.7	0.54	0.17	0.05	0.81
23	8.9	0.6	10.1	0.96	1.23	1.00	1.13
24	8.4	0.6	8.4	0.36	0.00	0.22	0.70
25	8.5	0.6	8.1	1.44	0.32	0.54	1.56
26	8.4	0.6	8.7	0.58	0.32	0.10	0.84
27	7.3	0.6	6.3	1.41	0.96	1.18	1.53
28	6.9	0.6	6.8	0.42	0.13	0.35	0.73
29	7.2	0.6	6.1	0.91	1.12	1.34	1.09
30	6.1	0.6	6.2	0.47	0.11	0.11	0.76

To evaluate the performance of the method, ΔA is compared with the expanded uncertainty U_Δ . If $\Delta A \leq U_\Delta$ then there is no significant difference between the measurement results and the certified value. The

same comparison can be carried out for the mean corrected value ΔA_C . The results of the comparison are presented in Figure 86. For the offset correction, the erroneous value of the 2nd harmonic is neglected.

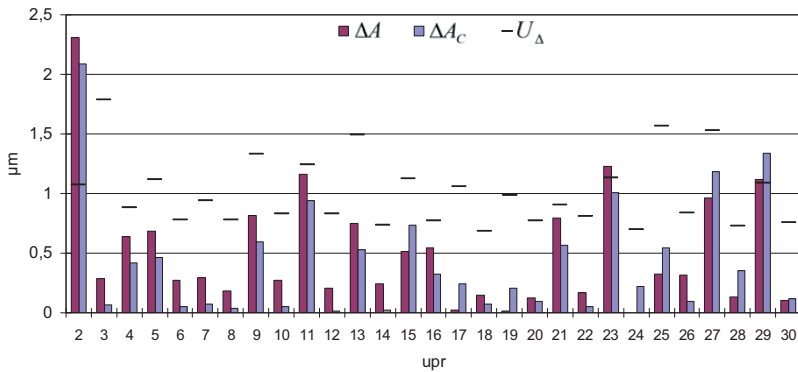


Figure 86 The absolute difference between the mean and the certified value ΔA is evaluated against the expanded uncertainty U_Δ . The corrected value ΔA_C eliminates systematic errors from the measurement.

According to the analysis it can be stated that with the prerequisites the expanded uncertainty of the measurement for the dynamic geometry measurement device is

$$U \leq 2 \mu\text{m}. \quad (56)$$

In many cases especially the harmonic components with the even number of undulations per revolution the expanded uncertainty of measurement is lower, $U_{\text{even}} \leq 1 \mu\text{m}$.

There are still some doubts in the expanded uncertainty of measurement when the surface characteristics of the measured target differ from the one that were used in the measurement. These results apply for ground steel surfaces, and most likely for other ground surfaces with constant optical properties. The laser sensor has an automatic gain control if the intensity of the reflected light changes during the measurement process.

5.4 Backing roll behavior

Roundness profiles and their change as a function of running speed are presented at all measured 13 cross-sections (c-s) of the test roll for further validation of the FE model. The measured roundness profiles are shown in Figure 87 to get an impression of the dynamic geometry change. The

maximum roundness value $267\ \mu\text{m}$ was measured at the middle cross-section.

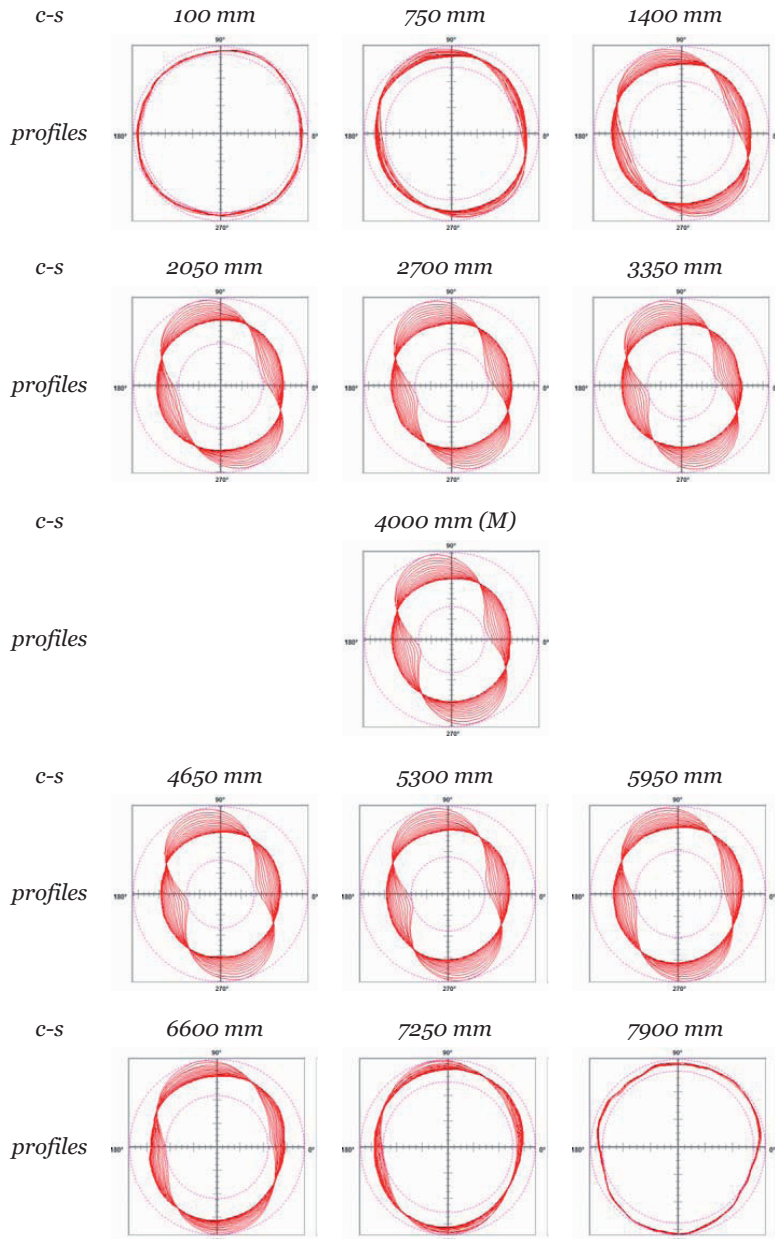


Figure 87 All measured profiles for a quick review of the results at each cross-section in the speed range from 0.2 Hz to 5.9 Hz.

A cylindricity model is created from the individual measurement results at selected speeds of 50, 400, 800, 1200 and 1600 m/min (Figure 88). The static geometry is included in the model, but the eccentricity and the dynamic bending are excluded to emphasize the effect of the dynamic

roundness. The radial deflection is amplified with a factor of 1000. The scale and color bar are the same in all models. It is evident that the change in the dominating 2nd harmonic component (both amplitude and phase) is very fluent and there are no discontinuities in any of the measurements.

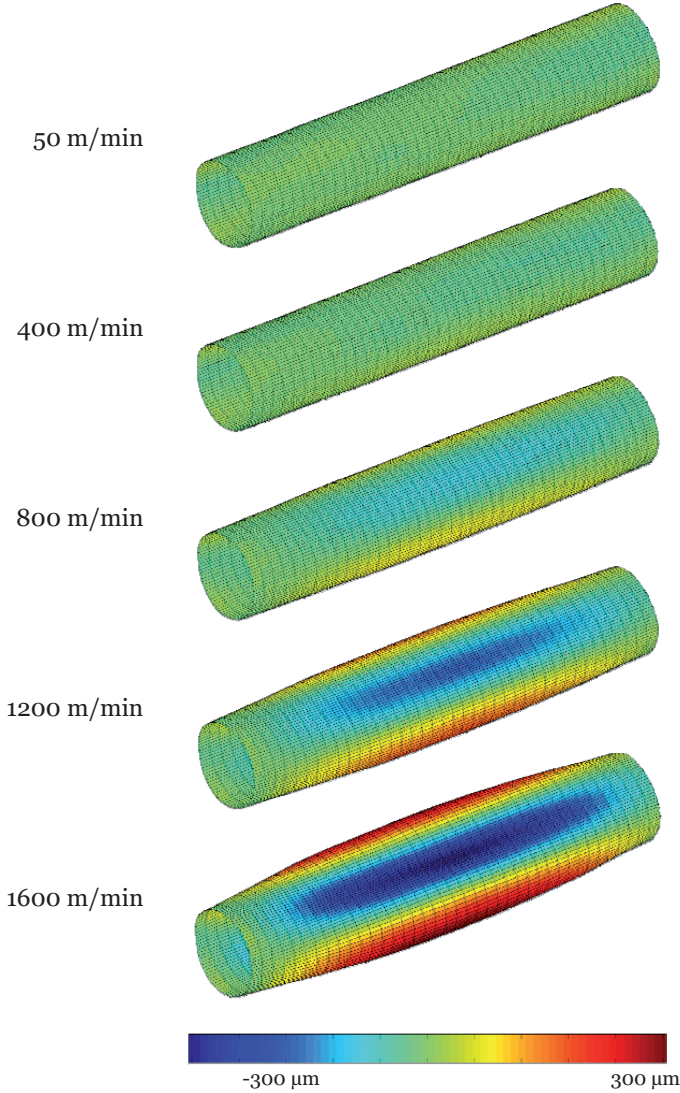


Figure 88 Representation of the dynamic cylindricity created from measurement results as a function of running speed. All 13 measured cross-sections are included in all models.

The change is moderate up to 800 m/min, and at that speed the 50 μm dynamic run-out tolerance is exceeded already by the roundness error only.

The roundness measurement results are also presented as graphs across the length of the roll (Figure 89). It can be seen that the change increases fluently towards the center of the roll indicating the stiffening effect of the fixed end plates, and each extra speed step of 400 m/min has an increasing effect on the roundness.

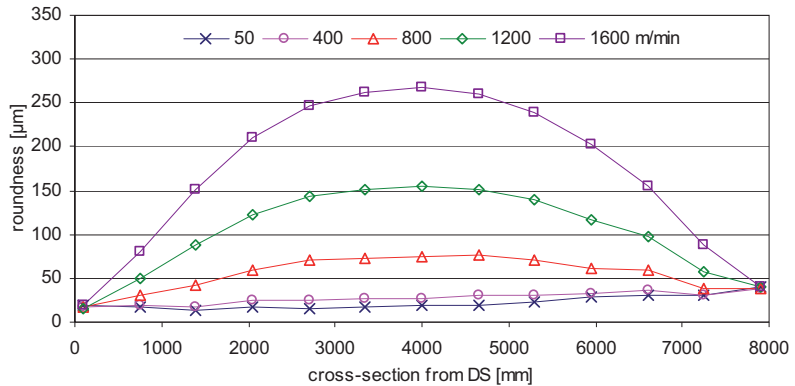


Figure 89 Roundness at each cross section as a function of running speed.

The dynamic geometry change of the second harmonic component (ovality) as a function of running speed is shown in Figure 90. The values are calculated by subtracting the static (50 m/min) measurement vector from each measurement at higher running speed of 400, 800, 1200 and 1600 m/min. The result shows consistent behavior throughout the length of the roll and through the speed range. The maximum change in the 2nd harmonic component of the roundness profile is at the middle cross-section of the roll, 250 μm .

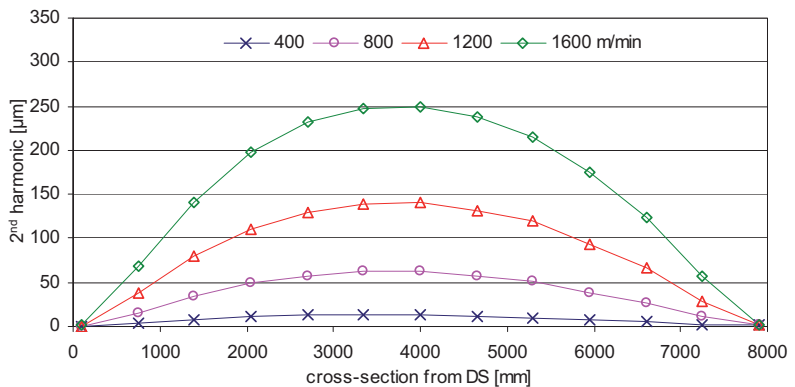


Figure 90 Change in the 2nd harmonic component of the roundness profile at each cross section as a function of running speed.

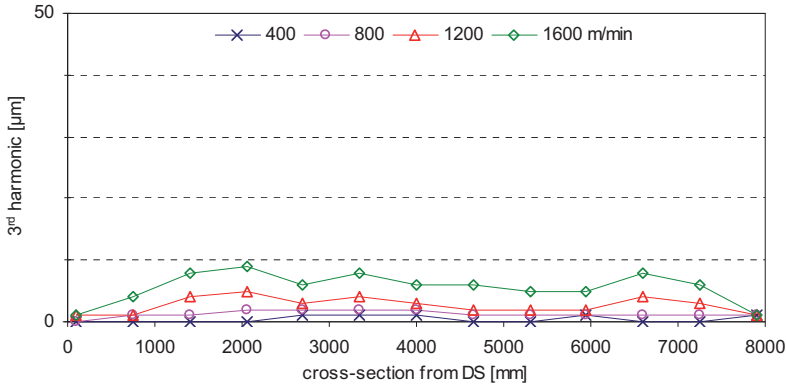


Figure 91 Change in 3rd harmonic component of the roundness profile at each cross section as a function of running speed.

The change in 3rd harmonic component is presented in Figure 91, respectively. The dynamic change is substantially less and not as fluent. The maximum values are reached close to the ends of the roll. To study this behavior the phase values of the 3rd harmonic were checked.

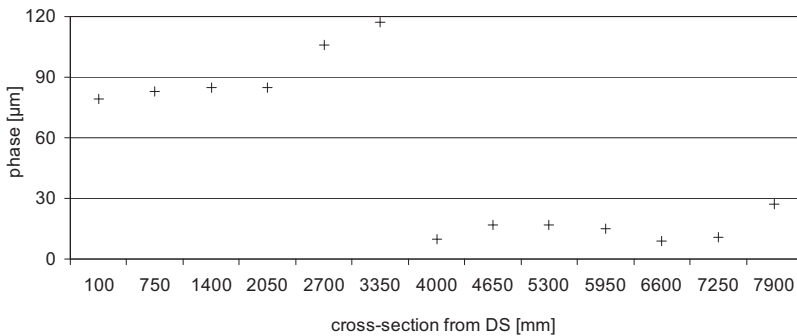


Figure 92 The phase of the third harmonic component of roundness profile at 1600 m/min at measured cross-sections.

The phase of the 3rd harmonic roundness component changes along the length of the roll as shown in Figure 92. This behavior could be affected by the roll structure. The roll shell is welded together from two shorter cylinders end-on-end. Each of the cylinders has been rolled separately with an axial weld. Typically, the rolling process causes a systematic geometry error in the cylinder. Because the axial welds of two cylinders are usually on the opposite sides (180° rotational phase shift) the triangular geometry component is phase shifted on the contrary to the oval geometry which is not strongly affected by a rotation of 180°.

It is obvious that the 2nd harmonic components are significantly higher than the 3rd harmonic components at normal operating speeds. There are two explanations for the behavior:

- Wall thickness variation at lower harmonics cause more dynamic roundness change than the same amount of wall thickness variation at higher harmonics due to the shell stiffness as was shown in the first FE analysis.
- The manufacturing of steel rolls typically leads to symmetric (mirrored) geometry error due to bending of the steel sheet and welding.

The dynamic geometry change of the 2nd behavior is analyzed as a function of running speed in different cross-sections, as shown in Figure 93. The MS Excel function for a least squares quadratic polynomial fit is used to evaluate of the 2nd order function

$$\hat{u}_i = f(x_i) = c_1x_i^2 + c_2x_i + c_3 . \quad (57)$$

For a given set of data $i=1...M$ the set of coefficients c_1 , c_2 and c_3 are varied to minimize the quantity

$$\sum_{i=1}^M (u_i - \hat{u}_i)^2 , \quad (58)$$

where u_i is the i^{th} element in the data set. Correlation coefficient R determines the relationships between two data sets and calculated correlation coefficients for the shown quadratic fitting curves in Figure 93 where $R > 0.999$ which indicates a strong positive relationship. Therefore, this model could be used to evaluate the dynamic roundness behavior at higher speeds than measured e.g. for future paper machine speed increase projects.

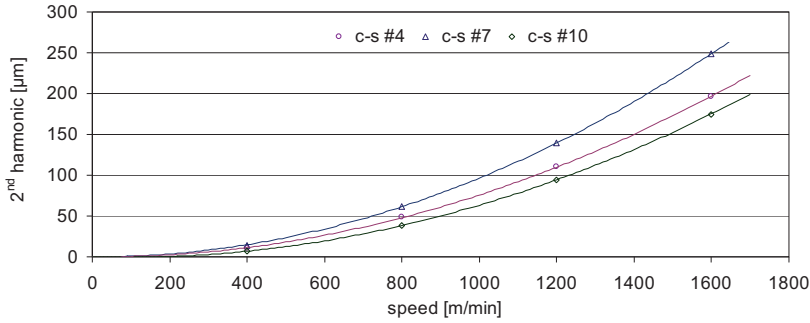


Figure 93 The 2nd harmonic component of roundness profile as a function of running speed at cross-sections #4, #7 (middle) and #10. Least squares quadratic polynomial fitting curves give the correlation coefficient $r > 0.999$.

5.5 Simulation model vs. measured behavior

The simulation model and the measurement results of the test roll are compared with each other for dynamic geometry change only. Dynamic and gravitational bending and other phenomena are not discussed.

The dynamic roundness results of the corresponding cross-sections are presented in Table 26.

Table 26 Comparison of modeled and measured roundness in cross-section #4, #7 and #10 as a function of running speed.

rotating speed [Hz]	Roundness [μm] at a cross-section					
	c-s #4		c-s #7 middle		c-s #10	
	model	measured	model	measured	model	measured
0.2	57	6	37	10	42	20
1.4	63	16	46	23	46	24
2.8	81	54	74	71	65	54
4.2	116	116	124	148	96	110
5.6	169	203	196	258	142	190

The result shows that there is less deformation in the model at higher running speeds. The values at the highest rotating frequency are approximately 20 % lower than the measured values. Also, the values at low speed differ from the model to the measured values.

It is evident that the model of the roll is stiffer than the test roll. The measured wall thickness variation did not cover the whole length of the roll, approximately 7200 mm. The welding seams were not modeled and the seams might be one of the big issues in the dynamic behavior.

The model and the documentation were finished before the dynamic geometry measurements were carried out, therefore the verification of the model was done with another model and simple systematic geometry error along the length of the cylinder.

The original model was built for a roll shell only and the ends were fixed. The result shows that the model is stiff giving smaller changes in the dynamic behavior than in the measurements. The boundary conditions should be checked, or the end plates and the shafts should be included in the model. Also, the sensitivity to a change in the Young's modulus and in the density should be studied.

The most significant improvement should be in the utilization of the wall thickness measurement matrix. Using sparse mesh with only a little over 30000 elements, thousands of the wall thickness values are neglected and only the values that are next to the element nodes are taken into account in Lagrangian interpolation. This can be solved using mesh size that corresponds to the wall thickness measurement matrix. The other solution is to filter the measurement matrix using for instance a Fourier transform and an inverse transform to cut out the higher harmonics from the measurement result. In the study, the welding seams are not analyzed, and thus the significance is unknown.

Besides uneven mass distribution, point and surface forces that are generated by the added mass on the inside surface of the roll might be a cause for uneven mass distribution. The mass might have been added for the balancing without realizing the effect on dynamic geometry.

For more detailed analysis of the effects a more advanced and validated model should be generated.

5.6 Roll behavior differences by roll structure

The studied backing rolls were classified by the shell structure. When the dynamic behavior is observed at the same surface speed, it was found that dynamic roundness is the major source for run-out with eight rolls and dynamic bending is dominating in six rolls.

A traditional dynamic behavior measurement on a balancing machine may not detect dynamic roundness component, because

- dynamic geometry has only minor effect on the state of balance. The change is mainly symmetric around the mass centerline, and
- the measuring system of a balancing machine may filter out the dynamic roundness component, because only the rotating frequency component is relevant for balancing purposes.

The dynamic behavior of different generations of rolls has improved, but at the same time the running speed of a paper machine and even the requirements for the paper quality have been increasing. Therefore, the need to control the runnability and dynamic performance of even the latest backing rolls still exists.

In general, dynamic deformation does not seem to affect the state of balance significantly. The effect can't be seen on static measurements on a grinding machine in a roll shop of a paper mill. Typically, the run-out measurement of a balancing machine filters out the 2nd harmonic component of the measurement result. The dynamic geometry change might be the largest run-out component of a balanced roll.

5.7 Roll maintenance

Current backing rolls are manufactured using the latest knowledge of the dynamic geometry changes. The rolls are optimized at the manufacturing facilities to meet the very high requirements of the coating process. The mechanical manufacturing accuracy is improved with measuring and correction methods.

In paper industry the maintenance of currently operating backing rolls is carried out by the maintenance organization of the paper mill or the maintenance is outsourced to a maintenance partner. A mechanical renovation of the roll shell is typically realized by a specialized company. In some mills there are machines and devices to actively put a new maintenance strategy into practice. These advanced maintenance organizations have implemented 3D grinding technology together with dynamic geometry measurement to be used to continuously monitor and improve the dynamic behavior of backing rolls - as well as other rolls of a paper machine. The challenge is that the most advanced methods require information of the roll behavior in process conditions and that typically requires knowhow and special competence from the personnel. The first results have been promising, as shown in Figure 96 in the next chapter.

The other challenge to be tackled is how to manage and finance the development of maintenance procedures. Typically, there is a fixed price tag on the maintenance services to keep a certain level of production capability and quality. In this case, the maintenance organization tries to be as efficient as possible to maintain that agreed level of service. The development of the maintenance procedures are not focused on improving the quality or efficiency of the production. However, in the latest strategies this has been taken into account.

5.8 Coating quality variations

Paper samples were acquired just before and right after maintenance downtime during which some other measurements at a coating station were carried out.

The relation of the measured run-out of backing rolls versus coating grammage variation was analyzed using measurement results from four rolls of two station coating machine and respective analyses of paper samples taken from the middle and from both edges of the paper web. The run-out value is the peak-to-peak value of time synchronous average of 100 revolutions. A TapioPMA's *sos*-analysis was used to identify the variation and its harmonics caused by the backing rolls. In Figure 94, the run-out of backing rolls versus grammage variation shows a positive correlation coefficient $R = 0.89$.

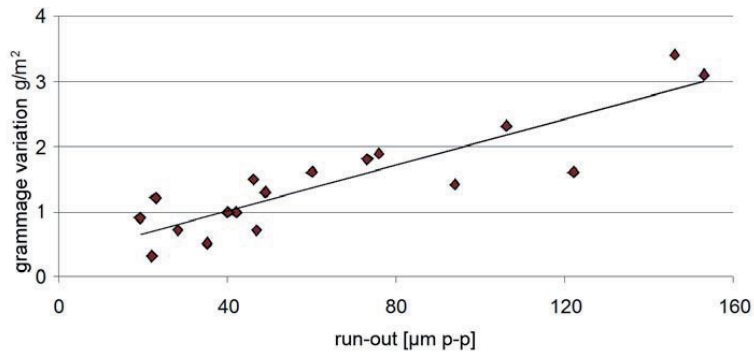


Figure 94 Run-out of a backing roll versus coating grammage variation caused by that very roll.

When a single run-out versus coating grammage analysis is carried out using harmonic components, a very good correlation can be observed, as shown in Figure 95. The correlation is not always as evident as in this analysis, because there are a few parameters affecting roll behavior in operating conditions (such as flexible bearing supports). Also, run-out measurements are not necessarily carried out in the direction of a coating blade.

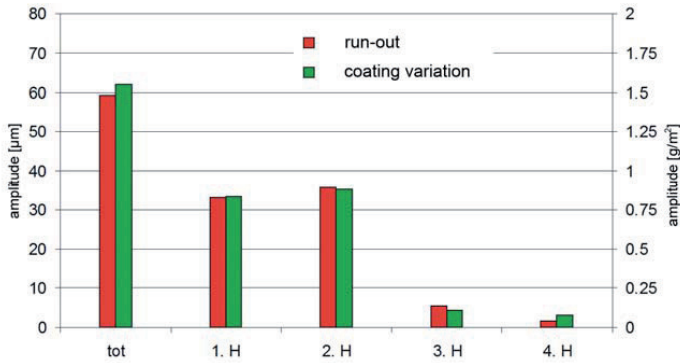


Figure 95 Run-out of a backing roll and its harmonic components versus respective paper grammage variation.

Maintenance of the roll decreased the run-out in the center of the roll down to 1/3 of the original run-out and the coating variation down to 1/6 of the original variation (Figure 96). On the edges of the web the reduction was a little less.

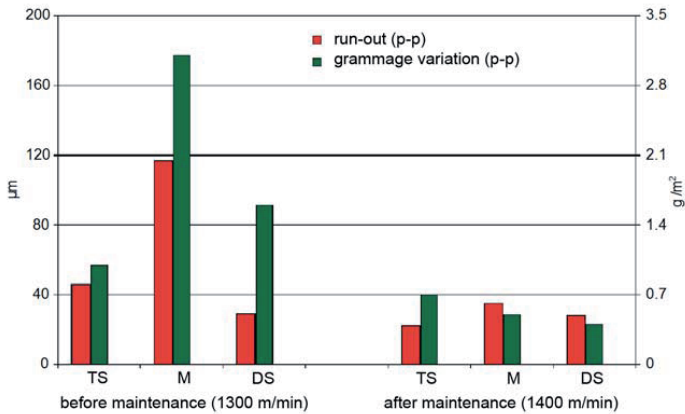


Figure 96 Run-out of a backing roll and the respective coating grammage variation before and after a maintenance procedure of the roll.

The renewal using stiffening rings proved to be beneficial. The procedure is described in more detail by Juhanko (1999). Other possible maintenance methods are described briefly in Chapter 5.7.

6 Summary

In this research dynamic geometry change of a paper machine roll is studied using several engineering tools. There are few references on quasi-static analyses on the dynamic geometry of paper machine rolls which are rotating hollow cylindrical shells. Paper machine rolls are apparently one of few rotor types that have this type of cylindrical structure.

Increasing design speed has affected the design of paper machine rolls. The eigenfrequency of the first bending mode had to be increased to avoid the unwanted natural frequency vibrations in the running speed range. The increased frequency can be obtained by higher stiffness or lower total mass. In most cases, the material selection is restricted to either steel or cast iron due to the cost of the material. Although there are some special rolls made of composite alloys, these high cost materials are not yet commonly used in standard paper machine rolls. The usage of the composite alloys would lead to stiffer and more lightweight rolls. Anyway, at the moment the most common materials used for rolls are steel and cast iron.

In practice, the development has led to a larger outer diameter of new rolls because the bending stiffness increases more rapidly than the mass compared with the increasing cylinder wall thickness. With the larger diameter, the surface velocity increases without increasing the rotating frequency.

The ever widening paper machines have had a similar effect on the dimensions of the rolls. Increasing the diameter of long rolls holds the bending stiffness efficiently. Hence the bending of the roll has been kept in normal tolerances.

When increasing the outer diameter, the total mass of the rolls has been restricted by holding the wall thickness close to original values. The diameter increase has led to decreasing shell stiffness, and therefore centrifugal forces due to manufacturing inaccuracies have stronger influence on the dynamic geometry of the roll.

It had been known that the coating variation of light weight coated paper is in synchronization with a backing roll of a coating station. The cause of the variation was the neither unbalance nor resonance vibration of the roll. It is shown that the frequency of the largest peak in the paper quality variation corresponds to the effect of an oval geometry of a backing roll, but no such a phenomenon has been measured in the roll shop when the

backing roll has been measured during the grinding process. It was realized that a cause of the problem could be the change in geometry as a function of running speed.

The wall thickness measurement shows systematic thickness variation on the studied roll due to manufacturing inaccuracy. The main variation component is used in a finite element analysis of a single cross-section to find out if manufacturing inaccuracy is the cause for dynamic geometry change. The analysis shows that the wall thickness variation can cause dynamic geometry change. The dynamic geometry change is more sensitive to lower harmonic variation components i.e. minimizing ovality component profits most in the manufacturing process.

For a more detailed study, a cylindrical FE model is created and the measured wall thickness matrix is used to define the inner surface nodes. This analysis shows similar dynamic geometry change although the dynamic geometry is more complex due to fixed end plates of the roll. Furthermore, the studied behavior could explain the observed quality variation of LWC paper. The measured wall thickness variation is in the magnitude that can be the cause for the dynamic geometry change.

To carry out experimental research on the dynamic geometry change of a rotating cylinder, such as a paper machine roll, a measuring device is developed. The device is calibrated and validated using a developed multi-lobe calibration disc as a reference standard. Using the principles of GUM (Guide to the expression of uncertainty in measurements) it is shown that the expanded uncertainty U of the device is less than $2\ \mu\text{m}$ in a typical measuring case.

A backing roll formerly used in a paper mill is used as a test roll in laboratory experiments. The wall thickness data from this particular roll is used in the above mentioned FE analysis. The measurements show similar behavior that was observed in the FE analyses. The magnitude of the dynamic geometry change in simulation was about 20 % lower than in the measurements. It is concluded that at least some of the difference can be explained by too stiff FE model of the roll shell. Also, the boundary conditions should be reformulated. Also, the processing of the measured wall thickness data could utilize more of the actual data points by advanced filtering and reduction methods.

The significance of the phenomenon is studied using a quite large sample of backing rolls that are used at paper mills in Finland and abroad. The measured rolls are classified according to different generations of manufacturing processes and materials used. Although the manufacturing processes have developed during the last decades, there are still challenges to achieve the required tolerances. It must be noted that the increase in

speed of a modern paper machine as well as the tightening requirements for the paper quality have put pressure on the development of even better rolls. A finite element model together with an ultrasonic wall thickness measurement system can be used in an advanced manufacturing process to minimize dynamic deformations in operating conditions.

A correlation analysis between quality variations of paper in the machine direction and the dynamic behavior of a backing roll showed a very strong correlation. It is shown that in many cases the dynamic geometry change is the most significant single component causing run-out, and thus the main cause for the paper quality variation. In some cases the bending of the roll has to be taken into account, if the variation is to be minimized.

During the research, some methods were used for maintenance purposes to improve the dynamic behavior of backing rolls. According to the dynamic behavior measurements, the used maintenance methods proved to be useful, and depending whether it is a question of manufacturing new rolls or maintaining the current ones, there is a suitable method available.

References

- Aoki Y. and Ozono S. 1966. On a New Method of Roundness Measurement Based on the Three-point Method (in Japan). *Journal of JSPE*, 32:12. pp. 831-836.
- Bathe K.J. and Wilson E.L. 1976. *Numerical methods in finite element analysis*. Prentice-Hall, Englewood Cliffs. 528 p.
- Braun S. 1975. The extraction of periodic waveforms by time domain averaging, *Acoustica* 32. pp. 69-77.
- Chetwynd D. G. and Phillipson P. H. 1980. An investigation of reference criteria used in roundness measurement. *Journal of Physics E: Scientific Instruments*, Vol 13, pp.530-538.
- Combet F. and Gelman L. 2007. An automated methodology for performing time synchronous averaging of a gearbox signal without speed sensor. *Mechanical Systems and Signal Processing* 21. pp. 2590-2606.
- Doebelin E. 1990. *Measurement systems - Applications and design*. McGraw-Hill, Inc. ISBN 0-07-017338-9. 960 p.
- Dorsch R. G., Hausler G. and Hermann J. M. 1994. Laser triangulation: fundamental uncertainty in distance measurement. *Applied Optics* Vol. 33:7. pp. 1306-1314.
- EA-4/02. 2003. Expression of uncertainty of measurement in calibration, European Co-operation for Accreditation. 79 p.
- EA-4/16. 2003. EA guidelines on the expression of uncertainty in quantitative testing, European Co-operation for Accreditation. 27 p.
- Estler W. T., Evans C. J. and Shao L. Z. 1997. Uncertainty estimation for multiposition form error metrology. *Precision Engineering* 21, pp. 72-82.
- Forsberg K. 2006. Modelling of the shell deformations of a tube roll. Master's thesis. Helsinki University of Technology, Otaniemi. 79 p.
- Fowler K. A., Elfbaum G. M., Smith K. A. and Nelligan T. J. 1997. Theory and application of precision ultrasonic thickness gaging. *NDTnet* Vol.2 No.10 *The Journal of the British Institute of Non-Destructive Testing*, www.ndt.net/article/wt1097/panam/panam.htm [referred 30.1.2011]
- Frennberg M and Sacconi A. 1996. International comparison of high accuracy roundness measurements. *Metrologia* 33, pp. 539-544
- Ganesan R. 1997. Nonlinear vibrations and stability of a rotor-bearing system with nonsymmetric clearances. *Journal of Engineering for Gas Turbines and Power, Transactions of the ASME*, 119(2):418-424.

- Gao W., Kiyono S and Nomura T. 1996. A new multiprobe method of roundness measurement. *Precision Engineering* 19. pp 37-45.
- Gao W. and Kiyono S. 1997b. On-machine roundness measurement of cylindrical workpieces by the combined three-point method. *Measurement* 21:4, pp.147-156.
- Gao W., Kiyono S. and Sugawara T. 1997a. High accuracy roundness measurement by a new error separation method. *Precision Engineering* 21. pp. 123-133.
- Ghosh A.K., Rae C. and Youdan J. 2001. Off-line analysis of properties of the paper web: A diagnostic tool to reduce variability. *Appita Journal* 54: 5, pp. 413-419.
- Haarla A. 2000. Printing and writing papers. in: Paulapuro H. (Ed.) Paper and board grades. Gummerus, Jyväskylä. 134 p. ISBN 952-5216-18-7.
- Hagberg L., Hautanen S., Henrikkson T., Laine H. S. and Löppönen P. (editors). 1998. Keep it running - Industrial asset management. Scandinavian Center for Maintenance Management ry. Loviisa. 200 p.
- Haikio J. 1997. A turning system to minimize the geometrical error of a roll. Master's thesis. Helsinki University of Technology, Otaniemi. 78 p.
- Haitjema H., Bosse H., Frennberg M., Sacconi A. and Thalmann R. 1996. International comparison of roundness profiles with nanometric accuracy. *Metrologia* 33, pp. 67-73.
- Halim E. B., Shoukat Choudhury M. A. A., Shah S. L. and Zuo M. J. 2008. Time domain averaging across all scales: A novel method for detection of gearbox faults. *Mechanical Systems and Signal Processing* 22. pp. 261-278.
- He P. 2001. Simultaneous measurement of sound velocity and wall thickness of a tube. *Ultrasonics* 39. pp. 4007-411.
- von Herten R. and Jorkama M. 1994. Lagrangian approach to spinning elastic shafts. In Mäkinen R. A. E. and Neittaanmäki P. (editors) *Proceedings of the 5th Finnish Mechanics Days*. pp. 127-134.
- von Herten R. and Jorkama M. 1995. On the modal analysis of rotating asymmetrical Rayleigh beams. *Proceeding of the 13th International Modal Analysis Conference*. pp. 1362-1367.
- Hilden K. and Perento J. 2000. Paper analysis: The key to optimizing and troubleshooting paper machines. *Pulp and Paper Canada*, Vol. 101, No. 7, Don Mills, Ontario, pp. 37-42, ISSN: 0316-4004.
- Hochmann D and Sadok M. 2004. Theory of synchronous averaging. 2004 IEEE Aerospace Conference Proceedings. 18 p.
- ISO 1101. 2004. Geometrical Product Specifications (GPS) - Geometrical tolerancing - Tolerances of form, orientation, location and run-out. 54 p.
- ISO 11342. 1994. Mechanical vibration - Methods and criteria for the mechanical balancing of flexible rotors. 1. p.
- ISO 1925. 1990. Mechanical vibration - Balancing vocabulary. 33 p.

ISO 1940/1. 1986. Mechanical vibration - Balance quality requirements of rigid rotors - Part 1: Determination of permissible residual unbalance. 1. p.

JCGM 100:2008. 2008. Evaluation of measurement data - Guide to the expression of uncertainty in measurement, Joint Committee for Guides in Metrology. 134 p.

JCGM 101:2008. 2008. Evaluation of measurement data - Supplement 1 to the "Guide to the expression of uncertainty in measurement" - Propagation of distributions using a Monte Carlo method, Joint Committee for Guides in Metrology. 90 p.

Järvelä J. 1989. Balancing of flexible paper machine rolls. Master's thesis. Tampere University of Technology, Faculty of Mechanical Engineering, Tampere. 137 p.

Jei Y.-G. and Lee C.-W. 1992. Modal analysis of continuous asymmetrical rotor-bearing systems. *Journal of Sound and Vibration*, 152(2):245-262.

Joh C.-Y. and Lee C.-W. 1996. Use of dFRFs for diagnosis of asymmetric/anisotropic properties in rotor-bearing system. *Journal of Vibration and Acoustics, Transactions of the ASME*, 118(1):64-69.

Jorkama M. 2001. Contact mechanical model for winding nip. Dr Thesis, Acta Polytechnica Scandinavica, Mechanical Engineering Series No. 146. Espoo. 96 p. ISBN 951-666-559-4.

Jorkama M. and Herten R. 1998. Optimal dynamic absorber for a rotating Rayleigh beam. *Journal of Sound and Vibration*, 217 (4), pp. 653-664.

Juhanko J. 1999. Dynamic behavior of a paper machine roll. Licentiate's thesis, Helsinki University of Technology, Otaniemi. 82 p.

Juhanko J. and Väänänen P. 1999. Geometry of paper machine rolls. Paper machine rolls seminar 27.-28.1.1999. Finnish Maintenance Society. Lahti. 13 p.

Juhanko J. and Kuosmanen P. 2007. New method for proactive maintenance of paper machine rolls. The 2nd World Congress on Engineering Asset Management (EAM) and the 4th International Conference on Condition Monitoring, 11 - 14 June 2007, Harrogate, United Kingdom. pp. 912-921.

Juhanko J., Porkka E., Widmaier T. and Kuosmanen P. 2010. Dynamic geometry of rotating cylinder with shell thickness variation. *Estonian Journal of Engineering* 16: 4, pp. 285-296.

Julkunen T. 1974. On the balancing of steel tube paper machine rolls. Dissertation. Helsinki University of Technology, Faculty of Mechanical Engineering, Otaniemi. 106 p.

Julkunen T. 1983. Vibration and balancing of rolls. In: Paper manufacturing III, Part 2, Handbook of Paper Engineers' Association. Turku. pp. 1143-1165. ISBN 951-99479-1-4.

Jusko O. and Lüdicke F. 1999. Novel multi-wave standards for the calibration of form measuring instruments. Precision engineering - nanotechnology, Proceedings of the 1st International EUSPEN Conference, Vol. 2, Bremen 31 May - 04 June 1999. 4 p.

- Kang Y., Lee A.-C. and Shih Y-P. 1994. A modified transfer matrix method for asymmetric rotor-bearing systems. *Journal of Vibration and Acoustics, Transactions of the ASME*, 116(3):309-317.
- Kang Y., Shih Y.-P. and Lee A.-C. 1992. Investigation on the steady-state responses of asymmetric rotors. *Journal of Vibration and Acoustics, Transactions of the ASME*, 114(2):194-208.
- Karhunen J. (1995). Minimization of half critical run-out of steel tube framed paper machine rolls. Dissertation. Oulu University, Oulu.
- Kärkkäinen T. and von Hertzen R. 1999. Report 3009991. Helsinki University of Technology, Laboratory of Mechanics, Otaniemi. 20 p.
- Karlsson M. 1997. Paper machine of the future. PaperHitech 97, 1st Seminar 6.2.1997. Otaniemi. 9 p.
- Kato H., Nakano Y and Nomura Y. 1990. Development of in-situ measuring system of circularity in precision cylindrical grinding. *Bulletin of the Japan Society for Precision Engineering*. Vol. 24:2. pp. 130-135.
- Kerttula R. 1997. Paper machines of the future. PaperHitech 97, 5th Seminar 15.5.1997. Jyväskylä. 14 p.
- Keskiniva M. 1997. Simulation and Balancing of Flexible Rotors in Terms of Semidefinite Modal Coordinates. Dissertation. Tampere University of Technology, Faculty of Mechanical Engineering, Tampere. Publications 220. 125 p.
- Keskiniva M. and Lauste L. 1995. Dynamic balancing of flexible rolls of paper machines subject to distributed unbalance loads. Ninth World Congress on the Theory of Machines and Mechanisms, August 30-31/ September 1-2 1995, Milano, Italy. 6 p.
- Kim N.-H. and Kim S.-W. 1996. Geometrical tolerances: Improved linear approximation of least squares evaluation of circularity by minimum variance. *International Journal of Machine Tools Manufacturing*, Vol. 36, No 3, pp. 355-366.
- Knowpap. 2009. Paper and paperboard grades. e-learning environment for papermaking and automation, www.knowpap.com [checked at 10.3.2011].
- Koskinen J. 1989. Development of a coating station for surface treatment of paper. Master's thesis. Helsinki University of Technology, Otaniemi. 133 p.
- Kuosmanen P. 1992. Optimization of the contact pressure in the nip of two non-ideal cylinders. Licentiate's thesis. Helsinki University of Technology, Otaniemi. 77 p.
- Kuosmanen P. 2004. Predictive 3D roll grinding method for reducing paper quality variations in coating machines. Dissertation. Helsinki University of Technology Publications in Machine Design 2/2004, Espoo. 91 p. ISBN 951-22-7014-5.
- Kuosmanen P. and Juhanko J. 2004. Reducing paper quality variations by predictive 3D grinding. Proceedings of 4th Euspen International Conference, Glasgow, Scotland. 6 p.

Kuosmanen P. and Väänänen P. 1996. New Highly Advanced Roll Measurement Technology. Proceedings of 5th international conference on new available techniques. The World Pulp and Paper Week, June 4-7 1996. Stockholm, Sweden. pp. 1056-1063.

Kuosmanen P., Juhanko J. and Pullinen J. 1998. Influence of modernization on the dynamic behavior of the backing roll. Proceedings of NordDesign '98, 26-28.8 1998, Royal Institute of Technology, Stockholm. pp. 269-278.

European patent EP 1 722 126 A2. 2006. Kuusinen A., Pullinen J., Salonen J. and Mattila J. Method and apparatus for balancing a tubular piece, such as a roll.

Lee A.-C., Kang Y., Tsai K.-L. and Hsiao K.-M. 1992. Transient analysis of an asymmetric rotor-bearing system during acceleration. Journal of Engineering for Industry, Transactions of the ASME, 114(4):465-475.

Lee A.-C., Shih Y.-P. and Kang Y. 1993. The analysis of linear rotor-bearing systems: A general transfer matrix method. Journal of Vibration and Acoustics, Transactions of the ASME, 115(4):490-497.

Lees A. W. and Friswell M. I. 1997. The evaluation of rotor imbalance in flexibly mounted machines. Journal of Sound and Vibration, 208(5):671-683.

Lehtinen E. 2000. Introduction to pigment coating of paper. Book 11: Pigment coating and surface sizing of paper, ed. E. Lehtinen. In: Papermaking Science and technology, editors Gullichsen J. and Paulapuro H. Fapet Oy, Helsinki. 810 p. ISBN 952-5216-11-X.

Leinonen T. E. 1969. On the influence of slight curvature in the bending behavior of a rotating shaft. Dissertation. Acta Polytechnica Scandinavica, Mechanical Engineering Series No. 47. 39 p.

Leinonen T. E. 1971. Notes on the bending behavior of slightly curved rotating shafts. Acta Polytechnica Scandinavica, Mechanical Engineering Series 63.

Leinonen T. E. 1994. On the structural nonlinearity of rotating shafts. Journal of Vibration and Acoustics, Transactions of the ASME, 116(3):404-407.

Li C. J., Li S. and Yu J. 1996. High-resolution error separation technique for in-situ straightness measurement of machine tools and workpieces. Mechatronics 6: 3, pp. 337-347.

Li H., Lam Y.-K. and Ng T.-Y. 2005. Rotating shell dynamics. Studies in Applied Mechanics 50. Elsevier. 263 p. ISBN 0-08-04477-6.

Linnonmaa J. 1988. The effect of blade geometry on the coat weight and coating quality in pigment coating of fine paper. Master's thesis. Helsinki University of Technology. Otaniemi. 83 p.

Linnonmaa J. and Trefz M. 2000. Pigment coating techniques. in: Lehtinen E. (Ed.) Pigment coating and surface sizing of paper. Gummerus, Jyväskylä. 810 p. ISBN 952-5216-11-X.

Linsinger T. 2005. Comparison of a measurement result with the certified value. ERM Application Note 1, European Reference Materials, IRMM. 2p.

- MacFadden P. D. and Toozhy M. M. 2000. Application of synchronous averaging to vibration monitoring of rolling element bearings. *Mechanical Systems and Signal processing* 14:6, pp. 891-906.
- Mark W. D., Lee H., Patrick R. and Coker J. D. 2010. A simple frequency-domain algorithm for early detection of damaged gear teeth. *Mechanical Systems and Signal Processing* 24. Elsevier. pp. 2807-2823.
- McFadden P. D. 1987. A revised model for the extraction of periodic waveforms by time-domain averaging, *Mechanical Systems and Signal Processing* 1 (1). pp 83-95.
- Melanson J. and Zu J.W. 1998. Free vibration and stability analysis of internally damped rotating shafts with general boundary conditions. *Journal of Vibration and Acoustics, Transactions of the ASME*, 120(3):776-783.
- Moore D. 1989. Design considerations in multiprobe roundness measurement. *Journal of Physics E: Scientific Instruments* 22, pp. 339-343.
- Nataraj C. 1993. On the interaction of torsion and bending in rotating shafts. *Journal of Applied Mechanics, Transactions of the ASME*, 60(1):239-241.
- Nielsen H. S. and Malburg M. C. 1996. Traceability and correlation in roundness measurement. *Precision Engineering* 19, pp. 175-179.
- Nikolajsen J.L. 1998. The effect of misalignment on rotor vibrations. *Journal for Engineering for Gas Turbines and Power, Transactions of the ASME*, 120(3): 635-640.
- Niskanen E. 1970. *Strength of materials Va. Theory of thermal stresses*. Publication 287, Otaniemi. 141 p.
- Ozono S. 1974. On a New Method of Roundness Measurement on the Three Point Method. *Proceedings of the ICPE, Tokyo*. pp. 457-462.
- Paloheimo T. 2000. A model and simulation program for rotor vibrations. Master's thesis. Helsinki University of Technology, Otaniemi. 73 p.
- Perento J. Paper trials help to improve quality and printability. *Paper Asia*, Vol. 15, No. 7, 1999, Singapore, pp. 15-17, ISSN: 0218-4540.
- Pirttiniemi J. 2004. Development of rotor balancing method. Master's thesis. Helsinki University of Technology. Otaniemi. 84 p.
- Plaut R.H. and Wauer J. 1995. Parametric, external and combination resonances in coupled flexural and torsional oscillations of an unbalanced rotating shaft. *Journal of Sound and Vibration*, 183(5):889-897.
- Proakis J.G. and Manolakis D.G. 1992. *Digital signal processing - Principles, algorithms and applications*. MacMillan Publishing Company, New York. ISBN 0-02-396815-X. 969 p.
- Puckett A. D. and von Herten R. 1999. State-of-the-art review of rotordynamics. Technical Report 56, Helsinki University of Technology Publications in Laboratory of Theoretical and Applied Mechanics, Espoo. 24 p. ISBN 951-22-4656-2.

- Pullinen J., Juhanko J. and Kuosmanen P. 1997. The effect of renewing on the dynamic behavior of a backing roll. Helsinki University of Technology, Laboratory of Machine Design, Publication C 286. 75 p. ISBN 951-22-3741-5.
- Rajalingham C., Bhat R.B. and Xistris G.D. 1993. Influence of external damping on stability and response of a horizontal rotor with anisotropic bending stiffness. *STLE Tribology Transactions*, 36(3):393-398.
- Sällinen P. 1998. Geometry error control of tube rolls of a paper machine. Master's thesis. Tampere University of Technology, Faculty of Mechanical Engineering, Tampere. 79 p.
- Savolainen M. 1996. Development of the measuring and balancing system for the paper machine rolls. Master's Thesis. Helsinki University of Technology, Faculty of Mechanical Engineering, Otaniemi. 68 p.
- Deutsche Patent DE 43 11 936 A1. 1993. Schachenhofer R. Balancing weight positioning system for roller, drum or cylinder casing - using hard positioning pins with pointed ends for penetrating material of cylinder inside wall around central support.
- Sekhar A. S. and Prabhu B. S. 1995. Effects of coupling misalignment on vibrations of rotating machinery. *Journal of Sound and Vibration* 185(4). pp. 655-671.
- Shao Y., Wang S., Ou J., Zhou X. Zhou B and Wang H. 2007. A new algorithm of time domain synchronous averaging analysis. International Conference on Control, Automation and Systems 2007, Oct. 17-20 2007 COEX, Seoul, Korea. pp. 2528-2531.
- Shaw J. and Shaw S. W. 1991. Non-linear resonance of an unbalanced rotating shaft with internal damping. *Journal of Sound and Vibration* 147(3). pp. 435-451.
- SKF bearing maintenance. 1994. Catalog 4100 Fi. 335 s.
- Slocum A. H. 1992. Precision machine design. New Jersey, Prentice Hall, Inc. 750 s. ISBN 0 13-690918-3.
- Snellman J. 1983. The effect of manufacturing accuracy on the dynamic behavior of guide rolls of a paper machine. Master's thesis. Oulu University, Oulu. 90 p.
- Stephenson R. W. and Rouch K. E. 1993. Modeling rotating shafts using axisymmetric solid finite elements with matrix reduction. *Journal of Vibration and Acoustics, Transactions of the ASME*, 115(4). pp. 484-489.
- Stoebener D. and Dijkman M. 2007. An Ultrasound In-Process-Measuring System to Ensure a Minimum Roundness Deviation for Rings During Turning. *Annals of the CIRP Vol. 56:1*. pp. 513-516.
- Suh J.-H., Hong S.-W. and Lee C.-W. 2005. Modal analysis of asymmetric rotor system with isotropic stator using modulated coordinates. *Journal of Sound and Vibration* 284. pp. 651-671.

- Tan J., Li D., Qiang X. and Yang W. 1992. The least squares circle model and parametric estimating method for the superprecision measurement of circle contour. Proceedings of the International Conference on Industrial Electronics, Control, Instrumentation and Automation. pp. 813-817.
- Tervonen, M. (1984). Barring of newsprint in the machine calender – The vibration models of the calendar. Licentiate's thesis, University of Oulu, Department of Mechanical Engineering. Oulu. 89 p.
- Tervonen, M. (1997). Numerical models for plane viscoelastic rolling contact of covered cylinders and a deforming sheet. Dissertation. Acta Universitatis Ouluensis Technica C100, University of Oulu, Department of Mechanical Engineering. Oulu. 123 p.
- Thalmann R. 2006. Basics of the highest accuracy roundness measurement. CENAM Metrology Symposium, 25.10.2006. 31 p.
- Thompson R. B. 1996. Ultrasonic measurement of mechanical properties. IEEE Ultrasonics Symposium 1996. pp. 735-744.
- Toiva J. 2002. Effect of structural imperfections on rotor dynamic response. Master's thesis, Helsinki University of Technology, Otaniemi. 75 p.
- Toiva J. 2006. Barring induced by nip contact. Licentiate's thesis, Helsinki University of Technology. Otaniemi. 64 p.
- U.S.Pat. 4,429,464. 1984. Burrus, B. M. Roundness calibration standard.
- U.S.Pat. 4,773,760. 1988. Makkonen T. Procedure and means for measuring the thickness of a film-like or sheet-like web.
- U.S.Pat. 5,096,734. 1992a. Nikulainen O., Koistinen J. Method and device for balancing a roll.
- U.S.Pat. 5,170,547. 1992b. Nikulainen O., Koistinen J. Method and device for balancing a roll.
- U.S.Pat. 5,331,737. 1994. Järvelä J. Method for fixing a balancing material in a roll.
- U.S.Pat. 5,397,291. 1995. Järvelä J. Method for fixing a balancing material in a roll.
- U.S.Pat. 5,940,969. 1999. Kuosmanen P. and Väänänen P. Method of continuously balancing and reducing the elastic asymmetry of a flexible rotor, particularly a roll or a cylinder.
- U.S.Pat. 6,370,953 B1. 2002. Ahokas M., Saari A., Kalapudas E. and Snellman J. 2002. Method for balancing a cylinder roll or equivalent part with a thin mantle and balanced cylinder, roll or equivalent part with a thin mantle.
- Uski T. 1999. Ultrasonic inspection of the coatings of paper machine rolls. Master's thesis. Helsinki University of Technology. Otaniemi. 53 p.
- Väänänen P. 1993. Turning of flexible rotor by high precision circularity profile measurement and active chatter compensation. Licentiate's thesis, Helsinki University of Technology. Otaniemi. 104 p.

- Wah T. 1964. Circular symmetric vibrations of ring stiffened circular shells. *J. Soc. Indust. Appl. Math.* Vol 12:3. pp. 649-662.
- Wauer J. and Suherman S. 1998. Vibration suppression of rotating shafts passing through resonances by switching shaft stiffness. *Journal of Vibration and Acoustics, Transactions of the ASME*, 120(1):170-180.
- Wettergren H. L. 1997. The influence of imperfections on the eigenfrequencies of a rotating composite shaft. *Journal of Sound and Vibration*, 204(1):99-116.
- Wettergren H. L. and Olsson K.-O. 1996. Dynamic instability of a rotating asymmetric shaft with internal viscous damping supported in anisotropic bearings. *Journal of Sound and Vibration*, 195(1):75-84.
- Whitehouse D. 1976. Some theoretical aspects of error separation techniques in surface metrology. *Journal of Physics E: Scientific Instruments*, Vol. 9. pp. 531-536.
- Whitehouse D. 1994. *Handbook of Surface Metrology*. Bristol, Institute of Physics Publishing. 988 p. ISBN 0-7503-0039-6.
- Widmaier T., Kiviluoma P., Pirttiniemi J., Porkka E. and Kuosmanen P. 2010. Thermal effects on the run-out of chilled cast thermo rolls. 7th International DAAAM Baltic Conference "Industrial Engineering", April 22-24 2010, Tallinn, Estonia. 6 p.
- Widmaier T., Kuosmanen P., Haikio J and Väänänen P. 2004. A non-circular turning system to minimise roll geometry errors. 4th International DAAAM Conference, 29th - 30th April, Tallinn, Estonia. 4 p.
- Widmaier T., Kuosmanen P., Haikio J. and Väänänen P. 2004. A 3D turning system to reduce geometry errors of flexible rotors. *Proceedings of Estonian Academy of Science and Engineering*, Vol 10: 4. pp. 251-260.
- Wirtz W. 2002. Advanced thermo rolls for high speed modern calendars. 7th International Conference on New Available Technologies, June 4-6 2002 Stockholm, Sweden. 5 p.
- Wong E. and Zu J. W. 1999. Dynamic response of a coupled spinning Timoshenko shaft system. *Journal of Vibration and Acoustics, Transactions of the ASME*, 121(1). pp. 110-113.
- Zhao W. Q., Xue Z., Tan J. B. and Wang Z. B. 2005. SSEST: A new approach to higher accuracy of cylindricity measuring instrument. *International Journal of Machine Tools & Manufacture* 46, pp. 1869-1878.

The coating variation of light weight coated LWC paper is found to be in synchronization with a backing roll of a coating station. A research hypothesis is set: The geometry of a roll changes as a function of running speed which has an effect on the harmonic quality variations of paper. Finite element analyses using measured wall thickness data show dynamic geometry change as a function of running speed. A device is developed to measure the dynamic geometry. A multi-lobe disc is used as a reference standard. A full scale backing roll is used for laboratory measurements which show similar behavior that was observed in the finite element analyses. Measurement series of backing rolls at paper mills show that dynamic geometry change is the most significant single component causing run-out and harmonic paper quality variation. Some examples of possible maintenance methods are introduced to improve the dynamic behavior of backing rolls.



ISBN 978-952-60-4363-0
ISBN 978-952-60-4364-7 (pdf)
ISSN-L 1799-4934
ISSN 1799-4934
ISSN 1799-4942 (pdf)

Aalto University
School of Engineering
Department of Engineering Design and Production
www.aalto.fi

**BUSINESS +
ECONOMY**

**ART +
DESIGN +
ARCHITECTURE**

**SCIENCE +
TECHNOLOGY**

CROSSOVER

**DOCTORAL
DISSERTATIONS**